

Summer 7-22-2022

## DESIGNING DYNAMIC AND DEGRADABLE POLYMERIC MATERIALS WITH THIOL-X CHEMISTRIES

Reese Sloan

Follow this and additional works at: <https://aquila.usm.edu/dissertations>

 Part of the [Materials Chemistry Commons](#), [Organic Chemistry Commons](#), [Physical Chemistry Commons](#), and the [Polymer Chemistry Commons](#)

---

### Recommended Citation

Sloan, Reese, "DESIGNING DYNAMIC AND DEGRADABLE POLYMERIC MATERIALS WITH THIOL-X CHEMISTRIES" (2022). *Dissertations*. 2063.  
<https://aquila.usm.edu/dissertations/2063>

This Dissertation is brought to you for free and open access by The Aquila Digital Community. It has been accepted for inclusion in Dissertations by an authorized administrator of The Aquila Digital Community. For more information, please contact [aquilastaff@usm.edu](mailto:aquilastaff@usm.edu).

DESIGNING DYNAMIC AND DEGRADABLE POLYMERIC MATERIALS WITH  
THIOL-X CHEMISTRIES

by

Reese Keeling Sloan

A Dissertation  
Submitted to the Graduate School,  
the College of Arts and Sciences  
and the School of Polymer Science and Engineering  
at The University of Southern Mississippi  
in Partial Fulfillment of the Requirements  
for the Degree of Doctor of Philosophy

Approved by:

Dr. Derek L. Patton, Committee Chair  
Dr. Sarah E. Morgan  
Dr. Yoan C. Simon  
Dr. Sergei Nazarenko  
Dr. James W. Rawlins

December 2022

COPYRIGHT BY

Reese Keeling Sloan

2022

*Published by the Graduate School*



THE UNIVERSITY OF  
**SOUTHERN**  
**MISSISSIPPI**

## ABSTRACT

With plastic production poised to increase in coming years, there arises a need to develop new polymeric materials designed to combat the global pollution crisis. A commonly utilized approach in addressing this challenge is to employ a responsive functional moiety into the polymer architecture. Thiol-X reactions, a commonly utilized class of “click” reactions, have garnered broad implementation in new stimuli-responsive materials. This work specifically focuses on utilizing radical-mediated thiol-ene coupling and base-catalyzed thiol-isocyanate reactions to develop a library of ternary thiol-ene/thiourethane covalent adaptable networks (CANs) and hydrolytically labile poly(thioether ketal) thermoplastics. CANs are a class of network materials capable of undergoing dynamic exchange, rendering the material reprocessable while maintaining the high-performance properties traditionally associated with thermosets. Herein, the thiourethane moiety, formed via the thiol-isocyanate reaction, is employed as the dynamic covalent chemistry (DCC) utilized in our approach to CANs. Additionally, linear thiol-ene photopolymerizations are employed to develop a series of poly(thioether ketal) thermoplastics. The ketal moiety incorporated into the polymer backbone of these materials render the resulting material hydrolytically labile – allowing the material to readily degrade at its end-of-lifetime. The work presented herein should provide a framework by which new environmentally friendly materials can be developed.

Chapter I of this dissertation focuses on the various utility of thiol-X reactions within the realm of polymeric materials – with specific interest on implementation within CANs and thermoplastic synthesis. Chapter II outlines the methods by which the thiol-X based materials, described herein, were developed and studied. Chapter III focuses on

understanding the specific structure-property relationship of ternary thiol-ene/thiourethane CANs affecting vitrimeric relaxation behaviors and material property retention throughout reprocessing. Chapter IV elaborates on the stoichiometric effects of ternary thiol-ene/thiourethane on the dynamic exchange equilibrium – ultimately dictating thermal relaxation behaviors. Finally, Chapter V utilizes linear thiol-ene photopolymerizations to develop a library of poly(thioether ketals) capable of undergo hydrolysis within an acidic environment while remaining stable in basic and neutral conditions.

## ACKNOWLEDGMENTS

First and foremost, I would like to acknowledge my advisor, Dr. Derek L. Patton, for taking a chance on me and giving me the opportunity to succeed. Thank you for teaching me how to ask the correct questions and how to move through the struggles of research. Thank you for the opportunities, fellowships, and professional connections you helped me to establish. I would not be where I am today without your guidance. To the members of my research group, both past and present, thank you for your support and input throughout my academic journey. In particular, I need to thank Matthew Fisher, Sarah Landrum, Dr. William Walker, Dr. Benjamin Alameda, Pritha Bhunia, and Jaylen Davis for each of your input and contributions to the work presented in this document.

To the members of my committee and other faculty members of the School of Polymer Science and Engineering, thank you for your guidance and support throughout my academic career.

To Charles Collen, David Delatte, John Peyrefitte, and Logan Dugas, thank you for your continued support and conversations in the shared lab. To everyone else in the department, thank you for great conversations and productive time wasting. We make it through graduate school together.

Finally, thank you to my funding sources for making this work possible; CHE-1710589, DGE-1449999, and the National Science Foundation Graduate Research Fellowship Program.

## DEDICATION

*To my dad Rick and brother Case,*

*Thank you for your love and support through this journey.*

*To the two strongest women in my life,*

*My mom Cindy and my wife Leah,*

*I would not have made it to where I am today without your love, support, and constant encouragement. You have helped me through the highs and pushed me through the lows of this journey.*

*Psalms 112:8*

*For they are confident and fearless and will face their foes triumphantly.*

## TABLE OF CONTENTS

ABSTRACT .....	ii
ACKNOWLEDGMENTS .....	iv
DEDICATION .....	v
LIST OF TABLES .....	x
LIST OF ILLUSTRATIONS .....	xii
LIST OF ABBREVIATIONS .....	xviii
CHAPTER I - Introduction .....	1
1.1 Motivation .....	1
1.2 Diverse Utility of Thiol-X “Click Chemistries” .....	2
1.3 Radical-Mediated Thiol-Ene Photopolymerization .....	3
1.4 Thiourethane Formation Through Thiol-Isocyanate Reactions .....	4
1.5 Thiol-x Reactions as a Route to Covalent Adaptable Networks and Vitrimeric Materials .....	5
1.6 Thiol-ene Reactions as Route Towards Hydrolytically Labile Materials .....	10
CHAPTER II – Materials and Methods .....	13
2.1 Materials .....	13
2.2 Material Preparation and Synthesis .....	13
2.2.1 Ternary Thiol-ene/Thiourethane CANs – Altering Diisocyanate Monomer Structure .....	13

2.2.2 Ternary Thiol-ene/Thiourethane CANs – Altering Reactive Functionality ....	14
2.2.3 Synthesis of Thiourethane Small Molecule .....	14
2.2.4 Synthesis of Bisalkene Diketal Monomers .....	15
2.2.5 Synthesis of Poly(thioether ketals) using DTT and EDDT Monomers .....	15
2.2.6 Synthesis of Poly(thioether ketals) using PPGMP 2200 as the Dithiol Monomer.....	16
2.3 Covalent Adaptable Network Material Characterizations .....	16
2.3.1 Real Time and Variable Temperature FTIR .....	16
2.3.2 Gel Content Determination .....	17
2.3.3 Thermogravimetric Analysis .....	17
2.3.4 Dynamic Mechanical Analysis .....	17
2.3.5 Stress Relaxation Analysis.....	18
2.3.6 Non-isothermal Creep Analysis.....	19
2.3.7 Creep/Recovery Analysis.....	19
2.3.8 Dynamic Scanning Calorimetry.....	20
2.3.9 Material Reprocessing .....	20
2.3.10 Tensile Testing.....	20
2.4 Poly(thioether ketal) Thermoplastic Material Characterization .....	21
2.4.1 Nuclear Magnetic Resonance (NMR) Analysis.....	21
2.4.2 Size Exclusion Chromatography (SEC).....	21

2.4.3 Hydrolytic Stability Analysis.....	21
2.4.4 Contact Angle Analysis .....	22
CHAPTER III - Ternary Thiol-Ene/Thiourethane Covalent Adaptable Networks: A Rapid and Versatile Route to Vitrimeric Materials .....	23
3.1 Objective.....	23
3.2 Formation of Ternary Thiol-ene/Thiourethane Covalent Adaptable Networks .....	24
3.3 Thermomechanical Characterization of the Ternary Thiol-ene/Thiourethane Networks .....	27
3.4 Probing the Dynamic Thiourethane Behavior within Networks.....	29
3.5 Material Reprocessing and Physical Property Retention.....	35
3.6 Concluding Remarks.....	38
CHAPTER IV – Understanding the Effects of Altering Functional Stoichiometry on the Vitrimeric Behavior of Ternary Thiol-ene/Thiourethane Covalent Adaptable Networks	40
4.1 Objective.....	40
4.2 Effects of Altering Thiol Content on the Dynamic Behavior of Ternary Thiol-ene/Thiourethane CANs.....	41
4.3 Effects of Thiol Stoichiometry on Thermomechanical and Mechanical Property Retention.....	49
4.4 Concluding Remarks.....	54

CHAPTER V – Development of hydrolytically labile poly(thioether ketal) thermoplastics .....	56
5.1 Objective .....	56
5.2 Polymer Synthesis.....	57
5.3 Hydrolytic Stability Analysis of Poly(thioether ketal) thermoplastics .....	59
5.4 Material Properties of Poly(thioether ketal) Thermoplastics.....	68
5.5 Concluding Remarks.....	70
CHAPTER VI Conclusions and Future Work.....	71
APPENDIX A - Supplemental Information to Chapter III.....	74
APPENDIX B – Supplemental Information to Chapter IV .....	80
APPENDIX C Supplemental Information to Chapter V .....	83
REFERENCES .....	99

## LIST OF TABLES

Table 3.1 Summary of conversion kinetics and gel content of cured ternary thiol-ene/thiourethane networks. ....	27
Table 3.2 Summary of virgin material thermal properties determined by DMA. ....	28
Table 3.3 Summary of vitrimeric topological freezing temperature and relaxation behaviors. ....	33
Table 3.4 Summary of key mechanical properties of <b>F1 – F3</b> throughout reprocessing..	37
Table 3.5 Summary of thermomechanical (properties determined by DMA) of <b>F1 – F3</b> throughout reprocessing.....	37
Table 4.1 Vitrimeric thermal relaxation behavior of the <b>F1</b> , <b>+5%</b> , and <b>+10%</b> systems..	42
Table 4.2 Summary of small molecule thiourethane systems.....	44
Table 4.3 Summary of obtained $T_v$ . ....	49
Table 4.4 Summary of thermal and thermomechanical properties of virgin <b>F1</b> and virgin altered thiol compositions. ....	50
Table 4.5 Summary of mechanical properties. ....	52
Table 4.6 Summary of reprocessed mechanical property retention relative to the respective virgin material properties.....	53
Table 5.1 Summary of model degradation kinetics determined using Mw data from polymers <b>11 – 14</b> fitted to the model developed by Lyu et al. <sup>140</sup> .....	67
Table 5.2 Summary of molecular weights, contact angle, and thermal properties of polymers <b>9 – 14</b> .....	69
Table B.1 Summary of $\tau^*$ values of the excess thiol systems. ....	80

Table B.2 Summary of  $\tau^*$  values of the deficient thiol systems..... 80

## LIST OF ILLUSTRATIONS

Figure 1.1 Reaction mechanism of the radical-mediated thiol-ene photoreaction. ....	3
Figure 1.2 Reaction mechanism of the base catalyzed thiol-isocyanate coupling reaction.	5
Figure 1.3 Generic scheme to the dissociative (ex. Diels-Alder) and associative (ex. transesterification) dynamic pathways in CANs.....	7
Figure 1.4 Dual dynamic behaviors of the thiourethane DCC.....	8
Figure 1.5 Proposed synergistic dual dynamic behavior of the thiourethane moiety when using DBN as the exchange catalyst. <sup>72</sup> .....	9
Figure 1.6 Mechanism of ketal hydrolysis.....	11
Figure 3.1 A) Reaction scheme of the “one-pot two-step” method to achieve ternary thiol-ene/thiourethane networks with B) illustrating the commercially available monomers utilized.....	24
Figure 3.2 A) FTIR analysis of F1 before and after the addition of DBN. B) Decrease in <b>F1</b> thiol peak absorbance as at various UV exposure times. C) Thiol conversion kinetics of <b>F1 – F3</b> as a function of UV exposure time. ....	26
Figure 3.3 DMA thermograms of virgin A) <b>F1</b> , B) <b>F2</b> , and C) <b>F3</b> . ....	28
Figure 3.4 VT-FTIR of <b>F1 – F3</b> (A – C, respectively) at varying temperature profiles. Additionally, the structures of <b>F1 – F3</b> are depicted to show the primary (blue) and secondary (green) thiourethane moieties. ....	30
Figure 3.5 Stress relaxation experiments of A) <b>F1</b> , B) <b>F2</b> , and C) <b>F3</b> with their respective primary (blue) and secondary (green) thiourethane structures as dictated by the parent diisocyanate monomer selection. D) Results from stress relaxation experiments plotted in terms of the Arrhenius relationship.....	32

Figure 3.6 Nonisothermal creep results obtained for <b>F1</b> , <b>F2</b> , and <b>F3</b> .....	34
Figure 3.7 Basic process by which materials ( <b>F1</b> being shown) were reprocessed.....	35
Figure 3.8 Thermomechanical (A-C; determined via DMA) and mechanical properties (D-F; determined via tensile testing) of <b>F1</b> – <b>F3</b> throughout two material reprocessing cycles.....	36
Figure 4.1 Stress relaxation analysis of the A) +5% and B) +10% systems. ....	41
Figure 4.2 Stress relaxation of results plotted in terms of the Arrhenius relationship.....	42
Figure 4.3 Formation of <b>SM1</b> . ....	44
Figure 4.4 VT-FTIR of <b>SM1</b> . ....	45
Figure 4.5 VT-FTIR analysis of <b>SM1</b> , <b>SM2</b> , and <b>SM3</b> (increasing DBN content) at 90°C (solid), 100°C (dash), and 110°C (dash dot).....	46
Figure 4.6 VT-FTIR analysis of <b>SM1</b> – <b>SM3</b> and <b>SM4</b> – <b>SM6</b> (respective increased thiol counterpart) at 110°C.....	46
Figure 4.7 Stress relaxation analysis of the A) -5% and B) -10% systems. ....	47
Figure 4.8 Arrhenius plot of the -5% and -10% systems from the obtained stress relaxation data, where it hypothesized that the lower temperature regime (VFT behavior) is indicative of thiourethane dissociation, and the upper temperature regime (Arrhenius behavior) is due to the presence of the associative behavior. ....	48
Figure 4.9 Non-isothermal creep analysis of <b>F1</b> and all altered thiol systems. ....	49
Figure 4.10 A) DMA and B) DSC thermograms of virgin <b>F1</b> and virgin altered thiol compositions. ....	50
Figure 4.11 Virgin tensile properties of each altered thiol system. ....	51

Figure 4.12 Virgin and reprocessed tensile test results of the A) +5%, B) +10%, C) -5%, and D) -10% systems.....	51
Figure 4.13 DMA thermograms of the +10% system throughout reprocessing. ....	54
Figure 5.1 General synthetic scheme for cyclic bisalkene diketal monomers <b>3</b> and <b>5</b> from the acid-catalyzed ketalization of diketones ( <b>2</b> and <b>4</b> ) and 3-allyloxy-1,2-propanediol ( <b>1</b> ). .....	58
Figure 5.2 General synthetic scheme for polymers <b>9</b> , <b>10</b> , <b>11</b> , <b>12</b> , <b>13</b> , and <b>14</b> from the radical mediated thiol-ene photopolymerization of monomers <b>3</b> and <b>5</b> with commercially available dithiol monomers <b>6</b> , <b>7</b> , and <b>8</b> . ....	58
Figure 5.3 Gravimetric analysis of polymers <b>9</b> and <b>10</b> upon exposure to acidic (1M HCl:Acetonitrile – 90:10 by volume), neutral (pH 7.4 PBS buffer:acetonitrile – 90:10 by volume), and basic (1M NaOH:Acetonitrile – 90:10 by volume) aqueous environments versus time. ....	60
Figure 5.4 A) Illustration of the potential crosslinking reactions of polymers <b>9</b> and <b>10</b> that could occur during the degradation process under acidic conditions and B) molecular structure of crosslinks (yellow) and reformed hydroxyl groups (green) as a result of acidic catalysis (crosslink formation) and degradation.....	62
Figure 5.5 SEC chromatograms of A) polymer <b>12</b> and B) polymer <b>14</b> throughout degradation under acidic conditions and SEC analysis of C) polymers <b>11</b> and <b>12</b> and D) polymers <b>13</b> and <b>14</b> throughout degradation under acidic conditions. ....	63
Figure 5.6 Molecular weight data of polymers <b>11</b> – <b>14</b> fitted to the model proposed by Lyu et al. <sup>140</sup> .....	67
Figure A.1 FTIR analysis of <b>F2</b> resin before and after the addition of DBN catalyst.....	74

Figure A.2 Reduction in the characteristic thiol peak of <b>F2</b> resin due to UV exposure. . .	74
Figure A.3 FTIR analysis of <b>F3</b> resin before and after the addition of DBN catalyst. ....	75
Figure A.4 Reduction in the characteristic thiol peak of <b>F3</b> resin due to UV exposure. . .	75
Figure A.5 ATR spectra of <b>F1</b> throughout reprocessing. ....	76
Figure A.6 ATR spectra of <b>F2</b> throughout reprocessing. ....	76
Figure A.7 ATR spectra of <b>F3</b> throughout reprocessing. ....	77
Figure A.8 TGA thermogram of <b>F1</b> throughout reprocessing. ....	77
Figure A.9 TGA thermogram of <b>F2</b> throughout reprocessing. ....	78
Figure A.10 TGA thermogram of <b>F3</b> throughout reprocessing. ....	78
Figure A.11 Creep/recovery results for <b>F1 – F3</b> . ....	79
Figure B.1 Bar graphs of key physical properties throughout reprocessing for each of the altered thiol systems. ....	80
Figure B.2 Bar graphs of key physical property retention throughout reprocessing for each of the altered thiol systems. ....	81
Figure B.3 DMA of the <b>-10%</b> thiol system throughout reprocessing. ....	81
Figure B.4 DMA of the <b>-5%</b> thiol system throughout reprocessing. ....	82
Figure B.5 DMA of the <b>+5%</b> thiol system throughout reprocessing. ....	82
Figure C.1 <sup>1</sup> H-NMR Spectrum of Polymer <b>9</b> . ....	83
Figure C.2 <sup>13</sup> C-NMR Spectrum of Polymer <b>9</b> . ....	83
Figure C.3 <sup>1</sup> H- <sup>13</sup> C HSQC Spectrum of Polymer <b>9</b> . ....	84
Figure C.4 COSY Spectrum of Polymer <b>9</b> . ....	84
Figure C.5 <sup>1</sup> H-NMR Spectrum of Polymer <b>10</b> . ....	85
Figure C.6 <sup>13</sup> C-NMR Spectrum of Polymer <b>10</b> . ....	85

Figure C.7 $^1\text{H}$ - $^{13}\text{C}$ HSQC Spectrum of Polymer <b>10</b> .....	86
Figure C.8 COSY Spectrum of Polymer <b>10</b> .....	86
Figure C.9 $^1\text{H}$ -NMR Spectrum of Polymer <b>11</b> .....	87
Figure C.10 $^{13}\text{C}$ -NMR Spectrum of Polymer <b>11</b> .....	87
Figure C.11 $^1\text{H}$ - $^{13}\text{C}$ HSQC Spectrum of Polymer <b>11</b> .....	88
Figure C.12 COSY Spectrum of Polymer <b>11</b> .....	88
Figure C.13 $^1\text{H}$ -NMR Spectrum of Polymer <b>12</b> .....	89
Figure C.14 $^{13}\text{C}$ -NMR Spectrum of Polymer <b>12</b> .....	90
Figure C.15 $^1\text{H}$ - $^{13}\text{C}$ HSQC Spectrum of Polymer <b>12</b> .....	90
Figure C.16 COSY Spectrum of Polymer <b>12</b> .....	90
Figure C.17 $^1\text{H}$ -NMR Spectrum of Polymer <b>13</b> .....	91
Figure C.18 $^{13}\text{C}$ -NMR Spectrum of Polymer <b>13</b> .....	91
Figure C.19 $^1\text{H}$ - $^{13}\text{C}$ HSQC Spectrum of Polymer <b>13</b> .....	92
Figure C.20 COSY Spectrum of Polymer <b>13</b> .....	92
Figure C.21 $^1\text{H}$ -NMR Spectrum of Polymer <b>14</b> .....	93
Figure C.22 $^{13}\text{C}$ -NMR Spectrum of Polymer <b>14</b> .....	93
Figure C.23 $^1\text{H}$ - $^{13}\text{C}$ HSQC Spectrum of Polymer <b>14</b> .....	94
Figure C.24 COSY Spectrum of Polymer <b>14</b> .....	94
Figure C.25 Initial SEC chromatograms of polymers 9-14. ....	95
Figure C.26 SEC Chromatograms of Polymer <b>11</b> Throughout Degradation Under Acidic Conditions.....	95
Figure C.27 SEC Chromatograms of Polymer <b>12</b> Throughout Degradation Under Acidic Conditions.....	96

Figure C.28 SEC Chromatograms of Polymer <b>13</b> Throughout Degradation Under Acidic Conditions .....	96
Figure C.29 SEC Chromatograms of Polymer <b>14</b> Throughout Degradation Under Acidic Conditions .....	97
Figure C.30 DSC Thermograms of Polymers <b>9</b> and <b>10</b> .....	97
Figure C.31 DSC Thermograms of Polymers <b>11</b> and <b>12</b> .....	98
Figure C.32 DSC Thermograms of Polymers <b>13</b> and <b>14</b> .....	98

## LIST OF ABBREVIATIONS

DCC	Dynamic Covalent Chemistry
CAN	Covalent Adaptable Network
UV	Ultraviolet
DBN	1,5-diazobicyclo[4.3.0]non-5-ene
DBU	1,8-diazobicyclo[5.4.0]undec-7-ene
GDL	Glucarodilactone
EDDT	2,2'-(ethylenedioxy)diethanethiol
H <sub>12</sub> MDI	4,4'-methylenebis(cyclohexyl isocyanate)
TTT	Triallyl triazine
p-TsOH	p-Toluenesulfonic Acid
HDI	Hexamethylene Diisocyanate
IPDI	Isophorone Diisocyanate
DTT	Dithioerythritol
PPGMP 2200	Propyleneglycol 3-mercaptopropionate 2200
THF	Tetrahydrofuran
FTIR	Fourier-transform Infrared Spectroscopy
VT-FTIR	Variable-temperature Fourier-transform Infrared Spectroscopy
-NCO	Isocyanate Functional Group
-SH	Thiol Functional Group
DCM	Dichloromethane
TGA	Thermogravimetric Analysis

DMA	Dynamic Mechanical Analysis
DSC	Dynamic Scanning Calorimetry
MTS	Mechanical Testing Systems
NMR	Nuclear Magnetic Resonance Spectroscopy
SEC	Size Exclusion Chromatography
$T_g$	Glass Transition Temperature
$T_v$	Topology Freezing Temperature
$E_a$	Energy of Activation
FWHM	Full Width Half Maximum
VFT	Vogel-Fulcher-Tommann
PPO	Poly(propylene oxide)
LCST	Lower Critical Solution Temperature

## CHAPTER I - Introduction

### 1.1 Motivation

As a modern society, we have generated 6.3 billion metric tons of plastic waste since 1950 – a staggering 79% of this waste has accumulated in landfills or in the natural environment creating a global environmental problem. Despite an increase in plastic recycling programs, 75% of plastic products produced in 2015 were discarded in landfills – much of it from single use applications.<sup>1-2</sup> Thus, there arises a need to develop new materials of environmental relevance. Tackling this challenge is often difficult due to the stringent requirements arising in the development of these materials while also being cost competitive with products already being produced on an industrial scale. Two common approaches have arisen to address the challenge in combatting the plastic pollution issue. The first approach is the utilization of dynamic covalent chemistries (DCCs) within thermosetting network materials. Traditionally, thermosetting networks exhibit highly sought-after material properties due to the permanent crosslinks binding the polymer matrix into one molecular unit.<sup>3</sup> However, these high performance properties come at the expense of material reprocessability. By implementing DCCs into the polymer crosslinks, thermoset network reprocessability can be achieved while maintaining high performance material properties. The second approach is to utilize degradable linkages along the polymer backbone allowing the material to break down upon exposure to an appropriate trigger at the end-of-use lifetime of the thermoset. However, in many cases, these approaches require stringent synthetic processes to achieve these materials. Therefore, simple synthetic processes should be utilized in the development of materials implementing these approaches. It is the goal of this dissertation to exploit the simplicity

of various “click chemistries” to develop materials implementing these approaches rapidly and efficiently.

## **1.2 Diverse Utility of Thiol-X “Click Chemistries”**

“Click chemistry”, a term coined by Sharpless et al.<sup>4</sup>, embodies a group of reactions with simple reaction conditions using readily available starting materials to achieve a single product in high yield with little to no purification needed.<sup>4-6</sup> To be considered as a “click chemistry”, the reaction must be modular, wide in scope, high yielding, regio/stereoselective, mild reaction conditions, and orthogonal in selection to the chemical substrate.<sup>4-5</sup> While multiple chemistries have been found to satisfy these prerequisites, thiol-x reactions, where “x” often represents electron – deficient alkenes or isocyanates, have become widely associated with the class of “click chemistries”.

Thiol based reactions have been shown to exhibit rapid reaction rates, high conversion, and regioselectivity. The high reactivity of the thiol moiety is well known and is able to interact with a wide variety of chemical substrates via radical, base-catalyzed, or nucleophile-catalyzed mechanisms.<sup>5</sup> Example reactions include thiol-ene<sup>7-10</sup>, thiol-epoxy<sup>5, 11</sup>, thiol-Michael<sup>5, 12</sup>, and thiol-isocyanate<sup>13-16</sup>; each having found wide utilization in material and polymer science in forms of post-polymerization modification<sup>5, 17</sup>, linear<sup>18</sup> and network polymer formation<sup>5</sup>, surface modification<sup>19-21</sup>, and lithography<sup>22</sup>. The work described herein utilizes both the thiol-ene and thiol-isocyanate reactions to develop thermosetting covalent adaptable networks and hydrolytically labile thermoplastics.

### 1.3 Radical-Mediated Thiol-Ene Photopolymerization

Owing to their rapid reaction kinetics, chemical orthogonality, and high reaction efficiency, thiol-ene couplings have been shown to be effectively utilized in organic chemistry and polymer synthesis.<sup>5, 8-10</sup> The mechanism of the thiol-ene photoreaction, as illustrated in **Figure 1.1**, is driven by the UV induced formation of a thiyl radical *via* hydrogen abstraction from the activated initiator. The thiyl radical then adds across an alkene bond in an anti-Markovnikov fashion to form a  $\beta$ -centered carbon radical that then undergoes chain transfer with a free thiol to form the resulting thioether adduct and a new thiyl radical that continued to participate in the reaction.<sup>23-24</sup> Radical-mediated thiol-ene photopolymerization proceeds in a step growth manner<sup>10</sup>, providing inherent benefits and drawbacks in polymer synthesis depending on the class of polymer being developed (i.e., thermosetting or thermoplastic materials).

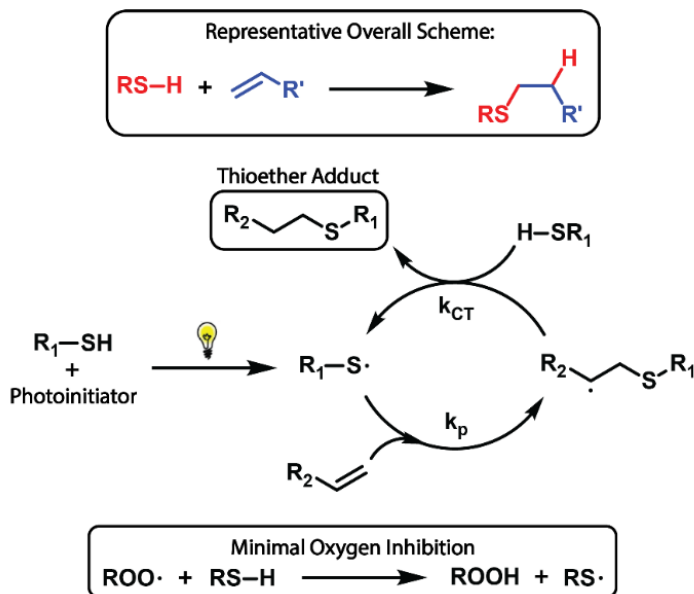


Figure 1.1 Reaction mechanism of the radical-mediated thiol-ene photoreaction.

Thermosetting materials formed by means of a step growth mechanism generally exhibit uniform network architecture with identical molecular weight between crosslinks, in contrast to those formed by a chain growth mechanism. In the case of thermoplastic materials, achieving high molecular weight polymers can be difficult due to the necessity of achieving high degrees of conversion. Furthermore, the step growth mechanism produces thermoplastics exhibiting a polydispersity in polymer chain lengths. Nevertheless, the thiol-ene photoreaction has garnered great attention in the realm of network materials and post-polymerization modification.<sup>10, 25-27</sup>

#### **1.4 Thiourethane Formation Through Thiol-Isocyanate Reactions**

Thiourethanes are sulfur-based analogs of the urethane moiety formed *via* the reaction of thiols with isocyanates. Early reports by Dyer et al.<sup>13</sup> showed that the thiourethane moiety could be formed using a base-catalyzed thiol-isocyanate coupling reaction, **Figure 1.2**. Here, a thiolate anion is formed *via* proton abstraction of a thiol by a base catalyst. The thiolate anion is then able to add to an isocyanate to form a deprotonated thiourethane intermediate, that subsequently undergoes chain transfer with a free thiol to produce the thiourethane moiety and a new thiolate anion to further catalyze the continued reaction<sup>5, 16</sup>. The base-catalyzed thiol-isocyanate and radical-mediated thiol-ene coupling reactions are mechanistically similar in that both undergo an alternating chain-transfer and propagation two-step process<sup>5</sup>. Importantly, the base-catalyzed thiol-isocyanate coupling reaction is classified as a “click chemistry” due to rapid reaction kinetics, high yield and efficiency, and no formation of byproducts.<sup>5, 28</sup> The thiourethane moiety has found useful implementation within a range of areas in material science.<sup>29-31</sup>

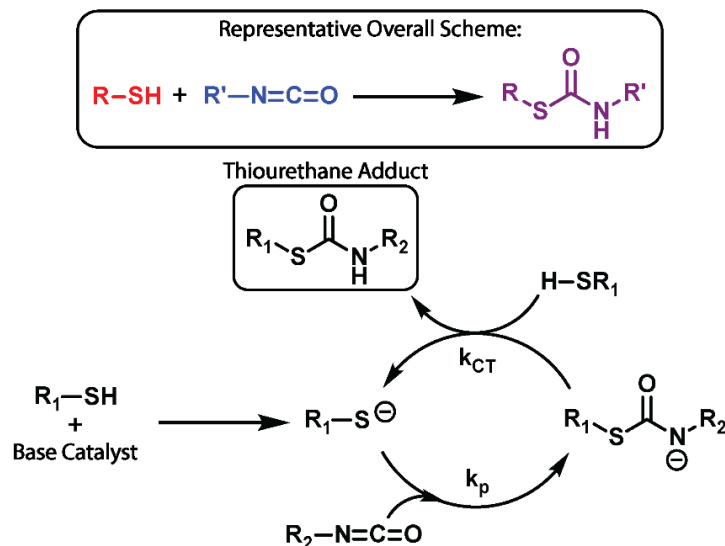


Figure 1.2 Reaction mechanism of the base catalyzed thiol-isocyanate coupling reaction.

## 1.5 Thiol-x Reactions as a Route to Covalent Adaptable Networks and Vitrimeric Materials

Vitrimeric materials have gained considerable attention within the realm of network forming polymers – offering an interesting alternative to traditional thermosetting polymers. Historically, thermosets have been differentiated from thermoplastic materials by permanent covalent crosslinks between polymer chains endowing the material with highly sought after thermal and mechanical properties. However, the resulting permanent three-dimensional architecture prevents traditional thermosetting materials from being reshaped, remolded, and reprocessed.<sup>32-34</sup> Significant efforts have since been placed on tackling the intellectual challenge of marrying thermal malleability associated with thermoplastic polymers with the desired high-performance properties of thermosetting networks.

Recent advancements in polymer science have provided insight into different methods by which supramolecular networks can be developed – i.e., thermoplastic polymers bound by noncovalent interactions. These noncovalent interactions act as physical crosslinks in the form of hydrogen bonding<sup>35-37</sup>, phase separation<sup>34-35</sup>,  $\pi$ - $\pi$  interactions<sup>38</sup>, and metal complexation<sup>37, 39</sup>. In contrast, covalent adaptable networks (CANs) incorporate the use of dynamic chemistries into covalently bound network architectures. This approach offers certain advantages over supramolecular networks, such as solvent resistance and prolonged material lifetime imparted by covalent interactions.<sup>34</sup> Significant research has been dedicated towards the synthetic development and fundamental understanding of the key structure-property relationships dictating the dynamic character of such materials.

CANs are a class of materials that incorporate the use of dynamic covalent chemistries (DCC) within the traditional three-dimensional architecture of thermosetting materials. These dynamic chemistries are employed within the polymeric crosslinks and can undergo dynamic exchange when exposed to an external stimulus. To date, various functional handles have been identified as viable dynamic chemistries for use in CANs. To be determined viable, the dynamic chemistry employed must exhibit rapid exchange kinetics to reach a thermodynamic equilibrium resulting in macroscopic flow and topological rearrangement.<sup>32, 34, 40-42</sup> The nature of the DCC employed must be considered when designing CANs, as the dynamic behavior has a distinct impact on the retention of macromolecular architecture. Furthermore, CANs are classified in terms of the dynamic behavior of the DCC, i.e., dissociative or associative behaviors (**Figure 1.3**). Dissociative CANs utilize DCCs that break into distinctly different functional groups that

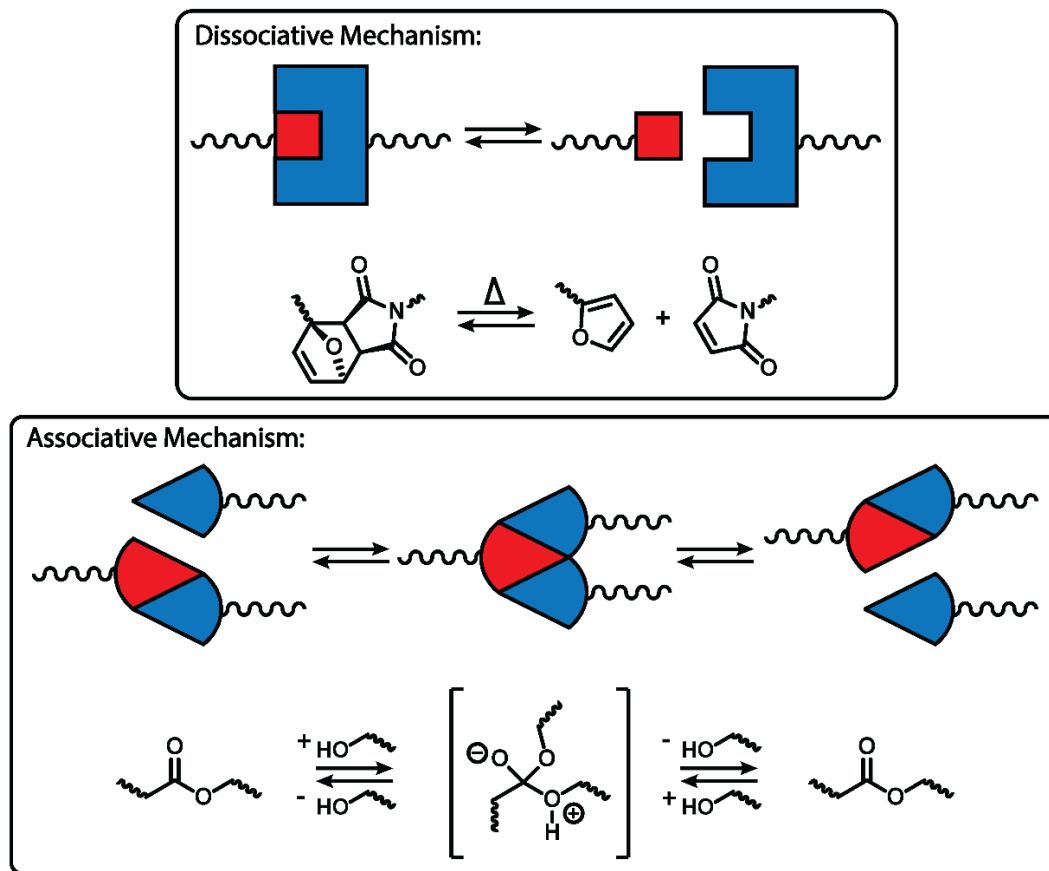


Figure 1.3 *Generic scheme to the dissociative (ex. Diels-Alder) and associative (ex. transesterification) dynamic pathways in CANs.*

rapidly reform the parent DCC in another location. This process is commonly characterized by a loss in crosslink density when the dynamic exchange process is occurring.<sup>33</sup> Common dissociative DCCs include Diels-Alder<sup>43-46</sup>, thiol-Michael<sup>47</sup>, alkoxyamines<sup>48</sup>, acylhydrazones<sup>49-50</sup>, and hindered ureas.<sup>51-53</sup> Associative CANs, although less common<sup>54</sup>, utilize DCCs that exchange between the dynamic functional handle and nearby free reactive functional group. This process is distinct from its dissociative counterpart in that crosslink density is retained throughout the dynamic exchange process.<sup>33</sup> Common associative DCCs include transesterification<sup>55-61</sup>, transamidation<sup>62</sup>, trithiocarbonates<sup>63-65</sup>, and vinylogous urethanes<sup>54, 66</sup>. Additionally,

specific DCCs – such as disulfides<sup>67-71</sup> and thiourethanes<sup>72-79</sup> – have been shown to exhibit both associative and dissociative behaviors.

Thiol-X reactions have recently received a great deal of attention in vitrimeric systems as both crosslinking formers<sup>22, 63, 68, 80</sup> and DCCs<sup>47, 81-83</sup>, due to their fast reaction kinetics and relatively benign reaction conditions<sup>5</sup>. In the CAN portion of this dissertation (Chapter III and IV), focus is placed on the thiourethane DCC. Li et al. recently showed that vitrimer networks could be formed via thiol-isocyanate click reactions.<sup>73</sup> On the small molecule scale, they were able to show that the thiourethane moiety exhibits both the associative and dissociative processes, **Figure 1.4**. Incorporating the thiourethane functional group into polymer networks, they demonstrated the ability of these materials to be reprocessed and recycled. Expanding on the work from Li et al., Wen and coworkers<sup>72</sup> were able to show that the exchange catalyst used in thiourethane vitrimeric systems dictates the dynamic process by which the thiourethane moiety undergoes upon exposure to elevated temperatures. Here it was determined that the associative behavior is promoted by a base catalyst and the dissociative behavior is promoted by a nucleophilic catalyst.

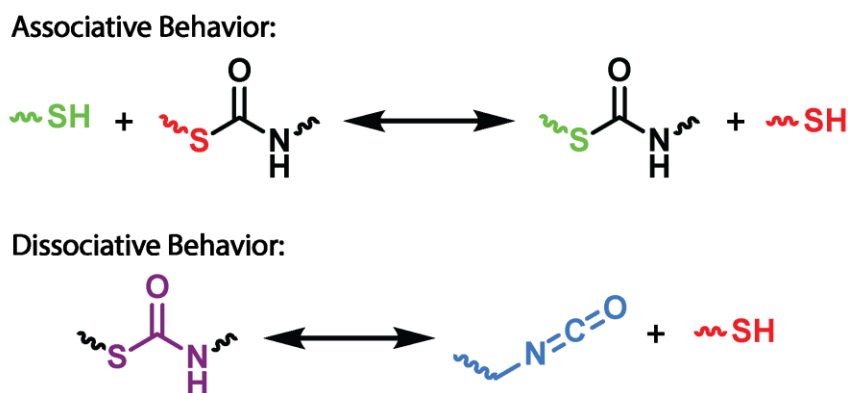


Figure 1.4 *Dual dynamic behaviors of the thiourethane DCC.*

Furthermore, Wen et al. explained that catalyst acting as both a good base and nucleophile, such as DBN or DBU, promote both the associative and dissociative behaviors (**Figure 1.5**). While these reports highlight the usefulness of the thiourethane DCC in vitrimeric networks, they do pose certain drawbacks inherent to the thiourethane moiety. Namely, these reports are unable to determine virgin material properties because of the rapid reaction kinetics between the parent thiol and isocyanate monomers. Alternative methods of thiourethane formation have been investigated utilizing tin catalyst systems.<sup>75-78</sup> However, these systems require extensive heating and solvents in the preparation of the final network material – which can be undesirable in vitrimer network applications. In the CAN portion of this dissertation (Chapter III and Chapter IV), we aim to exploit the orthogonality of thiol-ene and thiol-isocyanate reactions to circumvent these drawbacks inherent to thiourethane network preparation.

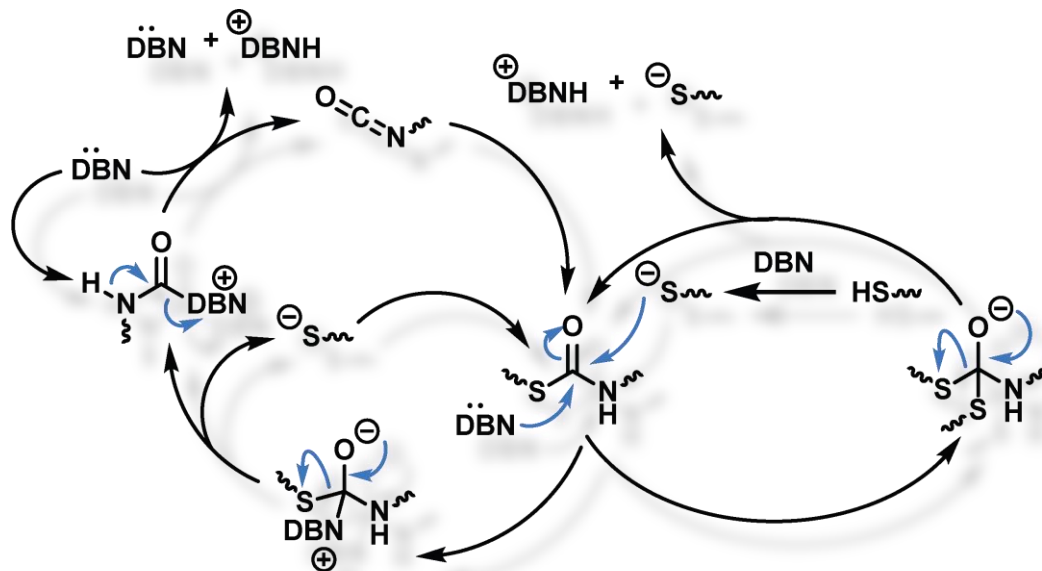


Figure 1.5 *Proposed synergistic dual dynamic behavior of the thiourethane moiety when using DBN as the exchange catalyst.*<sup>72</sup>

## 1.6 Thiol-ene Reactions as Route Towards Hydrolytically Labile Materials

A considerable amount of attention has been put into developing materials that rapidly degrade in the natural environment in an effort to combat the amount of plastic waste produced and discarded by the global population.<sup>84-85</sup> Polymers with hydrolytically labile linkages, such as esters,<sup>86-88</sup> anhydrides,<sup>89-91</sup> acetals,<sup>26, 92-94</sup> and ketals,<sup>25, 95-97</sup> along the polymer backbone have gained considerable interest within academic and industrial settings. These materials must adhere to stringent guidelines to be viable for their intended applications – i.e. shelf-life stability, performance lifetime, and end of use degradation. However, polymer degradation profiles are predominately limited by the nature of the labile chemistry employed in the polymeric design.

Polyketals – materials that exhibit tunable degradation profiles based on chemical architecture – have received considerable attention in medical applications,<sup>95, 98-99</sup> while remaining underutilized in broader applications. Polyketals have been shown to exhibit pH dependent degradation profiles which can be easily tuned based on the structure of the parent ketone.<sup>100</sup> Furthermore, ketals exhibit excellent stability under neutral and basic conditions while readily undergoing hydrolytic degradation under acidic conditions.<sup>101</sup> Upon hydrolysis, ketals are known to degrade into charge neutral byproducts *via* a well-established mechanism in which the formation of carbenium ion intermediate is the rate determining step (**Figure 1.6**).<sup>100-102</sup>

Thiol-ene photopolymerizations have been highly utilized in network formation and post-polymerization modification but have received minimal attention in the realm of thermoplastic synthesis. While the first report of using thiol-ene polymerizations as a route to linear thermoplastics was first published in 1948 by Marvel and Chambers,<sup>103</sup> it

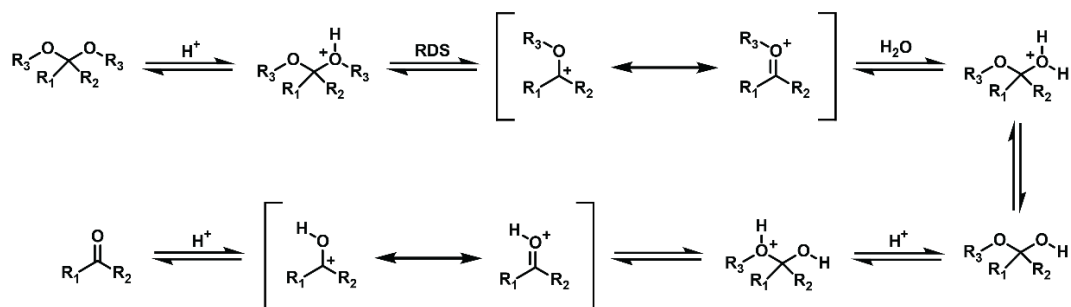


Figure 1.6 *Mechanism of ketal hydrolysis.*

has only recently received a growing interest in the development of thermoplastic polymers with a wide variety of architectures for multiple different uses.<sup>104-109</sup> Recently, Lillie and coworkers showed that thiol-ene photopolymerizations could be used as a route to incorporate glucarodilactone (GDL), a chemical analogue to isosorbide, into linear polymers.<sup>110</sup> By incorporating GDL into the polymer backbones, they were able to achieve materials that exhibited hydrolytic degradability as well as industrially relevant mechanical characteristics. As such, this polymerization route has been shown to be a promising route towards the development of hydrolytically labile materials.

A recent report from our group by Alameda et al. showed that a series of novel bisalkene diketone monomers could be utilized in thiol-ene photopolymerizations to develop homogenous hydrolytically labile networks.<sup>25</sup> They were able to show that the hydrolytic stability of the resulting materials was dependant on the stability of the ketal moiety, as it pertains to the parent ketone electronic and conformational characteristics.<sup>25</sup> We sought to build upon these findings, and develop linear thermoplastic polymers using the wide variety of commercially available dithiol monomers. Herein, we have developed a library of hydrolytically labile poly(thioether ketal) thermoplastics *via* thiol-ene photopolymerization which readily undergo hydrolysis into small-molecule

byproducts. We aim to show that these polymers represent a new class of degradable materials that could offer alternative methods for molecular design in the realm of environmentally degradable materials.

## CHAPTER II – Materials and Methods

### 2.1 Materials

All materials were used as received unless otherwise specified. 2,2'-(ethylenedioxy)diethanethiol (EDDT), 1,5-diazobicyclo[4.3.0]non-5-ene (DBN), 4,4'-methylenebis(cyclohexyl isocyanate) (H<sub>12</sub>MDI), triallyl triazine (TTT), 1-hexanethiol, p-toluenesulfonic acid (p-TsOH), and benzene were purchased from Sigma-Aldrich. Hexamethylene diisocyanate (HDI) and isophorone diisocyanate (IPDI) were purchased from Perstorp. Darocur 1173 was purchased from Ciba. Hexyl isocyanate was purchased from Fluka Chemical. 1,4-cyclohexanedione was purchased from Acros. 4,4'-bicyclohexanone, 3-allyloxy-1,2-propanediol, and dithioerythritol (DTT) were purchased from TCI Chemical. Propyleneglycol 3-mercaptopropionate 2200 (PPGMP 2200) was purchased from Bruno Bock.

### 2.2 Material Preparation and Synthesis

#### 2.2.1 Ternary Thiol-ene/Thiourethane CANs – Altering Diisocyanate Monomer Structure

Selected isocyanate monomers (HDI, IPDI, or H<sub>12</sub>MDI) (15.36 mmol), TTT (2.2 mL; 10.24 mmol), and Darocur 1173 (5 wt% of formulation) were first mixed in a vial equipped with a stir bar and allowed to stir until homogenous. EDDT (5 mL; 30.72 mmol) was then added to the mixture at 80 °C with stirring. DBN (0.5 wt% of formulation) was subsequently added to the reaction mixture at 80 °C and allowed to stir for 30 minutes, resulting in a viscous oligomeric resin. The reaction mixture was then sandwiched between two glass slides separated by 1mm Teflon spacers and irradiated with UV light using an Omnicure S-1000B light source (100 W mercury lamp,  $\lambda_{\text{max}} = 365$

nm, 320 – 500 nm filter) with a light guide at 100 mW/cm<sup>2</sup> for 10 min. The light source was calibrated using an International Light Model 1400A calibration radiometer. The resulting polymer films were then cut into strips for subsequent dynamic mechanical analysis. Additionally, dog bone tensile specimens were also prepared in the same manner using a silicon mold with both a thickness and width of 3.5mm.

### **2.2.2 Ternary Thiol-ene/Thiourethane CANs – Altering Reactive Functionality**

HDI (15.36 mmol), TTT (10.24 mmol), and Darocur 1173 (5 wt% of formulation) were first mixed in a scint vial equipped with a stir bar and allowed to stir until homogenous. EDDT was then added in various amounts to the mixture at 80°C with stirring. The amount of EDDT added varied based on the equation:

$$N_{NCO} + N_{ENE} = N_{SH} * X_{SH}$$

where  $N_{NCO}$  is the number of isocyanate functional groups,  $N_{ENE}$  is the number of alkene functional groups,  $N_{SH}$  is the number of thiol functional groups, and  $X_{SH}$  is the percentage of thiol functional group input into the system. Being that  $N_{NCO}$  and  $N_{ENE}$  are equivalent, five different formulations were developed: two systems in thiol excess (+5% and +10% -SH), one system being functionally equivalent, and two systems in thiol deficiency (-5% and -10% -SH). The resulting formulations were then photocured in accordance with that previously stated in section 2.2.1.

### **2.2.3 Synthesis of Thiourethane Small Molecule**

Functionally equivalent small molecule thiourethane systems were developed by first mixing hexyl isocyanate (3.52 mmol) with hexanethiol (3.52 mmol) in a scint vial. DBN (0.05 mmol) was then added to the mixture and allowed to stir for 10 minutes to catalyze the reaction. The system was then studied without any additional purification.

Additional systems were formulated using 10% excess hexane thiol and either 2x's or 5x's the original DBN content (**Table B.2**).

#### **2.2.4 Synthesis of Bisalkene Diketal Monomers**

Synthesis of bisalkene diketal monomers were conducted in accordance to procedures previously conducted by Alameda et al.<sup>25</sup>. Approximately 10 g (1 equivalent) of the appropriate ketone (monomer **3** – 1,4-cyclohexanedione; monomer **5** – 4,4'-bicyclohexanedione), 3-allyloxy-1,2-propanediol (4 equivalents), and 0.1 mol% of p-TsOH were solubilized in 50mL of benzene and refluxed at 115°C for 4hrs using a Dean-Stark apparatus. The reaction mixture was then washed with saturated NaHCO<sub>3</sub>, DI water, and brine. The organic layer was then dried over MgSO<sub>4</sub> and rotary evaporated to yield the crude product. The crude product was then dissolved in a minimal amount of dichloromethane and purified *via* flash chromatography using hexanes with 5% trimethylamine and acetone as the eluent. The collected fraction was then subject to rotary evaporation and left under vacuum overnight to yield the product as a clear viscous oil (yield ≈ 65%).

#### **2.2.5 Synthesis of Poly(thioether ketals) using DTT and EDDT Monomers**

Equimolar amounts of either monomers **3** or **5** (7 mmol) and either dithiol monomers **6** or **7** (7 mmol) were solubilized in THF (4.5 mL) in a scent vial. Darocur 1173 (5 mol%) was added and allowed to solubilize. The reaction mixture was then subject to UV irradiation for 30 min using a Reyonet Photochemical Reactor, and then allowed to cool. The solution was then precipitated into diethyl ether and centrifuged to obtain the polymer. The polymer was purified by resolubilizing in THF, precipitation

into diethyl ether, and centrifuging to reobtain the polymer (3x's). The resulting polymers were dried in a vacuum oven overnight at 50 °C (yield  $\approx$  70%).

### **2.2.6 Synthesis of Poly(thioether ketals) using PPGMP 2200 as the Dithiol Monomer**

Equimolar amounts of either monomers **3** or **5** (3 mmol), dithiol monomer **8** (3 mmol), and Darocur 1173 (5 mol%) were mixed in bulk and was subject to UV irradiation for 30 min. The mixture was then solubilized in THF, precipitated into hexanes, and centrifuged to obtain the polymer. The polymer was purified by resolubilizing in THF, precipitation into hexanes, and centrifuging to reobtain the polymer (3x's). The resulting polymers were dried in a vacuum oven overnight at 50°C (yield  $\approx$  50%).

## **2.3 Covalent Adaptable Network Material Characterizations**

### **2.3.1 Real Time and Variable Temperature FTIR**

FTIR kinetic data was collected using a Nicolet 8700 spectrophotometer with a KBr beam splitter and an MCT/A cryogenic detector under an inert nitrogen atmosphere. Samples were first analyzed before and after DBN addition to confirm consumption of the isocyanate moiety for all formulations as indicated by the disappearance of the -NCO peak at 2258  $\text{cm}^{-1}$ . Photocuring reaction kinetics were collected at a resolution of 2  $\text{cm}^{-1}$  at 1.34s intervals. Samples were irradiated at an intensity 100  $\text{mW}/\text{cm}^2$  using an Omnicure S1000B light source (100 W mercury lamp,  $\lambda_{max} = 365 \text{ nm}$ , 320-500 nm filter) under an inert nitrogen atmosphere. Thiol conversion was monitored by the change in peak area of the S-H stretch at 2550  $\text{cm}^{-1}$ . Variable temperature FTIR (VT-FTIR) used the same instrumentation with the addition of a heating stage. Films were

cured on NaCl windows and analyzed at temperature profiles ranging from 70°C to 120°C by monitoring the appearance of the -NCO peak at 2258 cm<sup>-1</sup>.

### 2.3.2 Gel Content Determination

To determine the gel content of polymer networks, samples from each formulation were cut into small pieces, swelled, and extracted in DCM for 24 hrs. The samples were then dried under vacuum at 50°C for 24hrs. The mass of the original ( $m_o$ ) and dried ( $m_1$ ) specimen were recorded, and the gel content (G(%)) of each formulation was calculated by:

$$G(\%) = \frac{m_1}{m_o} * 100\%$$

Each formulation was measured three times and the average of each was taken.

### 2.3.3 Thermogravimetric Analysis

Thermogravimetric analysis of all polymer formulations was conducted using a TGA Q500 analyzer (New Castle, DE, USA). Samples were heated from ambient to thermal degradation using a ramp rate of 10 °C/min.

### 2.3.4 Dynamic Mechanical Analysis

Dynamic mechanical analysis of all polymer formulations was conducted using a DMA Q800 analyzer from TA Instruments (New Castle, DE, USA). Samples were tested in tension at temperature profiles ranging from -60 °C to 120 °C with a heating rate of 3 °C/min. This process was further repeated for the reprocessed materials. The molecular weight between crosslinks was determined using:

$$M_c = \frac{3RTd}{E'_{Rubbery}}$$

where  $M_c$  is the molecular weight between crosslinks, R is the universal gas constant, T is the absolute temperature, d is the polymer density, and  $E'_{rubbery}$  is the storage modulus taken from the rubbery regime. The polymer density for each formulation was determined using the Archimedes' method.  $E'_{rubbery}$  was taken as  $T_g + 40^\circ\text{C}$ , with  $T_g$  being defined as the peak of the tan delta curve, to ensure that the values used were from the rubbery regime. Polymer crosslink density was determined using:

$$q = \frac{M_w}{M_c}$$

where q is the crosslink density and  $M_w$  is the molecular weight of the monomers.<sup>41, 111-</sup>

112

### 2.3.5 Stress Relaxation Analysis

Stress relaxation experiments were performed using a DMA Q800 analyzer from TA Instruments (New Castle, DE, USA) in tension. Sample specimens was first equilibrated at the predefined temperature profile, followed by the application of a constant strain of 5% allowing for the consequent stress level to be measured as a function of time. This process was repeated for each formulation, with one specimen being tested only once at a singular temperature (temperature profiles ranged from 80 °C – 120 °C at 10 °C increments).

The characteristic relaxation time ( $\tau^*$ ) of vitrimeric materials is defined as the time needed for the relaxation modulus to reach 37% (1/e) of its original value. By taking these values at varying temperature profiles, the obtained data was fitted to the Arrhenius relationship by:

$$\tau^*(T) = \tau_o e^{E_a/RT}$$

where  $\tau_o$  is the characteristic relaxation time at infinite T,  $E_a$  is the activation energy of bond exchange reaction (kJ/mol), R is the universal gas constant (8.314 JK<sup>-1</sup>mol<sup>-1</sup>), and T is temperature (K). This can be rewritten as:

$$\ln \tau^* (T) = \ln \tau_o + \frac{E_a}{RT}$$

By plotting this equation, the activation energy of bond exchange can be obtained from the resulting slope. Furthermore, the topological freezing temperature ( $T_v$ ) can be determined by utilizing the Maxwell equation in conjunction with the rewritten Arrhenius relationship. The Maxwell equation is defined by:

$$\eta = \frac{1}{3} E' * \tau^*$$

where  $\eta$  is the liquid to solid transition viscosity (taken as 10<sup>12</sup> Pa\*s) and E' is the storage modulus taken from the rubbery regime at  $T_g + 40$  °C. These equations can then be combined to determine  $T_v$ .<sup>58, 72, 113-115</sup>

### **2.3.6 Non-isothermal Creep Analysis**

Non-isothermal creep experiments were conducted using a DMA Q800 analyzer from TA Instruments (New Castle, DE, USA). Samples were tested in tension utilizing a constant stress of 0.1 MPa and a heating rate of 3 °C/min to analyze the change in strain as a function of temperature. The onset value of rapid deformation as a function of creep is taken as  $T_v$ .

### **2.3.7 Creep/Recovery Analysis**

Creep/Recovery experiments were conducted using a DMA Q800 analyzer from TA Instruments (New Castle, DE, USA). Sample were tested in tension utilizing a constant stress of 0.01 MPa at 80 °C to measure the change in strain as a function of time.

### **2.3.8 Dynamic Scanning Calorimetry**

Dynamic Scanning Calorimetry experiments were conducted using a DSC Q100 analyzer from TA Instruments (New Castle, DE, USA). Samples were tested in an aluminum hermetic pan using a heat/cool/heat cycle ranging from -90 °C to 120 °C a rate of 5 °C/min.

### **2.3.9 Material Reprocessing**

Materials were reprocessed by cutting the resulting polymer systems into small pieces and melt pressing using an appropriate mold and melt press apparatus. The materials were pressed at 100 °C for 10 min using approximately 5 metric tons of force. Two different molds were used for reprocessing. A strip mold with dimensions of 50mm x 10mm x 2mm was used to make reprocessed DMA samples. A dog bone mold, with both a thickness and width of 3.5mm, was used to prepare reprocessed tensile specimens in Chapter III. The dog bone samples tested in Chapter IV (virgin and reprocessed) were cut using a type V dye punch in accordance with ASTM D638-14.

### **2.3.10 Tensile Testing**

Tensile testing was conducted on all samples throughout reprocessing using a Mechanical Testing System (MTS) Insight material testing machine equipped with either a 1kN (Chapter III) or 500N (Chapter IV) load cell. Samples were carefully centered in the clamps and deformed in tensile mode at a strain rate of 0.2 in/min until failure. Each formulation was tested in triplicate for each reprocess to ensure consistent and accurate measurements.

## **2.4 Poly(thioether ketal) Thermoplastic Material Characterization**

### **2.4.1 Nuclear Magnetic Resonance (NMR) Analysis**

Polymer structure was confirmed by  $^1\text{H}$ ,  $^{13}\text{C}$  NMR, COSY, and HSQC experiments using a Bruker Avance<sup>TM</sup> 600 MHz NMR Spectrometer in Deuterated Chloroform.

### **2.4.2 Size Exclusion Chromatography (SEC)**

Polymer molecular weights were obtained using a TOSOH EcoSEC HLC-8320 GPC equipped with TSKgel® SuperMultiPore HZ-M. The instrument was calibrated using a linear calibration against a polystyrene standard – PSTquick MP-M polystyrene standard. All experiments were conducted at 40°C.

### **2.4.3 Hydrolytic Stability Analysis**

Polymer films were cast from THF (100 mg/mL) in the bottom of scent vials. The films were then allowed to dry in a vacuum oven overnight at 50 °C to achieve films of approximately 50 mg. Films were then subject to hydrolytic stability testing in acidic, neutral, and basic aqueous conditions. The vials were filled with approximately 20 mL of degradation media and incubated in a 30 °C oven. At varying time intervals, samples were removed, washed with DI water, and freeze dried for 24hrs. Samples were then subject to SEC and gravimetric analysis to determine the extent of hydrolysis. The various degradation media were prepared from 1M HCl, pH 7.4 PBS buffer, and 1M NaOH to obtain the acidic, neutral, and basic conditions, respectively. In each case, degradation solutions were prepared with 10%, by volume, acetonitrile to assist in the solubilization of the degradation byproducts.

#### **2.4.4 Contact Angle Analysis**

Contact angle analysis was performed using a Rame-hart STD Goniometer and analyzed using DROPimage Advanced Software. All experiments were conducted with a 6 $\mu$ L droplet of DI water at ambient conditions.

## CHAPTER III - Ternary Thiol-Ene/Thiourethane Covalent Adaptable Networks: A Rapid and Versatile Route to Vitrimeric Materials

### 3.1 Objective

This chapter describes the development of a rapid and versatile approach to the formation of vitrimeric materials. Specifically, this work expands upon results previously described by McNair et al.<sup>123</sup> in which a generic “one-pot two-step” method was developed to form ternary thiol-ene/thiourethane networks. This approach was modified to achieve certain key objectives:

- 1) Alteration of the thiourethane formation catalyst and content so that the thiourethane DCC employed would render the resulting polymer networks reprocessible.
- 2) Strict utilization of only commercially available materials to limit the number of synthetic processes and experience necessary in the development of CANs.
- 3) Provide a rapid and versatile route to vitrimeric materials to act as a platform to aid in developing and understanding of key properties influencing vitrimeric behavior.

Herein, a series of ternary thiol-ene/thiourethane covalent adaptable networks with altered polymeric network architecture was developed through this modified “one-pot two-step” approach to provide an understanding of key structure-property relationships on the vitrimeric behavior of such materials. Additionally, this approach enables the study of virgin material properties – an area of study that is generally lacking in thiourethane vitrimeric literature due to the rapid reaction kinetics of the thiourethane

formation – ultimately allowing for comparison to reprocessed materials to provide key insights into material property retention.

### 3.2 Formation of Ternary Thiol-ene/Thiourethane Covalent Adaptable Networks

Ternary thiol-ene/thiourethane vitrimers were prepared via a “one-pot two-step” bulk method, as illustrated in **Figure 3.1A**. In the first step of the process, the thiourethane moiety was first formed by the DBN catalyzed reaction between the thiol and isocyanate functionalities. The stoichiometric ratio of thiol and isocyanate functional groups was 2:1 (SH: NCO) to drive complete consumption of the isocyanate moiety while maintaining a stoichiometric equivalence of unreacted thiol to alkene necessary for

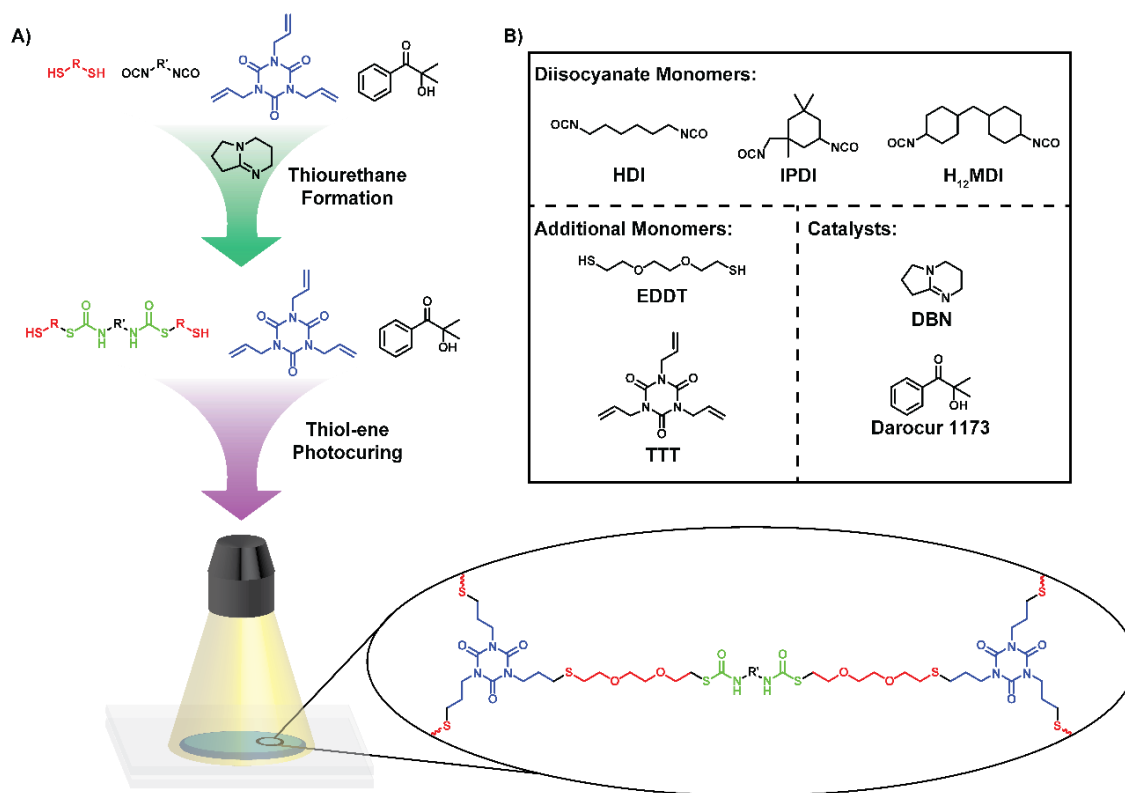


Figure 3.1 A) Reaction scheme of the “one-pot two-step” method to achieve ternary thiol-ene/thiourethane networks with B) illustrating the commercially available monomers utilized.

the second step of the “one-pot two-step” process. In the second step of the process, the resulting viscous mixture, formulated with 5 wt.% Darocur 1173 photoinitiator, was irradiated with UV light to produce a transparent solid thermoset. Three different thermosets were prepared varying only by the diisocyanate monomer used in the formulation – with **F1** containing HDI, **F2** using IPDI, and **F3** comprising H<sub>12</sub>MDI. The specific structures of all monomers are shown in **Figure 3.1B**. Each step of the “one-pot two-step” process was followed via FTIR analysis (**Figure 3.2A - 3.2B**). The consumption of the isocyanate moiety, as an indicator of the formation of the thiourethane moiety, was monitored by the disappearance of the -NCO peak at 2258 cm<sup>-1</sup> upon addition of the DBN catalyst to the reaction mixture. The complete disappearance of the -NCO peak was observed for all three formulations (**Figure. 3.2A, A.1, and A.3**) studied in this work. Furthermore, upon complete consumption of the isocyanate moiety, it was further determined that thiol functionality remained in the formulation as indicated by the peak at 2565 cm<sup>-1</sup> attributed to the -SH stretch. Following the formation of the thiourethane moiety, the kinetics of the photoinduced thiol-ene crosslinking reaction was monitored via real-time FTIR with focus placed on the -SH peak at 2565 cm<sup>-1</sup> (**Figure 3.2B, A.2, and A.4**). Rapid, near quantitative conversion of the thiol was observed for each formulation, as shown in the conversion vs. time plots in **Figure 3.2C**. The **F2** formulation exhibited the highest apparent viscosity upon formation of the thiourethane, which translates into slower photopolymerization kinetics and longer irradiation times necessary to achieve 95% thiol conversion (**Table 3.1**). To provide further validation of network formation, gel content studies were performed on the resulting thermoset. As

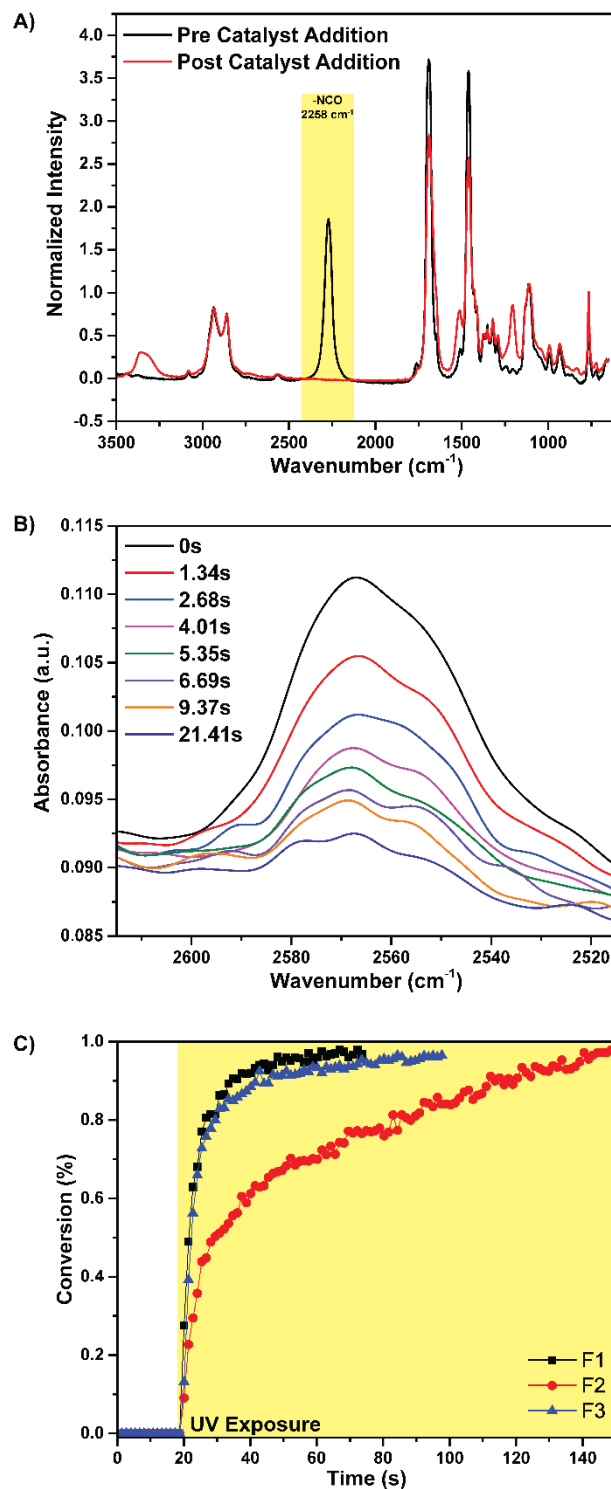


Figure 3.2 A) FTIR analysis of *F1* before and after the addition of DBN. B) Decrease in *F1* thiol peak absorbance as at various UV exposure times. C) Thiol conversion kinetics of *F1* – *F3* as a function of UV exposure time.

indicated in **Table 3.1**, the synthetic approach yielded thermosets with greater than 90% gel content.

### 3.3 Thermomechanical Characterization of the Ternary Thiol-ene/Thiourethane Networks

The thermomechanical properties of the resulting thermosets were investigated via dynamic mechanical analysis (DMA). Samples were subjected to a small oscillatory strain as a function of temperature to resolve the storage modulus ( $E'$ ), loss modulus ( $E''$ ) and  $\tan \delta$  ( $E''/E'$ ). **Figure 3.3** shows the  $\tan \delta$  and  $E'$  curves for the **F1**, **F2**, and **F3** networks. Relatively narrow  $\tan \delta$  distributions ( $< 23$  °C at FWHM, specific values summarized in **Table 3.2**) were observed for all thermosets – a typical characteristic of the step-growth thiol-ene polymerization process indicative of homogeneous polymer networks. Glass transition temperatures were determined from the peak maximum of the  $\tan \delta$  curves. As shown in **Figure 3.3**, the glass transition temperature for **F1**, **F2**, and **F3** was 0.37 °C, 48.3 °C, and 43.9 °C, respectively. The more rigid and compact framework of IPDI endowed **F2** with the highest  $T_g$ . DMA also showed glassy storage moduli in the range of 1000-2000 MPa and a rubbery plateau region for each thermoset that indicated rubbery moduli of between 4 - 6 MPa at approximately 80 °C.

Table 3.1 *Summary of conversion kinetics and gel content of cured ternary thiol-ene/thiourethane networks.*

Formulation	Time to 95% Conversion (s)	Gel Percent (%)
<b>F1</b>	29.5	93.1
<b>F2</b>	132.1	>99
<b>F3</b>	54.9	>99

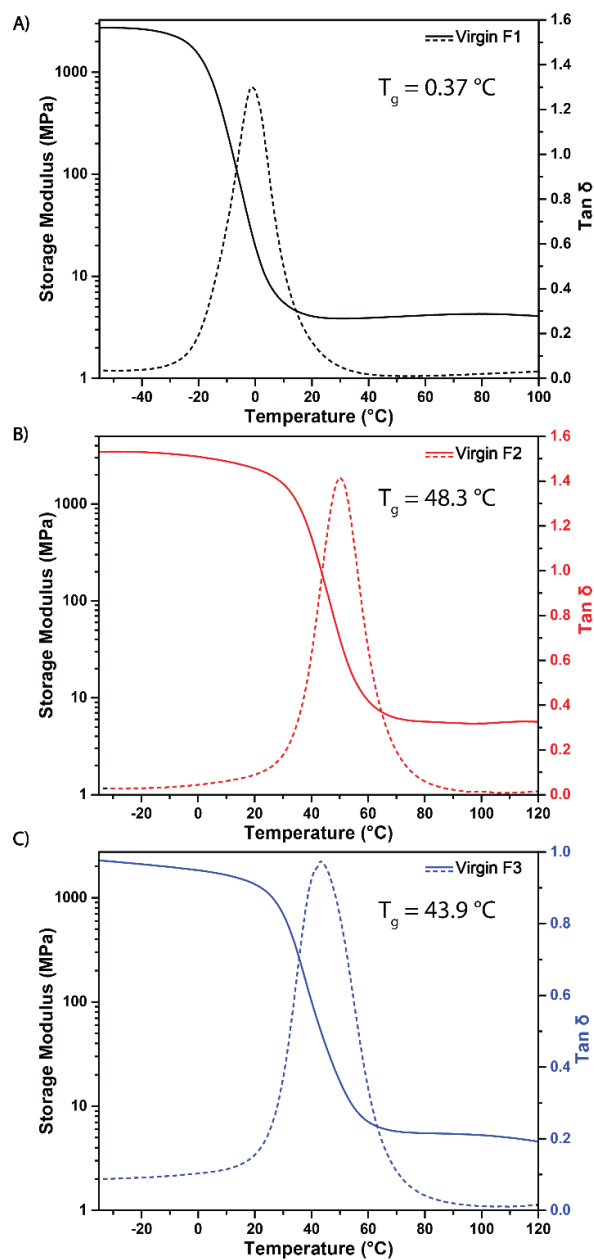


Figure 3.3 DMA thermograms of virgin A) **F1**, B) **F2**, and C) **F3**.

Table 3.2 Summary of virgin material thermal properties determined by DMA.

Formulation	Tan $\delta$ (°C)	FWHM <sup>a</sup> (°C)	Storage Modulus (MPa)	Crosslink Density
<b>F1</b>	-0.37	18.6	4.15	0.261
<b>F2</b>	48.3	18.9	5.61	0.337
<b>F3</b>	43.9	22.6	6.19	0.395

<sup>a</sup>Full width at half maximum of the Tan Delta peak used to describe network homogeneity. <sup>b</sup>Storage Modulus value taken from the rubbery regime at  $T_g+40^\circ\text{C}$ , with  $T_g$  being defined as the tan  $\delta$  peak.

### 3.4 Probing the Dynamic Thiourethane Behavior within Networks

Foundational work by Li and Torkelson<sup>73</sup> proposed an association/dissociation dual mechanism that governs the thiourethane bond exchange process. Building on the work by Li, Wen et al.<sup>72</sup> demonstrated the thiourethane moieties constructed from primary aliphatic isocyanates and aliphatic thiols are capable of undergoing both the associative and dissociative pathways depending on the nature of the exchange catalyst employed in the system. The catalysts 1,5-diazobicyclo[4.3.0]non-5-ene (DBN), as used in our system, promotes both associative and dissociative pathways since DBN exhibits both basic and nucleophilic characteristics. It is also plausible to assume that the structural characteristics of thiourethane (e.g., derived from primary or secondary isocyanates) would influence dynamic pathway. Initially, the dynamic nature of the thiourethane linkages within the **F1 – F3** networks was investigated using variable temperature Fourier transform infrared spectroscopy (VT-FTIR). Using literature precedent from urethane networks, an active dissociative mechanism is indicated by the appearance of the isocyanate peak in VT-FTIR experiments.<sup>116</sup> VT-FTIR experiments were carried out on thin films of the **F1 – F3** thiourethane thermosets at five temperature setpoints ranging from 80 °C to 120 °C. As shown in **Figure 3.4A**, the **F1** network comprised of primary aliphatic thiourethane linkages showed minimal changes in intensity at 2258 cm<sup>-1</sup>, the position expected for a free NCO functional group, as a function of temperature. This result would seem to indicate that the dissociative mechanism is minimally active within the polymer network at 0.5wt% DBN catalyst loading; however, it is noteworthy that we and others<sup>72</sup> observe the dissociation of the primary aliphatic thiourethane in small molecule analogs. In contrast, the VT-FTIR for

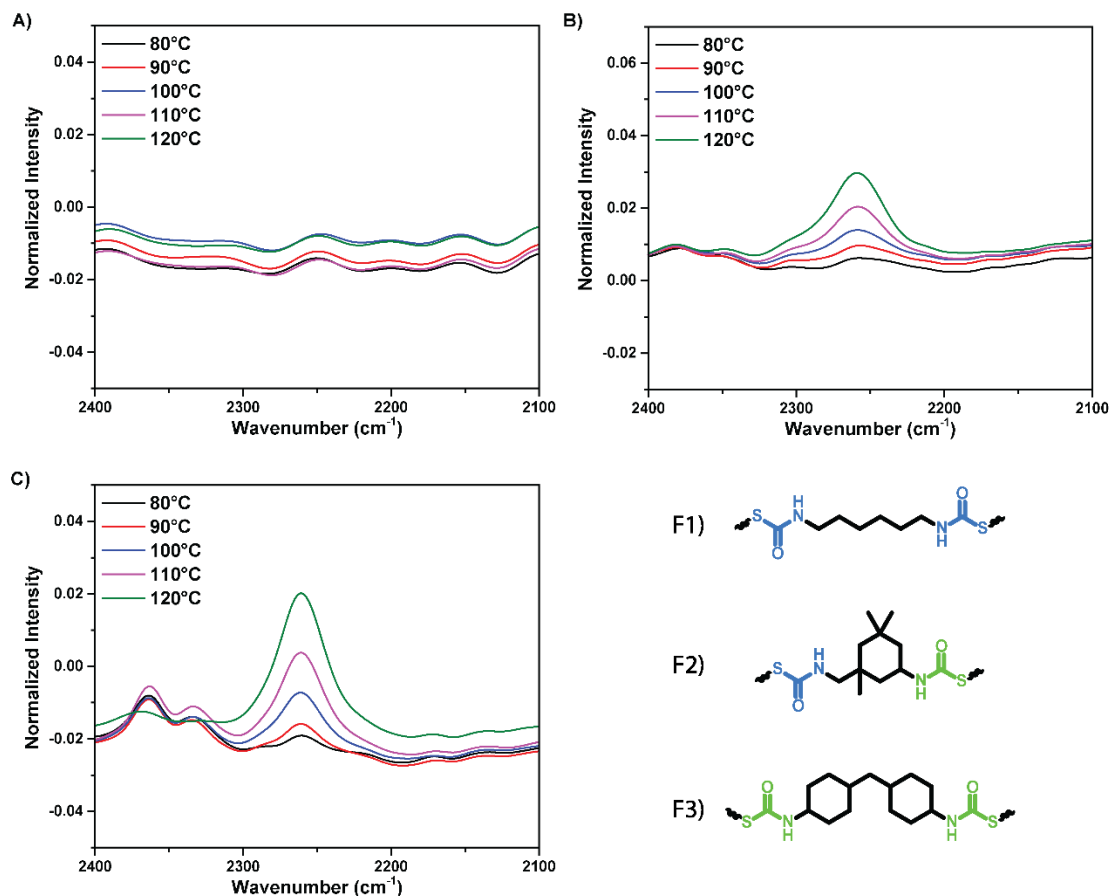


Figure 3.4 VT-FTIR of **F1** – **F3** (A – C, respectively) at varying temperature profiles. Additionally, the structures of **F1** – **F3** are depicted to show the primary (blue) and secondary (green) thiourethane moieties.

**F2** (Figure 3.4B, derived from IPDI containing one primary and one secondary isocyanate) and **F3** (Figure 3.4C, derived from H<sub>12</sub>MDI with two secondary isocyanates) polymer networks show clear evidence of the dissociative pathway as indicated by the appearance and growth of the NCO peak at 2258 cm<sup>-1</sup> with increasing temperature. While these experiments alone preclude the ability to comment on or identify a dominant dynamic pathway (e.g., dissociative vs. associative), the propensity of the secondary thiourethane linkage to undergo dissociation is clearly influenced by the structure and substitution of the isocyanate. The current observations are consistent with the reported

behavior of hindered ureas, which more readily undergo dissociation as the bulkiness of the urea substituents increases – a process driven by steric hindrance disruption of the conjugation of the  $\pi$ -electrons on the nitrogen atoms and carbonyl p-orbitals.<sup>117-120</sup>

The dynamic nature of the thiourethane linkages within the **F1-F3** polymer networks was investigated through a series of thermal stress relaxation experiments, with keen interest in understanding how the diisocyanate architecture influences the thiourethane bond exchange, and ultimately, the vitrimeric properties of the thermosets. **Figure 3.5** shows the stress relaxation behaviors at different temperatures (80 °C – 120 °C) for the stoichiometrically balanced polymer networks. As expected, the rate of stress relaxation significantly increases with increasing temperature for each formulation. From these stress relaxation curves, the corresponding characteristic relaxation times ( $\tau^*$ ) were determined as the time at which the material reached 1/e of the initial stress, indicated by the horizontal dotted lines in **Figure 3.5A-C**. An Arrhenius relationship (**Figure 3.5D**) was observed when plotting  $\ln \tau$  as a function of  $1000/T$  ( $K^{-1}$ ), from which we estimated the activation energy ( $E_a$ ) for **F1**, **F2**, and **F3** as 56.7 kJ/mol, 90.7 kJ/mol, and 105.8 kJ/mol, respectively (**Table 3.3**). These  $E_a$  values are in good agreement with previously reported thiourethane-based polymer networks; however, direct comparisons are precluded due to different thiol structures, catalysts, and catalyst loading.<sup>29, 72, 76-77</sup> It can be noted that the  $E_a$  values generally increase as the steric hindrance around the thiourethane linkage increases, where the **F3** network derived from H<sub>12</sub>MDI with two secondary isocyanates exhibits the highest energy of activation. Fitting these materials to a Maxwell element and assuming a Poisson's ratio of 0.5, we extrapolated the viscosity as a function of temperature ( $\eta = G'(\tau)$ ) and calculated the theoretical topology freezing

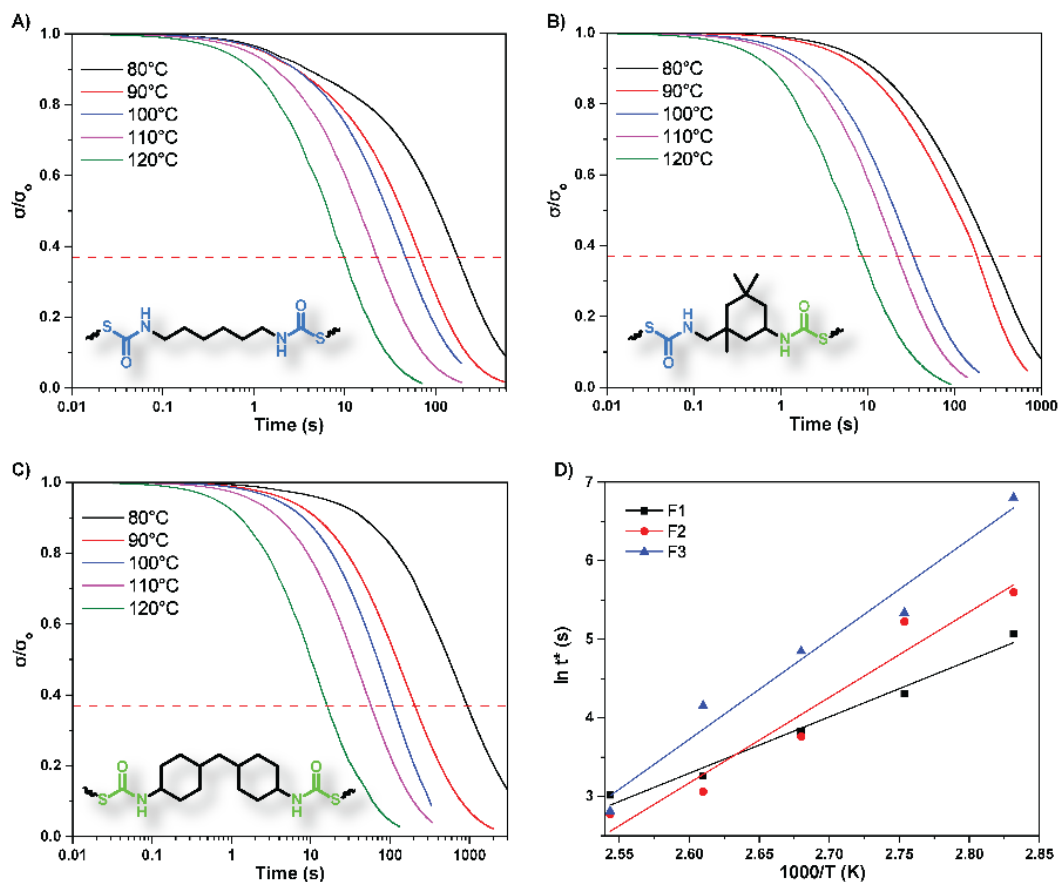


Figure 3.5 *Stress relaxation experiments of A) F1, B) F2, and C) F3 with their respective primary (blue) and secondary (green) thiourethane structures as dictated by the parent diisocyanate monomer selection. D) Results from stress relaxation experiments plotted in terms of the Arrhenius relationship.*

temperature ( $T_v$ ). Extrapolation of the calculated viscosities provided  $T_v$  values of -24.4 °C, 10.8 °C, and 57.4 °C, respectively, for networks **F1**, **F2**, and **F3**. While convenient for purposes of comparison across these three systems, the  $T_v$  values provided by the Maxwell fit of stress relaxation experiments offer minimal practical utility with regard to reprocessability. This approach does fails to accurately capture relaxation modes (e.g., Rouse and reptation) that typically occur over broad ranges of temperature and timescales. Additionally, since the vitrification temperature is extracted via extrapolation, the method likely ignores chemical and physical changes that may occur within the

Table 3.3 Summary of vitrimeric topological freezing temperature and relaxation behaviors.

Formulation	$E_a$ (kJ/mol)	$R^2$	$T_v^a$ (°C)	$T_v^b$ (°C)	$T_g^c$ (°C)
<b>F1</b>	56.7	0.9812	-24.4	61.9	0.37
<b>F2</b>	90.5	0.9495	10.8	68.8	48.3
<b>F3</b>	105.8	0.9682	57.4	77.5	43.9

$T_v^a$  determined by the Arrhenius equation in conjunction with the Maxwell equation.  $T_v^b$  determined by means of nonisothermal creep experiments.  $T_g^c$  determined by DMA.

extrapolated region. By this approach, the **F1** and **F2** networks would be considered  $T_g$ -limited networks, where  $T_v < T_g$ , while the **F3** network would be considered  $T_v$ -limited, where  $T_v > T_g$ . Although Nishimura and coworkers<sup>121</sup> report the classic WLF-to-Arrhenius transition just beyond  $T_g$  in lightly crosslinked polystyrene, significantly higher temperatures are often needed to reprocess  $T_g$ -limited dynamic thermosets. This suggests that direct  $T_g$  and  $T_v$  values are not immediately adequate for determining ideal material reprocessing conditions. As postulated by Dugas et al., the large discrepancy in these values of merit may be the result of the number of exchanges that must occur simultaneously to induce flow in highly crosslinked thermosets. Thus, a recent impetus in the area of vitrimers has focused on identifying of methods to quantify thermally induced dynamic exchanges that provide relevant information for reprocessing.<sup>122</sup>

Recently, non-isothermal creep analysis was employed by Serra and coworker for the analysis of poly(thiourethane) vitrimers.<sup>76-77</sup> In this approach,  $T_v$  is reported as the temperature at which the material deviates from a linear strain response (**Figure 3.6**). The transition values obtained from the non-isothermal creep experiments for the **F1**, **F2**, and **F3** thermosets were 61.9 °C, 68.8 °C, and 77.5 °C, respectively (**Table 3.3**). The general trend in  $T_v$  established previously for these materials by means of the Arrhenius relationship agree with the non-isothermal creep values, but the absolute values from the

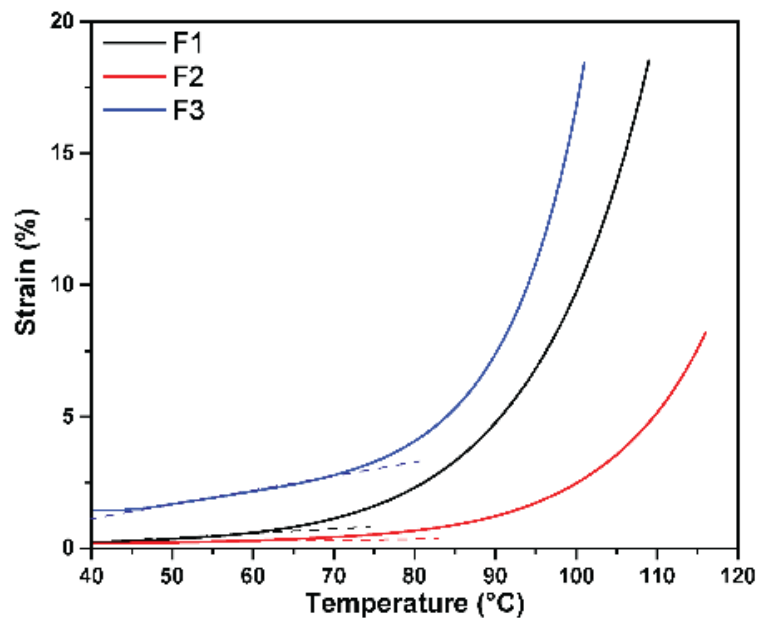


Figure 3.6 Nonisothermal creep results obtained for **F1**, **F2**, and **F3**.

creep experiments are more relevant to guide reprocessing conditions discussed in the next section. We postulate that the trend in increasing  $T_v$  values from **F1** to **F3**, established by both methods of  $T_v$  determination, is due to the structural conformation imparted from the parent diisocyanate monomer. For instance, **F1** is formed using HDI where both isocyanate moieties are primary, resulting in two primary thiourethane functionalities per parent diisocyanate within the final polymeric product. In contrast, **F2** and **F3** are formed using diisocyanate monomers with either one primary and one secondary isocyanate or two secondary isocyanates, respectively, resulting in primary and secondary thiurethanes as dictated by the parent diisocyanate monomer structure. We expect that these structural differences dictate the degree of steric interaction on thiourethane functionality, ultimately affecting the exchange behavior of these materials.

### 3.5 Material Reprocessing and Physical Property Retention

Reprocessability of covalent adaptable or vitrimeric materials is a distinguishing factor from traditional thermosetting polymers and is the predominant reason for significant interest in the field. To be industrially relevant, vitrimers should be able to retain key mechanical properties as a function of multiple reprocessing cycles. To investigate the reprocessability, **F1 – F3** were cured as tensile bars, cut into pieces, and reprocessed into tensile bar molds at 100 °C for 10 min using approximately 5 metric tons of force, as illustrated in **Figure 3.7**. Thermomechanical and mechanical properties were determined via DMA and tensile testing for each of the materials as a function of two reprocessing cycles. The storage modulus and  $\tan \delta$  curves for the **F1-F3** materials are shown in **Figure 3.8A-C**, while the stress-strain curves are shown in **Figure 3.8D – 3.8F**, **Table 3.4**). The summary of specific mechanical and thermomechanical properties is provided in **Table 3.4** and **Table 3.5**. Interestingly, **F1** exhibited the best performance in retention of properties after reprocessing. After the second reprocessing cycle, the

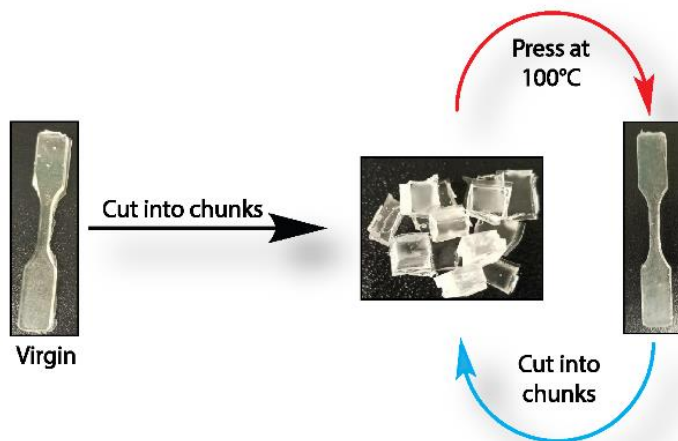


Figure 3.7 *Basic process by which materials (F1 being shown) were reprocessed.*

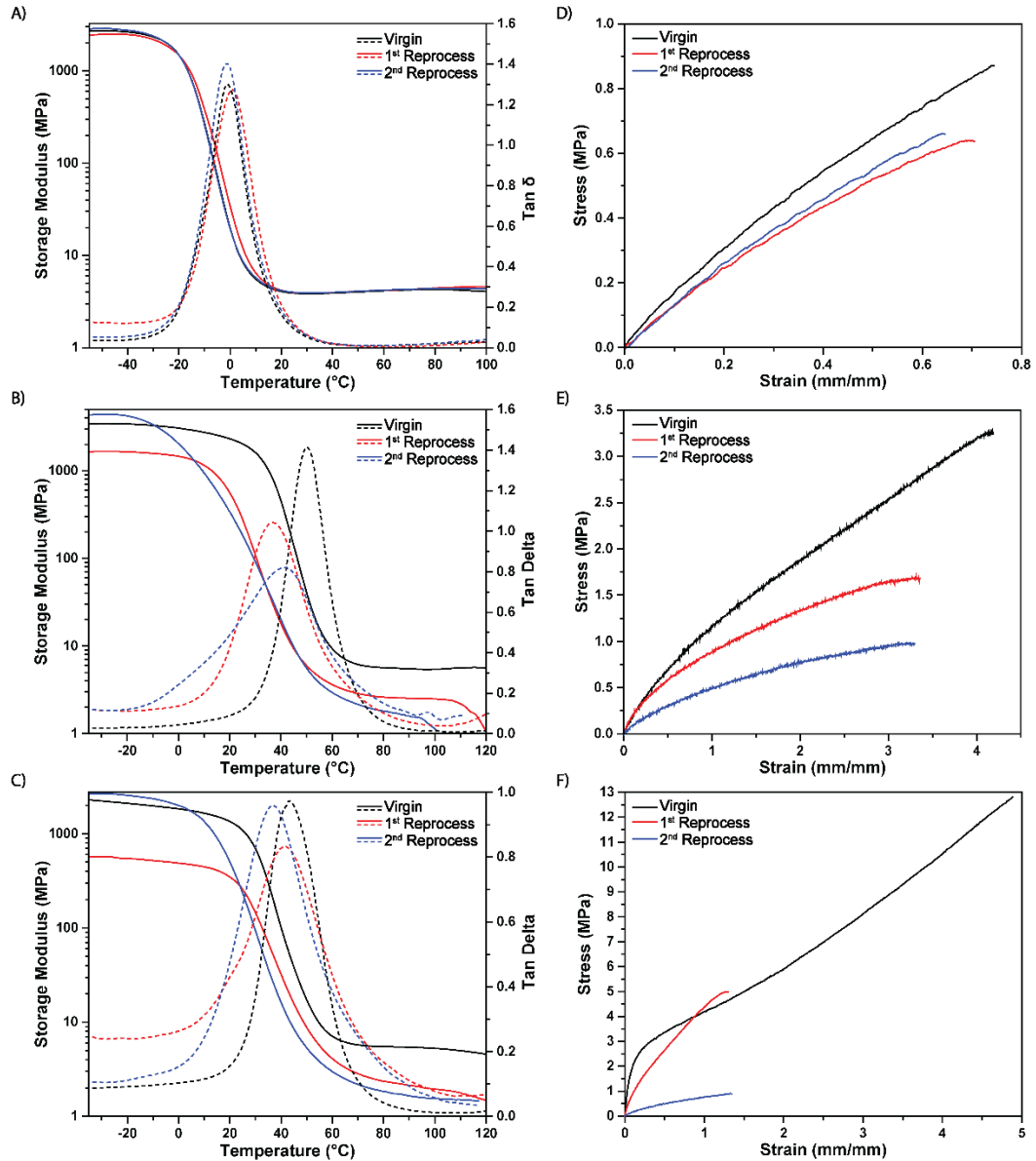


Figure 3.8 *Thermomechanical (A-C; determined via DMA) and mechanical properties (D-F; determined via tensile testing) of F1 – F3 throughout two material reprocessing cycles.*

Young's modulus for **F1** decreased from 1.74 MPa to 1.22 MPa, retaining 75% of the original value. Similarly, the **F1** network retained 90% of the original crosslink density with minimal shifts in the  $T_g$ . In contrast, **F2** and **F3** exhibited poor retention of Young's modulus after multiple reprocessing cycles, respectively retaining only 21% and 20% of

Table 3.4 Summary of key mechanical properties of **F1** – **F3** throughout reprocessing.

Formulation	Reprocessing Cycle	Young's Modulus (MPa)	Strain at Break (%)
<b>F1</b>	Virgin	1.74	63.98
	1 <sup>st</sup> Reprocess	1.22	56.70
	2 <sup>nd</sup> Reprocess	1.30	59.78
<b>F2</b>	Virgin	3.78	472.36
	1 <sup>st</sup> Reprocess	1.48	332.47
	2 <sup>nd</sup> Reprocess	0.81	312.45
<b>F3</b>	Virgin	5.57	550.52
	1 <sup>st</sup> Reprocess	4.53	144.08
	2 <sup>nd</sup> Reprocess	1.09	158.97

Table 3.5 Summary of thermomechanical (properties determined by DMA) of **F1** – **F3** throughout reprocessing.

Formulation	Reprocessing Cycle	Tan $\delta$ (°C)	FWHM <sup>a</sup> (°C)	Storage Modulus (MPa)	Crosslink Density
<b>F1</b>	Virgin	-0.37	18.55	4.15	0.261
	1 <sup>st</sup> Reprocess	1.01	19.39	3.54	0.221
	2 <sup>nd</sup> Reprocess	-2.08	18.46	3.72	0.235
<b>F2</b>	Virgin	48.27	18.95	5.61	0.337
	1 <sup>st</sup> Reprocess	40.53	31.51	2.37	0.148
	2 <sup>nd</sup> Reprocess	41.15	34.12	1.92	0.117
<b>F3</b>	Virgin	43.92	22.64	6.19	0.395
	1 <sup>st</sup> Reprocess	43.31	46.08	2.29	0.152
	2 <sup>nd</sup> Reprocess	35.89	36.43	2.04	0.134

<sup>a</sup>Full width at half maximum of the tan  $\delta$  peak used to describe network homogeneity. <sup>b</sup>Storage Modulus value taken from the rubbery regime at  $T_g+40^\circ\text{C}$ , with  $T_g$  being defined as the Tan Delta peak.

their original modulus values. Furthermore, the **F2** and **F3** networks exhibited more than 65% decrease in crosslink density following multiple reprocessing cycles. As previously described and supported by VT-FTIR, the **F2** and **F3** networks undergo some degree of thiourethane dissociation, driven by the increased steric hinderance of the secondary thiourethane, upon exposure to elevated temperature. When reprocessing these materials, the dissociation of the thiourethane likely plays an important role in possible side reactions. Upon dissociation, highly reactive free isocyanate groups are produced at the reprocessing temperature. Since the reprocessing methodology was carried out under ambient atmosphere in the laboratory, the free isocyanate groups are exposed to a combination of elevated temperatures and humidity, which can lead to unsought side reactions and, consequently, loss of properties. Likewise, thiols are known to undergo

some oxidation at elevated temperatures in ambient atmosphere – process that would decrease the number of thiols available for reaction with isocyanates, resulting in a loss of crosslink density in the reprocessed samples. Similar observations were reported by Li and coworkers<sup>73</sup> in thiourethane materials comprised from aromatic isocyanates, which tend to also undergo dissociation under reprocessing conditions, particularly when formulated with stoichiometric ratios of thiol.

### **3.6 Concluding Remarks**

Vitrimers represent an interesting class of materials showing potential in bridging the gap between the highly sought-after properties of both thermosetting and thermoplastic materials. As such, multiple different DCCs have been investigated as potential candidates for use in CANs. Herein, our attention focused on the dynamic thiourethane moiety, which has recently gained considerable attention as a platform for vitrimers. We expanded upon a “one-pot two-step” process, previously described by McNair and coworkers.<sup>123</sup> This approach utilizes the high degree of selectivity of thiol-X “click” reactions as well as their inherent rapid reaction kinetics. Furthermore, our approach utilizes all commercially available sources – an advantage not observed by many other approaches to vitrimeric materials. It was determined that the molecular structure of the parent diisocyanate monomer has a crucial impact on the vitrimer exchange behavior and kinetics. In particular, the steric strain imparted on the secondary thiourethanes of **F2** and **F3** force these formulations to exhibit dissociative exchange behavior – similar to hindered urea vitrimers. This dissociative behavior complicates mechanical property retention for these vitrimers due to a reduction in crosslink density. Nevertheless, we have shown that our “one-pot two-step” process rapid approach to

producing vitrimeric materials. The simplicity and commercial viability of our approach should provide a platform for further investigation into various physical properties of vitrimeric materials that are not yet fully understood.

## CHAPTER IV – Understanding the Effects of Altering Functional Stoichiometry on the Vitrimeric Behavior of Ternary Thiol-ene/Thiourethane Covalent Adaptable Networks

### 4.1 Objective

A primary advantage associated with the “one-pot two-step” approach to fabricate ternary thiol-ene/thiourethane covalent adaptable networks is that the order of monomer addition can be used to control the reactive functional equivalents with minimal changes to network formation behavior. This approach enables the design and development of ternary thiol-ene/thiourethane CANs with free reactive groups (e.g., thiols or alkenes). In knowing that the thiourethane moiety undergoes both the associative and dissociative pathways synergistically when DBN is used as the dynamic exchange catalyst, we hypothesize that altering the free thiol content within the networks will force the dynamic exchange pathway to favor one exchange mechanism versus the other – i.e., strongly associative in presence of excess thiol and strongly dissociative when the thiol concentration is deficient. The work presented herein is predicated on two main objectives:

- 1) Determine the effect that altering thiol content has on the dynamic behavior of the ternary thiol-ene/thiourethane networks using **F1** (derived from HDMI) as the model system.
- 2) Determine the effects that altering thiol content will have on the material properties and property retention of **F1** throughout reprocessing.

The results obtained herein provide valuable insights into the factors affecting the synergistic dynamic mechanism of the thiourethane moiety when DBN is used as the exchange catalyst.

## 4.2 Effects of Altering Thiol Content on the Dynamic Behavior of Ternary Thiol-ene/Thiourethane CANs

A series of four new ternary thiol-ene/thiourethane CANs was developed using the same monomers as **F1**, differing by dithiol monomer feed. The networks were formulated so that two systems had an excess of final free thiol (+10% and +5% functional excess thiol input) and two systems were formulated with thiol deficiency (-10% and -5% functional deficient thiol input) to be compared to the stoichiometrically equivalent **F1** system. The effects of altered thiol content of these networks on their dynamic behavior were then investigated via a series of thermomechanical analysis. We initially hypothesized that increasing free thiol content would promote the associative exchange mechanism relative to the dissociative reversible mechanism. Promoting the associative exchange mechanism should be manifested in the observation of decreased relaxation times ( $\tau^*$ ) and lower calculated  $E_a$  values. The stress relaxation analysis for the +5% and +10% systems, as shown in **Figure 4.1**, corroborates this hypothesis when fitted to the Arrhenius equation (**Figure 4.2, Table 4.1**). The larger increase in free thiol

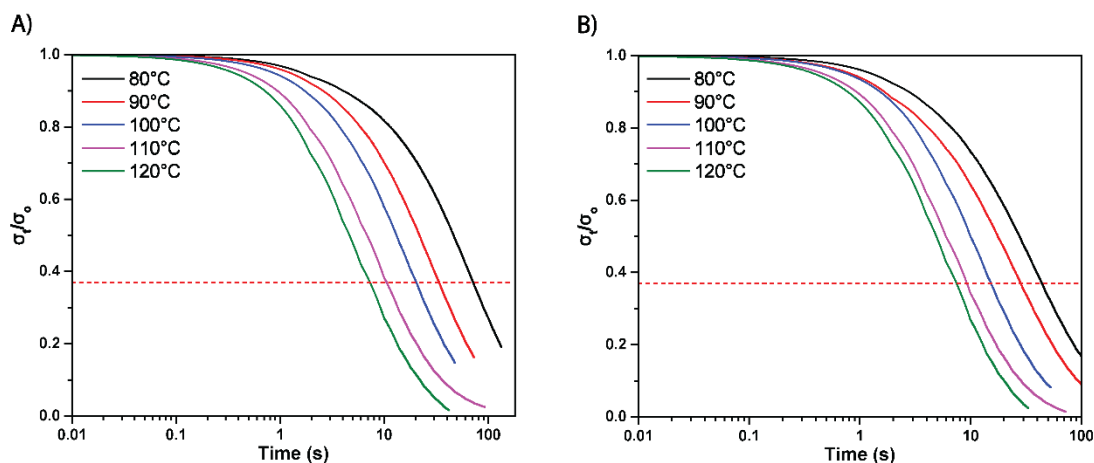


Figure 4.1 Stress relaxation analysis of the A) +5% and B) +10% systems.

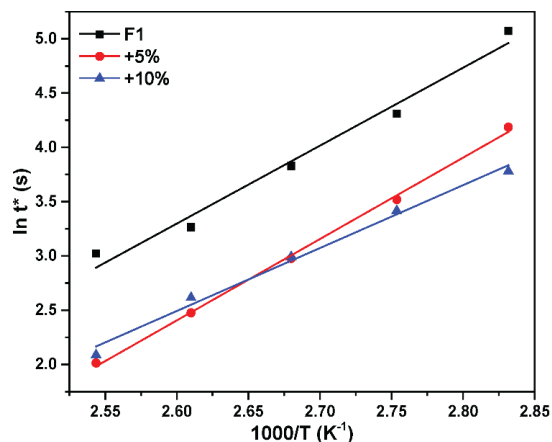


Figure 4.2 Stress relaxation of results plotted in terms of the Arrhenius relationship.

Table 4.1 Vitrimeric thermal relaxation behavior of the **F1**, **+5%**, and **+10%** systems.

Sample	$E_a$ (kJ/mol)	$r^2$	$T_v$ (°C)
<b>F1</b>	59.7	0.982	-24.4
<b>+5%</b>	62.3	0.998	-28.2
<b>+10%</b>	48.2	0.991	-55.5

content of the **+10%** system resulted in a decreased  $E_a$  and  $T_v$  (48.2 kJ/mol and -55.5°C, respectively) relative to the functionally equivalent **F1** system (59.7 kJ/mol and -24.4°C, respectively). Based on the results obtained the **+10%** system, it is reasonable to postulate that increasing the free thiol content shifts the equilibrium of dynamic exchange to favor the associative mechanism. However, the interpretation of the **+5%** system is more complicated. The **+5%** system exhibits a slightly increased  $E_a$  relative to **F1**, increasing from 59.7kJ/mol for **F1** to 62.3 kJ/mol for the **+5%** system. DBN has previously been shown to promote both the associative and dissociative exchange pathways synergistically resulting in elevated catalytic activity.<sup>72</sup> Adding this mechanistic understanding to the previously described hypothesis, we postulate that a critical free thiol content must be achieved to overcome the synergistic catalytic activity – reducing the level of dissociation ultimately resulting in higher degrees of maintained

crosslink density when exposed to elevated temperatures. This retention in crosslink density decreases chain mobility leading to a slight increase in  $E_a$  of the +5% system relative to **F1**. Interestingly, the  $\tau^*$  values of both the +5% and +10% systems were found to be dramatically lower than that of the **F1** system (**Table B.1**). This is attributed to the increased free thiol content within these systems. Although not immediately obvious, this provides further insight into the behavior of the +5% system. Ultimately, the reduction in  $\tau^*$  values result in a decreased  $T_v$  value of the +5% (-28.2°C) system relative to **F1** (-24.4°C). These results suggest that while the +5% system exhibits a slightly increased  $E_a$  relative to **F1**, due to the reduction of synergistic dynamic exchange imparted by DBN and the resulting retention of crosslink density, the rate of dynamic exchange and chain relaxation ultimately dwarfs the increased  $E_a$  resulting in decreased  $T_v$ . However, as established in previously **Figure 3.6**, the dissociative mechanism was not detectable via VTIR analysis of **F1** – meaning that the dissociative mechanism was either not occurring or occurring at levels undetectable to the instrument. Our attention then shifted to small molecule analysis as a potential route to provide validation to this hypothesis.

A series of six small molecule systems, **Figure 4.3**, were developed using hexyl isocyanate (3.52 mmol), hexanethiol (3.52 mmol), and DBN (0.05 mmol) to mimic the thiourethane moiety of **F1** and analyzed *via* VT-FTIR. They differ from each other based on the thiol input (3.52 mmol for **SM1-3** and 3.87 mmol for **SM4-6**) and DBN content (0.05 mmol, **SM1** and **SM4**; 0.11 mmol, **SM2** and **SM5**; 0.26 mmol, **SM3** and **SM6**) within the small molecule systems (**Table 4.2**). To establish a baseline, the first system analyzed (**SM1**) was formulated using functional equivalents of isocyanate and thiol with

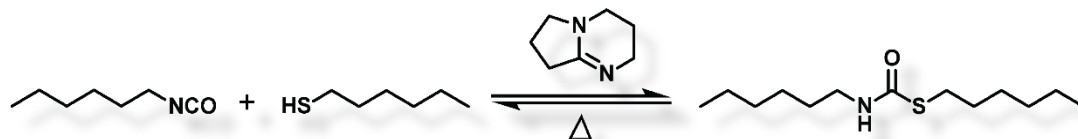


Figure 4.3 *Formation of SM1.*

Table 4.2 *Summary of small molecule thiourethane systems.*

Sample	Hexanethiol (mmol)	Hexyl isocyanate (mmol)	DBN (mmol)
SM1	3.52	3.52	0.05
SM2	3.52	3.52	0.11
SM3	3.52	3.52	0.26
SM4	3.87	3.52	0.05
SM5	3.87	3.52	0.11
SM6	3.87	3.52	0.26

a DBN content equivalent to that of the **F1** system relative to the thiourethane moiety. The **SM1** system was analyzed at varying temperature profiles with specific attention being placed on the appearance of the isocyanate peak at  $2258\text{ cm}^{-1}$  as a function of increasing temperature indicative of thiourethane dissociation (**Figure 4.4**). The VT-FTIR results from **SM1** suggest that the thiourethane does undergo dissociation under stoichiometric conditions for the small molecule analog of **F1**. However, as highlighted in Chapter III, VT-FTIR showed no evidence of dissociation within the network, or it is possible that dissociation in the network generated the free NCO occurred at levels below the instrument detection limit. The **SM1** system was then compared to **SM2** and **SM3** to determine the effects of increasing DBN content, as shown in **Figure 4.5**. As expected, the thiourethane dissociation is dependent on the concentration of DBN present within the system – with increasing DBN content resulting in increased levels of dissociation at each temperature profile, as indicated by the increase in NCO peak intensity in **Figure 4.5**. These results are consistent with work previously reported by Gamardella et al.<sup>76</sup> Each of these three small molecule systems were then reformulated using 10% excess

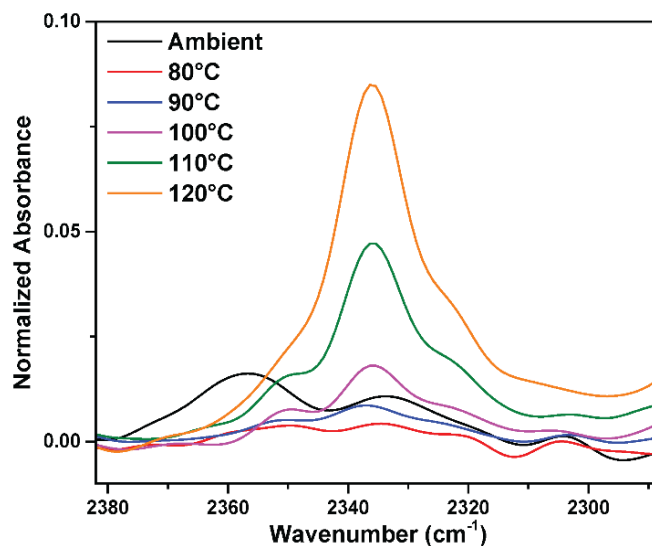


Figure 4.4 VT-FTIR of *SM1*.

thiol (**SM4** – **SM6**) and analyzed *via* VT-FTIR to determine if increasing the free thiol content within each system would affect the dynamic mechanism occurring, **Figure 4.6**. In each case, small molecule systems with excess thiol content (**SM4** – **SM6**) exhibited lower levels of thiourethane dissociation as a function of increasing temperature, relative to their respective functionally equivalent systems (**SM1** – **SM3**). This finding provides small molecule precedence to validate the previously developed hypothesis that excess free thiols in the +5% and +10% network systems will effectively shift the dynamic exchange equilibrium to favor the associative mechanism.

The thiol deficient systems were next analyzed by stress relaxation analysis (**Figure 4.7**), with the driving hypothesis being that the absence of free thiol content will favor the dissociative reversible mechanism for the thiourethane resulting in increased relaxation times and higher  $E_a$  and  $T_v$  values relative to **F1**. When fitted the Arrhenius relationship, both thiol deficient systems seemed to deviate from normal Arrhenius behavior, as illustrated in **Figure 4.8**. While unexpected, this behavior has previously

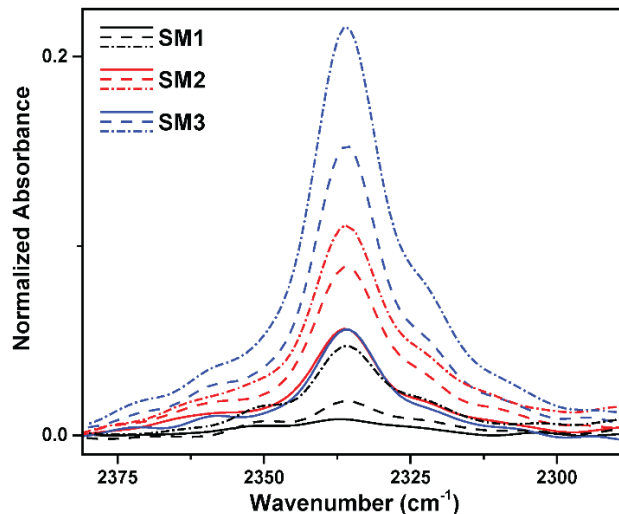


Figure 4.5 VT-FTIR analysis of *SM1*, *SM2*, and *SM3* (increasing DBN content) at 90°C (solid), 100°C (dash), and 110°C (dash dot).

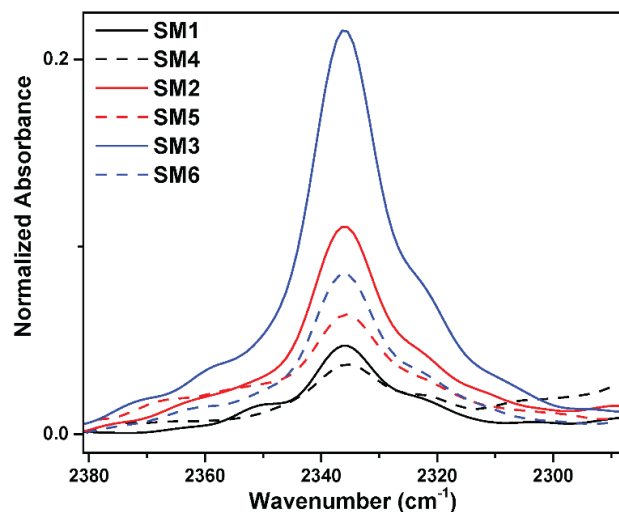


Figure 4.6 VT-FTIR analysis of *SM1* – *SM3* and *SM4* – *SM6* (respective increased thiol counterpart) at 110°C.

been observed by Jing et al.<sup>124</sup> when developing dynamic polyelectrolyte vitrimers.

They found that increasing salt content within their polyelectrolyte systems caused a shift towards the Vogel-Fulcher-Tammann (VFT) relationship due to the introduction of the dissociative mechanism.<sup>124</sup>

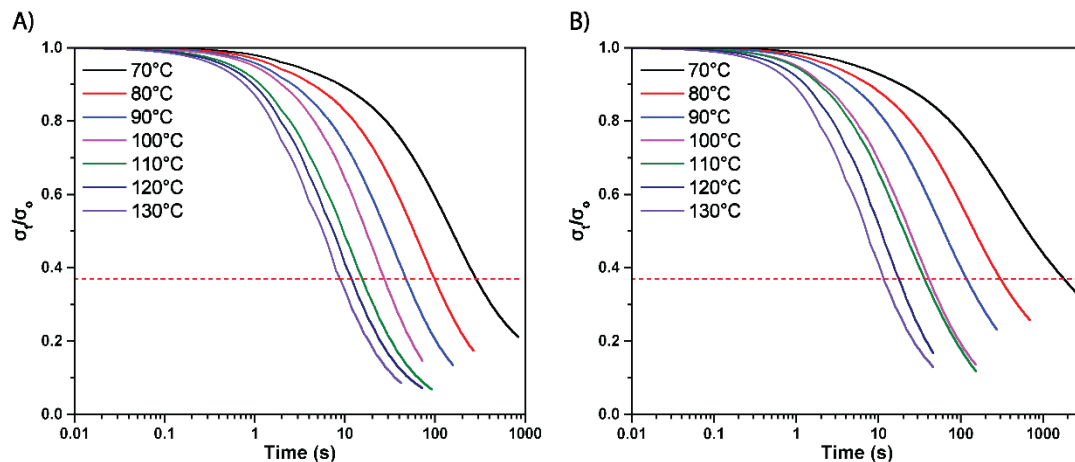


Figure 4.7 Stress relaxation analysis of the A) **-5%** and B) **-10%** systems.

VFT behavior in vitrimeric systems has also been described in various kinetic models.<sup>115, 125-126</sup> These models effectively separate an Arrhenius plot, exhibiting a change in slope, into a lower and upper temperature regime. In the lower temperature regime, material relaxation and network topological rearrangements are dominated by segmental motions and dynamics resulting VFT relaxation behavior. In the upper temperature regime, the rate of dynamic exchange outpaces chain relaxation resulting in Arrhenius behavior.<sup>125-126</sup>

In understanding the cause of VFT behavior in vitrimeric materials, a rationale can be developed to explain the unexpected relaxation behavior of the **-5%** and **-10%** thiol deficient systems. These systems were specifically formulated so that no free thiols would be present within the final network. Thus, the initial relaxation behavior ultimately comes in the form of thiourethane dissociation due to the absence of free thiol eliminating the possibility of the associative behavior taking place. It can then be inferred that the chain dynamics of these systems outpace the rate of thiourethane dissociation resulting in VFT behavior. Furthermore, since the stoichiometrically

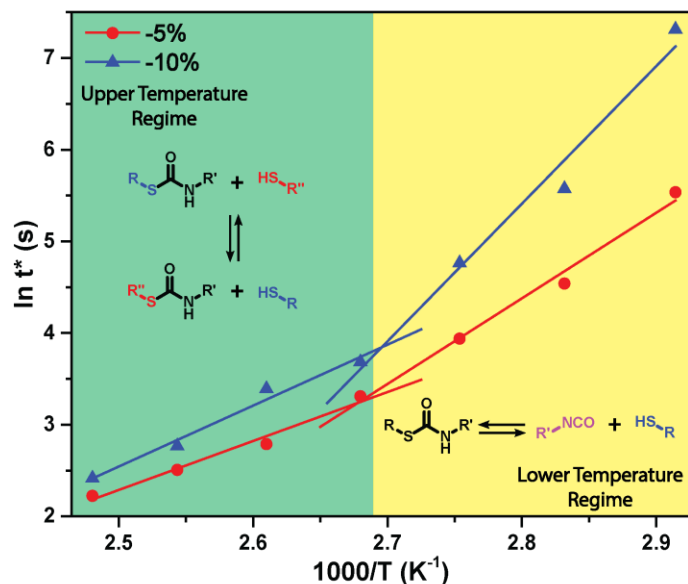


Figure 4.8 Arrhenius plot of the **-5%** and **-10%** systems from the obtained stress relaxation data, where it hypothesized that the lower temperature regime (VFT behavior) is indicative of thiourethane dissociation, and the upper temperature regime (Arrhenius behavior) is due to the presence of the associative behavior.

equivalent **F1** system does not exhibit VFT behavior, it can be assumed that there is a critical amount of dissociation that must occur to reduce the inherent crosslink density to a level for this behavior to be evident. However, network dissociation remains undetectable through VT-FTIR analysis.

Stress relaxation analysis now becomes inappropriate to compare the thiol excess and deficient systems, as they exhibit different mechanisms for relaxation. In contrast, non-isothermal creep analysis can be used to determine the effects of altered thiol content on the resulting material  $T_v$ . **Figure 4.9** clearly shows a distinct trend in  $T_v$ , with increasing free thiol content resulting in decreased  $T_v$  following an order of **10% > -5% > F1 > +5% > +10%** (specific values summarized in **Table 4.3**). The significant shifts in  $T_v$  values for the thiourethane systems containing either a stoichiometric excess or stoichiometric deficiency provide further evidence that stoichiometry effectively alters

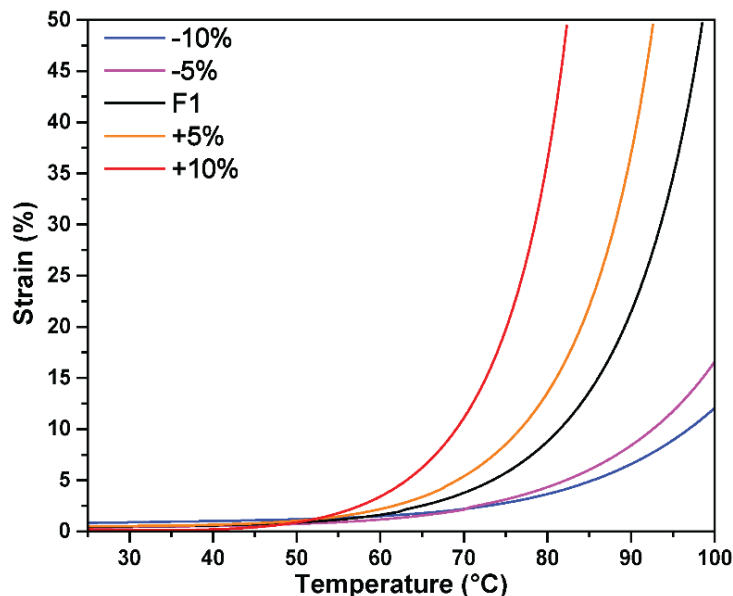


Figure 4.9 Non-isothermal creep analysis of **F1** and all altered thiol systems.

Table 4.3 Summary of obtained  $T_v$ .

Sample	$T_v^a$ (°C)	$T_v^b$ (°C)
-10%	NA	71.5
-5%	NA	68.9
<b>F1</b>	-24.4	61.8
+5%	-28.2	55.4
+10%	-55.5	48.2

<sup>a</sup>Determined by Arrhenius representation of the stress relaxation analysis. <sup>b</sup>Determined by non-isothermal creep measurements.

the thiourethane mechanism, favoring an associative exchange with thiol in excess and reversible dissociation when thiol is deficient.

### 4.3 Effects of Thiol Stoichiometry on Thermomechanical and Mechanical Property Retention

Not only does altering thiol content influence the dynamic relaxation behavior and apparent  $T_v$  of the networks, but it was also found to have a distinct effect on the virgin thermal and mechanical properties of these materials relative to the stoichiometrically equivalent **F1**. From DMA, as shown in **Figure 4.10A**, it was determined that decreasing free thiol content ultimately led to an increase in crosslink

density as determined from the plateau of the rubbery modulus, exhibiting a trend of  $-10\% > -5\% > \mathbf{F1} > +5\% > +10\%$ . Additionally, decreasing free thiol content leads to an increase in  $T_g$  as determined from the DMA  $\tan \delta$  peak (**Table 4.4**). Analysis of the networks by DSC showed similar trends in  $T_g$ . This trend also translated to the tensile properties, as shown in **Figure 4.11**, where decreasing free thiol content generally provided an increase in key mechanical properties such as Young's modulus and toughness (**Table 4.5**). Each of these materials were then reprocessed and retested *via* tensile testing, as shown in **Figure 4.12**, to determine how the altered thiol content would

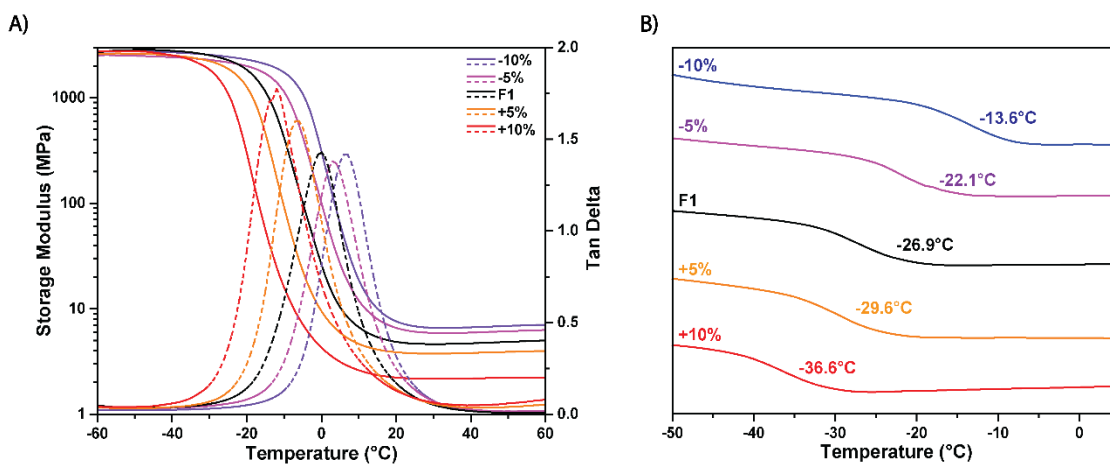


Figure 4.10 A) DMA and B) DSC thermograms of virgin **F1** and virgin altered thiol compositions.

Table 4.4 Summary of thermal and thermomechanical properties of virgin **F1** and virgin altered thiol compositions.

Sample	$T_g^a$ (°C)	$T_g^b$ (°C)	FWHM <sup>c</sup> (°C)	$M_c$ (g/mol)	$q$
-10%	-13.6	7.9	16.1	1373.1	0.44
-5%	-22.1	0.6	15.8	1787.8	0.34
<b>F1</b>	-26.9	-0.4	18.6	2305.2	0.26
+5%	-29.6	-7.1	16.2	2313.1	0.26
+10%	-36.6	-11.8	16.8	3871.7	0.15

$T_g^a$  determined by DSC.  $T_g^b$  determined from the DMA  $\tan \delta$  peak. <sup>c</sup>Full Width Half Maximum determined from the DMA  $\tan \delta$  peak.

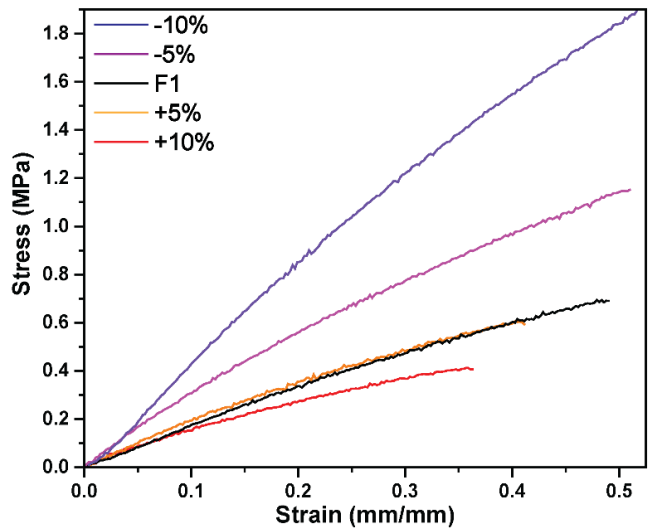


Figure 4.11 *Virgin tensile properties of each altered thiol system.*

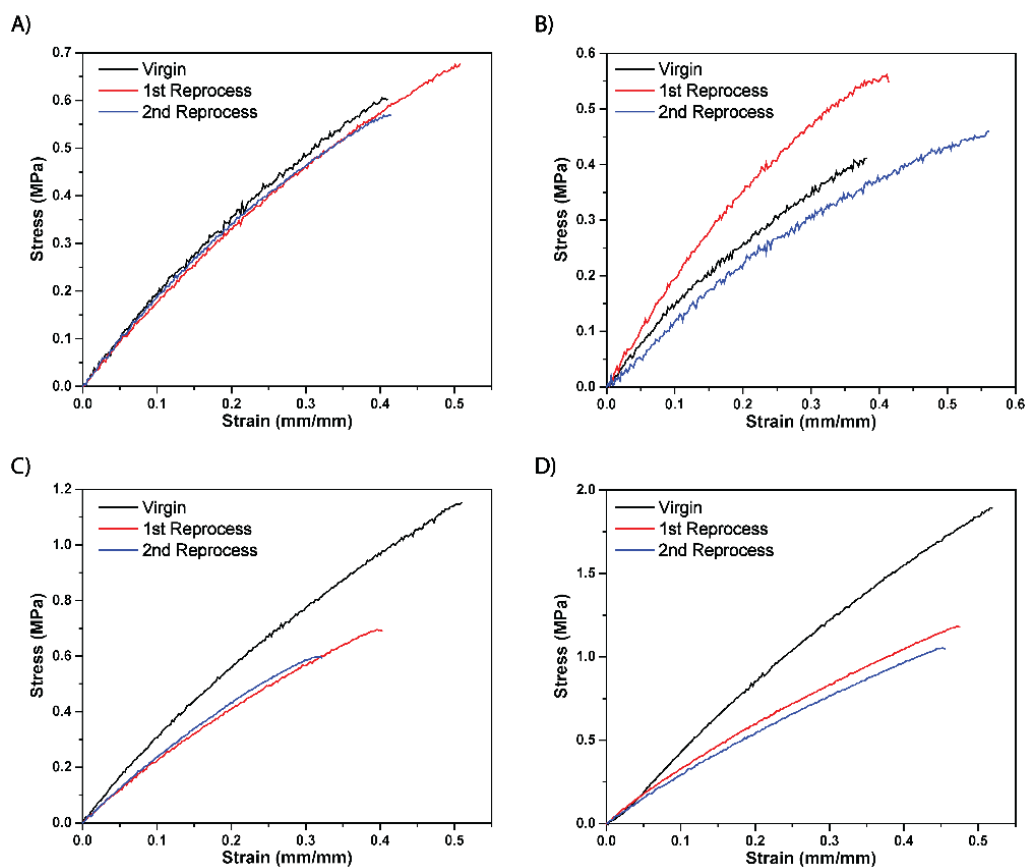


Figure 4.12 *Virgin and reprocessed tensile test results of the A) +5%, B) +10%, C) -5%, and D) -10% systems.*

influence the retention of these key material properties. Generally, the thiol deficient systems exhibit increased young's modulus, break stress, and toughness throughout reprocessing relative to **F1** and the thiol excess systems, **Table 4.5**, when observing the raw numerical values of the tensile experiments. For instance, the **-10%** exhibits toughness values of 0.42 J/m<sup>3</sup>, 0.31 J/m<sup>3</sup>, 0.28 J/m<sup>3</sup> (virgin, 1<sup>st</sup> reprocess, and 2<sup>nd</sup> reprocess respectively) while the **+10%** system exhibited values of 0.11 J/m<sup>3</sup>, 0.14 J/m<sup>3</sup>, and 0.15 J/m<sup>3</sup> (virgin, 1<sup>st</sup> reprocess, and 2<sup>nd</sup> reprocess respectively), **Table 4.5**. While the **-10%** system exhibits higher raw values than that of the **+10%** system, the property retention throughout reprocessing (relative to the virgin material) is better for the **+10%** system (132.9% and 146.1% - 1<sup>st</sup> reprocess and 2<sup>nd</sup> reprocess respectively) versus the **-10%** system (74.0% and 66.2% - 1<sup>st</sup> reprocess and 2<sup>nd</sup> reprocess respectively), **Table 4.6**. This trend in material property retention, however, appears predominantly within the break stress and material toughness categories. Nevertheless, these findings are in good agreement with work by Li et al.<sup>73</sup>, who described that increasing free thiol content

Table 4.5 Summary of mechanical properties.

Sample	Reprocess Cycle	Young's Modulus (MPa)	Break Strain (%)	Break Stress (MPa)	Toughness (J/m <sup>3</sup> )
<b>-10%</b>	Virgin	4.57	45.5	1.64	0.42
<b>-10%</b>	1 <sup>st</sup> Reprocess	3.41	47.8	1.14	0.31
<b>-10%</b>	2 <sup>nd</sup> Reprocess	3.47	43.9	1.09	0.28
<b>-5%</b>	Virgin	3.08	45.5	0.98	0.26
<b>-5%</b>	1 <sup>st</sup> Reprocess	2.60	41.6	0.79	0.20
<b>-5%</b>	2 <sup>nd</sup> Reprocess	2.61	40.8	0.76	0.18
<b>F1</b>	Virgin	1.93	44.3	0.67	0.17
<b>F1</b>	1 <sup>st</sup> Reprocess	1.86	44.3	0.56	0.15
<b>F1</b>	2 <sup>nd</sup> Reprocess	2.45	41.6	0.68	0.17
<b>+5%</b>	Virgin	2.12	41.5	0.63	0.15
<b>+5%</b>	1 <sup>st</sup> Reprocess	1.74	49.1	0.59	0.17
<b>+5%</b>	2 <sup>nd</sup> Reprocess	1.89	39.2	0.52	0.12
<b>+10%</b>	Virgin	1.77	39.30	0.44	0.11
<b>+10%</b>	1 <sup>st</sup> Reprocess	2.01	41.1	0.55	0.14
<b>+10%</b>	2 <sup>nd</sup> Reprocess	1.22	56.3	0.45	0.15

Table 4.6 *Summary of reprocessed mechanical property retention relative to the respective virgin material properties.*

Sample	Reprocess Cycle	Young's Modulus Retention (%)	Break Strain Retention (%)	Break Stress Retention (%)	Toughness Retention (%)
-10%	1 <sup>st</sup> Reprocess	74.6	104.9	69.7	74.0
-10%	2 <sup>nd</sup> Reprocess	76.0	96.4	66.3	66.2
-5%	1 <sup>st</sup> Reprocess	84.4	91.6	80.1	77.0
-5%	2 <sup>nd</sup> Reprocess	84.8	89.7	77.1	72.2
F1	1 <sup>st</sup> Reprocess	96.3	100.0	83.6	86.7
F1	2 <sup>nd</sup> Reprocess	127.1	94.1	102.0	100.5
+5%	1 <sup>st</sup> Reprocess	82.0	118.3	93.1	112.4
+5%	2 <sup>nd</sup> Reprocess	89.5	94.3	83.1	81.3
+10%	1 <sup>st</sup> Reprocess	113.7	104.6	125.5	132.9
+10%	2 <sup>nd</sup> Reprocess	69.2	143.2	103.2	146.1

results in higher levels of physical property retention due to the suppression of potential side reactions. Specifically, the thiourethane dissociative mechanism results in the formation of highly reactive NCO groups capable of reacting with atmospheric moisture due to reprocessing in an open environment – ultimately leading to crosslink density reduction and property loss. Relating this to the previously established VFT behavior of the **-5%** and **-10%** systems, it is reasonable to postulate that the reduction in material property retention of these systems is due to thiourethane dissociation.

Interestingly, the **+10%** system exhibited an increase in break stress, break strain, and toughness throughout each reprocessing cycle, relative to its virgin properties. DMA was conducted on the reprocessed **+10%** system in an effort to provide an explanation to this phenomenon, **Figure 4.13**. It was determined that the **+10%** system increased in crosslink density throughout reprocessing as determined from the rubber modulus. However, each of the other altered thiol systems showed either a maintained or decreased crosslink density throughout reprocessing. We expect that the increase in crosslink density of the **+10%** system is due to potential oxidation of the free thiols to form disulfides<sup>70, 127</sup> resulting in additional crosslinks relative to the virgin material.

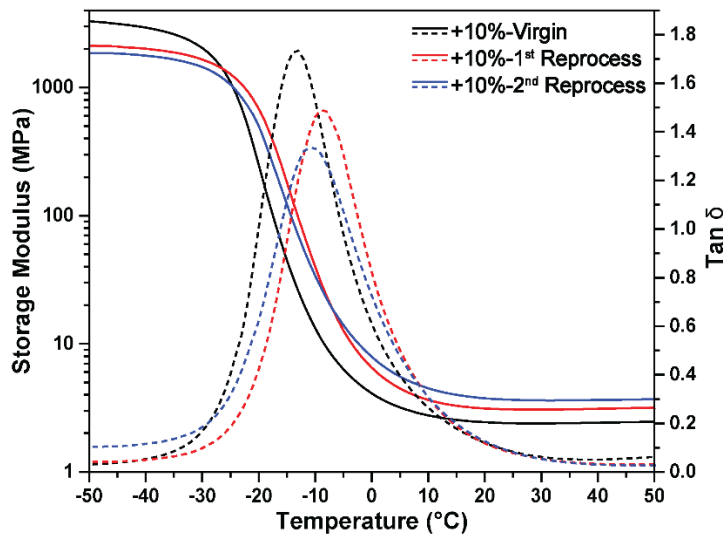


Figure 4.13 DMA thermograms of the +10% system throughout reprocessing.

#### 4.4 Concluding Remarks

Through previous investigations<sup>72-73</sup>, the thiourethane DCC has been shown to exhibit both the associative and dissociative pathways. Through systematic alterations in network thiol content, we aimed to investigate to what effect we could alter the dynamic equilibrium and the influence it would have on vitrimeric behavior and mechanical property retention. As initially expected, increasing free thiol content within the network resulted in decreased  $\tau^*$  and ultimately decreased  $T_v$ . In contrast, decreasing the thiol content within the network resulted in a deviation from the Arrhenius relationship to the VFT relationship. This was determined to be due to increased dissociative dynamic behavior, consistent with that previously observed by Jing et al.<sup>124</sup> A series of small molecule VTIR studies provided additional evidence that altering the free thiol content within the systems would result in a shift in the dynamic behavior equilibrium (i.e. associative vs. dissociative behavior). Furthermore, the altered thiol content was found to affect the virgin material properties and material property retention throughout

reprocessing. It was ultimately determined that decreasing thiol content within the systems resulted in an increase in virgin mechanical, thermal, and thermomechanical properties. However, these increased properties came at the expense of material property retention after reprocessing relative to the virgin property of the respective system.

## 5.1 Objective

Linear thiol-ene photopolymerizations have received minimal attention as compared to network formation and post-polymerization modification. However, early reports of thiol-ene photopolymerization as a route to step growth polymers have been reported to have exceptional reactivity circumventing problems commonly associated with achieving high molecular weight polymers traditionally associated with the step growth process.<sup>23, 104, 107, 128-129</sup> Herein, the overarching goal is to expand work previously established by Alameda et al.<sup>25</sup> on degradable thiol-ene networks into the realm of thermoplastic materials. A series of six different poly(thioether ketal) thermoplastics were synthesized in order to explore key structure-property relationships pertaining to polymer hydrolysis:

- 1) The effect of bisalkene diketone monomer structure on the relative rate of polymer hydrolysis.
- 2) The effect of dithiol monomer selection on the relative rate of polymer hydrolysis and degradation behavior.

As expected, the bisalkene diketone monomer structure had similar effects on the relative rate of polymer hydrolysis as previously reported by Alameda et al.<sup>25</sup> While it was expected that by changing the hydrophilic/hydrophobic character of the polymers would affect polymer hydrolysis rate, it also unexpectedly altered the degradation behavior of the materials. A mathematical model developed by Lyu et al. was then utilized to better compare the effects of changing polymer backbone architecture.

## 5.2 Polymer Synthesis

Previously in our lab, Alameda et al. synthesized a series of bisalkene diketone monomers from a series of common ketones and commercially available alkenyl-diol by means of classic acid catalyzed ketalization techniques.<sup>25</sup> They showed that through thiol-ene photopolymerization, poly( $\beta$ -thioether ester ketal) thermosets could be formed using the synthesized monomers and commercially available multifunctional thiols. These networks could then readily undergo rapid hydrolytic degradation under acidic conditions. Furthermore, these materials exhibited tunable degradation profiles based on the structure of the ketal monomer used. Building off these findings, we have developed a series of linear poly(thioether ketal) thermoplastics that exhibit tunable degradation profiles based on a variety polymer architectural features – i.e. ketal monomer stability and polymer backbone hydrophilic/hydrophobic characteristics.

We first focused our attention on utilizing monomers **3** and **5** (**Figure 5.1**), previously developed by Alameda et al.<sup>25</sup>, since they have been shown to exhibit moderate hydrolytic rates of degradation while maintaining consistency in monomer architectural features – i.e. similar structures with similar electronic effects. It has been proposed that the only aspect distinguishing these two monomers apart from each other in terms of hydrolytic stability stems from their respective structural conformations.

Hydrolytically labile poly(thioether ketals) were then synthesized *via* linear thiol-ene photopolymerizations using the bisalkene diketone monomers (**3** and **5**) and a series of commercially available dithiol monomers (**6**, **7**, and **8**). **Figure 5.2** illustrates the representative scheme for UV photopolymerization utilizing the bisalkene diketone monomers, commercially available dithiol monomers, and Darocur 1173 (5 mol%) as the

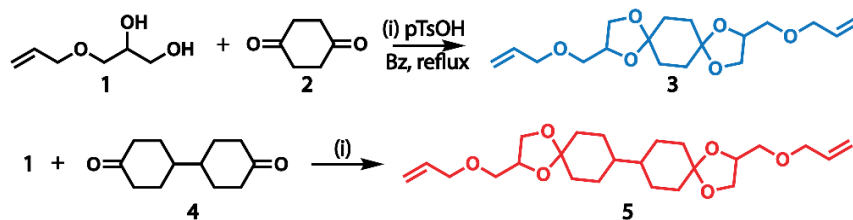


Figure 5.1 General synthetic scheme for cyclic bisalkene diketal monomers **3** and **5** from the acid-catalyzed ketalization of diketones (**2** and **4**) and 3-allyloxy-1,2-propanediol (**1**).

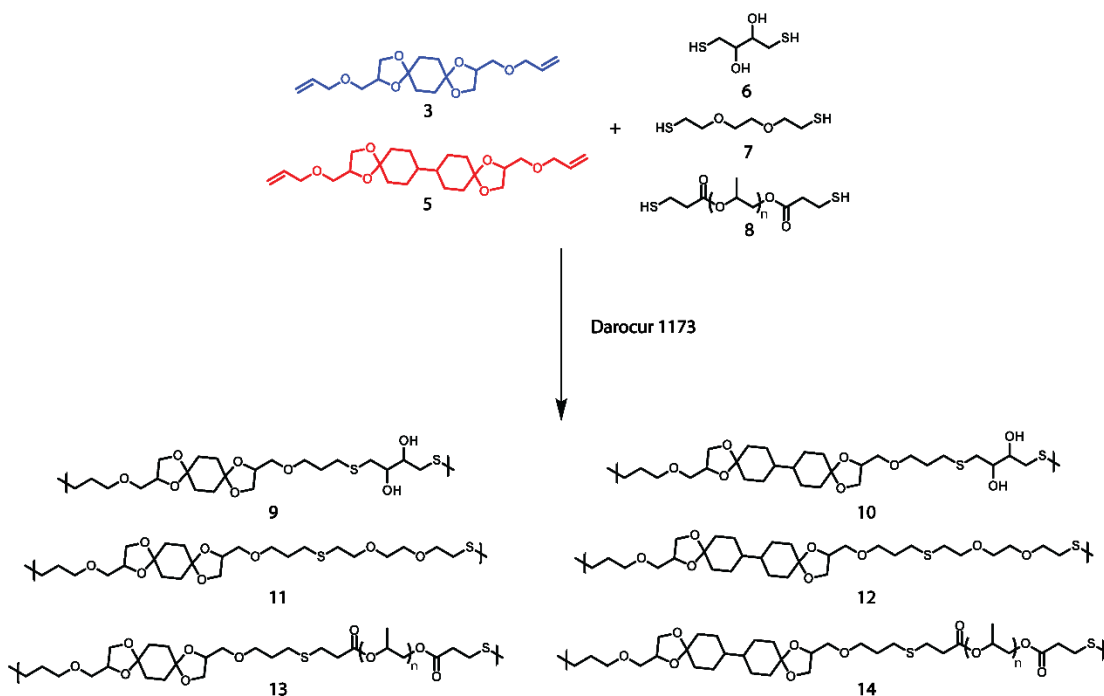


Figure 5.2 General synthetic scheme for polymers **9**, **10**, **11**, **12**, **13**, and **14** from the radical mediated thiol-ene photopolymerization of monomers **3** and **5** with commercially available dithiol monomers **6**, **7**, and **8**.

photoinitiator. Polymer structure and molecular weights were confirmed *via* NMR and SEC analysis (**Figure C.1** – **Figure C.25**). Although common for step growth polymers, there was a degree of difficulty in maintaining similar molecular weight profiles and  $X_n$  values across each class of polymers (class being defined by dithiol monomer), which we attributed to a number of factors; 1) inherent reactivity of the dithiol monomer,<sup>130</sup> 2)

steric effects of monomer structure, and 3) dramatic increase in the viscosity of the reaction medium.

### 5.3 Hydrolytic Stability Analysis of Poly(thioether ketal) thermoplastics

Each polymer system was subjected to hydrolytic stability testing *via* submersion into various degradation media. As previously stated, the wide variety of commercially available dithiol monomers enable us to tune the hydrophilic/hydrophobic characteristics of each polymer system by altering the polymer backbone architecture. In addition to the hypothesis that ketal stability will play a key role in polymer hydrolytic degradation, we further hypothesize that the polymer backbone contributions will endow our systems with another handle by which to tune the rates of degradation.

In analyzing our polymer hydrolytic stability of these systems, we first turned our attention to polymers **9** and **10**. Ketals commonly exhibit high degrees of stability under basic and neutral conditions, while readily undergoing hydrolysis under acidic conditions. We initially hypothesized that polymers **9** and **10** would only undergo hydrolytic degradation under acidic conditions, with their rates of hydrolysis being directly correlated to the stability of the ketal moiety. We found this to be true by monitoring the rates of hydrolytic degradation *via* gravimetric analysis (**Figure 5.3**). The results obtained suggest that polymers formed using monomer **5** would exhibit faster rates of degradation than that of polymers formed with monomer **3**. This is in agreement with results obtained by Alameda et al.<sup>25</sup> In which case, it has been proposed that the differences in the stability of the ketal moiety along the polymer backbone come from the structural conformation of the ketal monomer, where monomer **3** exhibits a somewhat “locked in” conformation while monomer **5** has more degrees of motion. This affects the

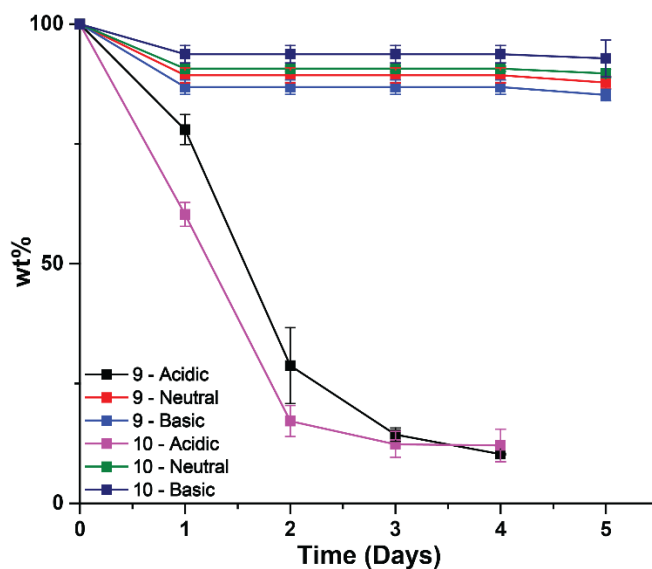


Figure 5.3 Gravimetric analysis of polymers **9** and **10** upon exposure to acidic (1M HCl:Acetonitrile – 90:10 by volume), neutral (pH 7.4 PBS buffer:acetonitrile – 90:10 by volume), and basic (1M NaOH:Acetonitrile – 90:10 by volume) aqueous environments versus time.

ability of the ketal to transition from a  $sp^3$  conformation to a  $sp^2$ . Since monomer **5** has more degrees of motion, it can more easily undergo the conformational transition making it more susceptible to hydrolytic degradation.

One of the interesting aspects of these two polymer systems is that we could not accurately monitor degradation by SEC throughout the degradation process due to the material being insoluble in THF. We attributed this to crosslinking reactions that could potentially occur throughout the degradation process. When the poly(thioether ketals) degrade, they form the parent ketone and polymer chains with diol end groups as degradation byproducts. Operating under the assumption that polymer hydrolytic degradation is a random chain scission process,<sup>131-132</sup> we can infer that polymer degradation results in smaller polymer chains of varying molecular weight. If we also assume that there is still some amount of the parent ketone that remains in the polymer

rich phase due to the inability to escape into solubilizing degradation media,<sup>133-134</sup> we can develop a rationale for why crosslinking is occurring. We expect that as degradation progresses in polymers **9** and **10**, the ketone degradation byproduct is able to react with the hydroxyl groups present along the polymer backbone, forming new ketal crosslinks catalyzed by the surrounding acidic media. A schematic for the proposed crosslinking mechanism is shown in **Figure 5.4**. This finding introduces yet another variable to quantifying the rate of degradation that in many mathematical models for describing polymer degradation is often excluded. Many of the mathematical models operate under the assumption that as hydrolytically labile polymers degrade into small molecule byproducts that are easily solubilized by the surrounding degradation media, and thus negligible towards the quantification of degradation rate. This assumption, in many cases, is made to simplify the models used. However, this is not the case for polymers **9** and **10**. Therefore, we hypothesize that the elimination of the parent ketone small molecule byproduct from the bulk polymer also affects the apparent rate of degradation for these systems.

We also sought to investigate the effects of altering the hydrophobic/hydrophilic character of the polymer backbone by systematically changing the dithiol monomer used when developing polymers **11** - **14**. Each of these polymer systems exhibited varying rates of degradation when subjected to aqueous degradation media while maintaining the initial mass of the starting polymer films. We attributed this mass retention to the degradation byproducts being insoluble in the surrounding media. This finding is opposite that of what was found for polymers **9** and **10** making direct comparisons to those polymer systems difficult without making large assumptions. Nevertheless,

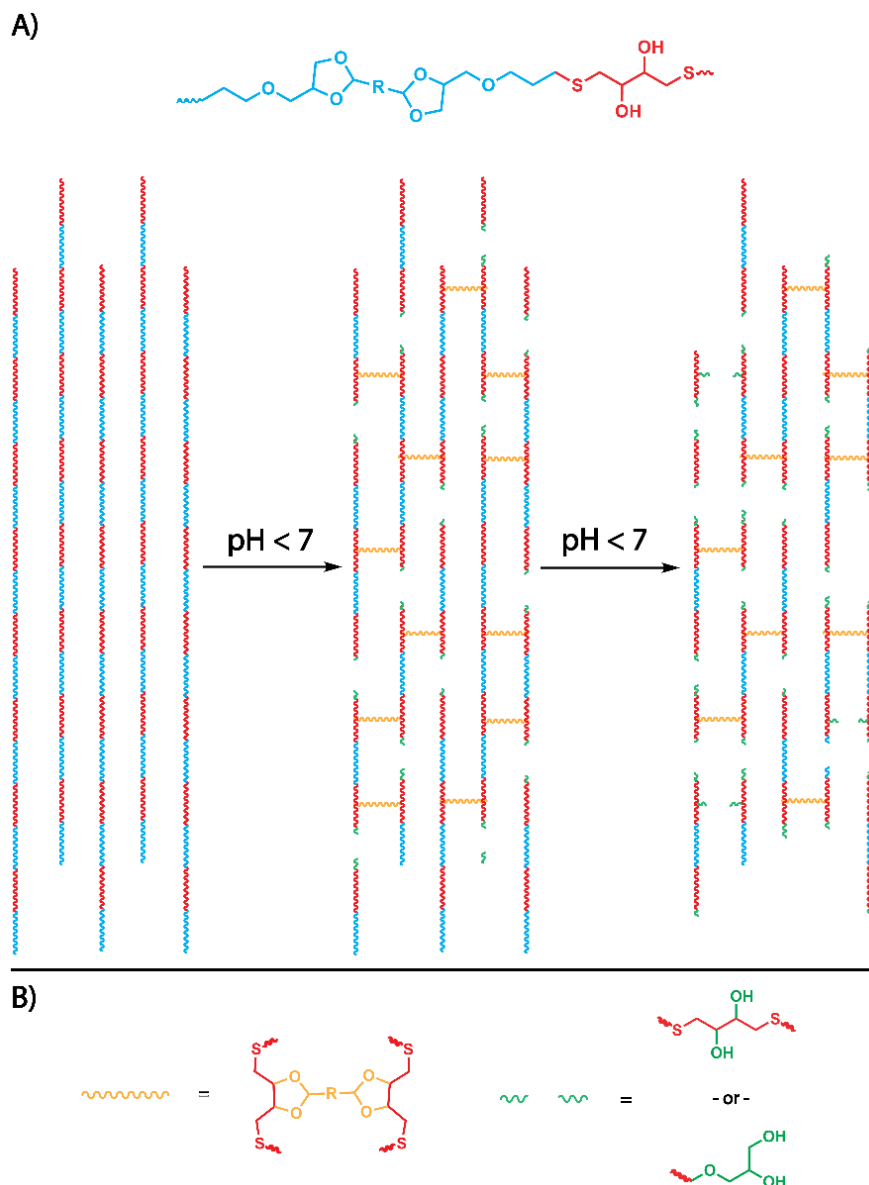


Figure 5.4 A) Illustration of the potential crosslinking reactions of polymers **9** and **10** that could occur during the degradation process under acidic conditions and B) molecular structure of crosslinks (yellow) and reformed hydroxyl groups (green) as a result of acidic catalysis (crosslink formation) and degradation.

polymer hydrolytic degradation of **11** – **14** could be tracked through SEC, with clear shifts in the chromatograms indicating a loss in molecular weight (Figure C.26 – Figure C.29). We found that polymers **11** and **12** only exhibited degradation in acidic media, due to the only hydrolysable linkage along the polymer backbone being the ketal moiety.

As shown in **Figure 5.5**, we found that polymers formed using monomer **5** exhibited faster rates of hydrolysis than those formed with **3**, which is in good agreement with previously stated results. When we analyzed the SEC results from polymers **11** and **12**, we noticed that there was some sort of an induction period (approx. 1 to 2 days) before high degrees of molecular weight loss became apparent. To understand why this induction period was occurring, we turned our attention to the various mathematical models that have been developed to describe polymer degradation and erosion. Polymer

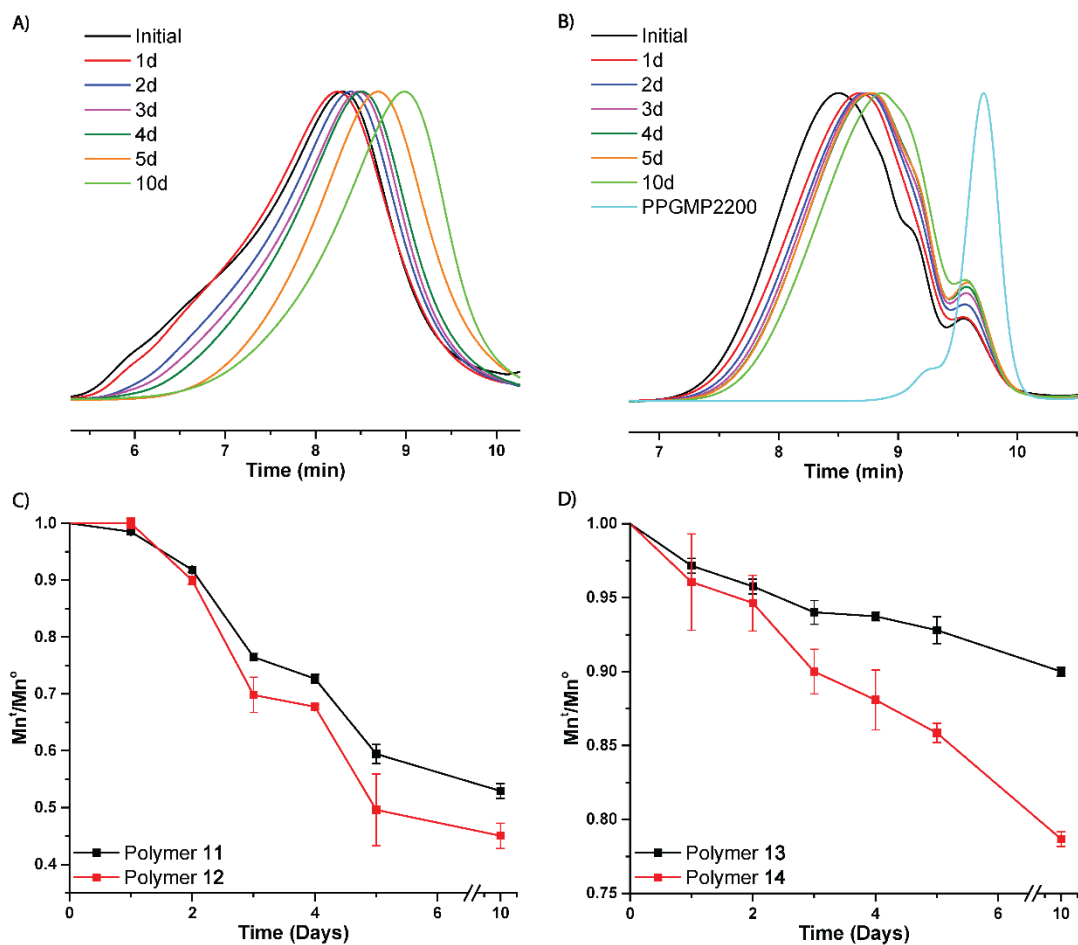


Figure 5.5 SEC chromatograms of A) polymer **12** and B) polymer **14** throughout degradation under acidic conditions and SEC analysis of C) polymers **11** and **12** and D) polymers **13** and **14** throughout degradation under acidic conditions.

degradation, process of chain cleavage at the sites of hydrolytically labile moieties, can commonly lead to erosion characteristics – a physical phenomenon that is commonly explored in biomedical polymers for controlled release applications and bioresorbable materials. Polymer erosion, in contrast to polymer degradation, is described as the mass loss behavior and depletion of the material.<sup>131-133, 135-136</sup> Polymer erosion mechanisms can be characterized into two categories; surface eroding and bulk eroding systems. In surface eroding systems, degradation occurs at a faster rate than the ingress of the degradation media leading to heterogenous phases. Thus, degradation and erosion is confined to the surface of the material.<sup>131, 133</sup> In bulk eroding systems, degradation occurs homogeneously throughout the bulk of the material due to the rate of hydrolytic degradation being slower than the ingress of the degradation media.<sup>131, 133</sup> In each case, surface and bulk erosion exhibit distinctly different changes in molecular weight profiles. Since degradation in surface eroding systems is confined to the surface, the molecular weight of the material in the bulk remains relatively unchanged. In bulk eroding systems, the molecular weight steadily decreases throughout the bulk of the material.<sup>133, 137-138</sup> In bulk eroding systems, the material retains its dimensions over the course of degradation and can degrade as much as 90% before any significant mass loss can be observed.<sup>133, 139</sup> This can help explain many of the phenomena that we observed pertaining to the degradation of polymers **11**, **12**, **13**, and **14**. With this in mind, we hypothesized that the reason for the sort of induction period for polymers **11** and **12** is due to the time it takes for the degradation media to penetrate the system enough to where some degree of bulk erosion to occurs.

To develop an understanding to what extent the role that the hydrophobic/hydrophilic character of the polymer backbone plays in hydrolytic degradation of our polymer systems, we turned our attention to polymers **13** and **14**. These polymers are unique in that they have a poly(propylene oxide) (PPO) spacer ( $n \approx 34.5$  units) in the polymer backbone. We initially expected that the PPO spacer would increase the hydrophilic character of these polymers in comparison to that of polymers **11** and **12**. This hypothesis was supported from initial contact angle studies where polymers **11** and **12** exhibited contact angles of  $84.9^\circ$  and  $110.8^\circ$  compared to polymers **13** and **14** contact angles of  $48.4^\circ$  and  $50.1^\circ$ , respectively. We expected that this increase in hydrophilic character would result in an increase in the rate of hydrolytic degradation. However, as shown in **Figure 5.5**, this was not the case. We found that after 10 days in the degradation media, polymers **13** and **14** never fell below 75% of the initial  $M_n$ . To our surprise, this was in direct contrast to our initial hypothesis. We attributed this finding to two potential aspects of these polymer systems: 1) Using the equation of  $M_n^t/M_n^0$  as a function of degradation time does not give an accurate comparison of degradation rates of these systems since the number of ketals in each systems varies by polymer  $X_n$  values, 2) The PPO spacer of polymers **13** and **14** could potentially act as a repulsive barrier due to its inherent LCST behavior, thus reducing the rate of degradation media ingress towards the ketal linkage.

In the aforementioned polymer systems, we initially used the equation  $M_n^t/M_n^0$  as a function of degradation time to describe the relative rates of hydrolysis. However, this method falls short in comparing polymers that do not exhibit the same  $X_n$  values, especially when trying to compare polymers **11** – **14** since they do not exhibit the same

starting  $X_n$  values or the same backbone architecture. Therefore, we used a set of fundamental equations, developed by Lyu and coworkers,<sup>140</sup> to relate the apparent rates of hydrolysis for these polymer systems. In which case, the diffusion of water molecules into the polymer systems is much faster than the hydrolysis of the ketal moieties along the polymer backbone. Therefore, polymer hydrolysis can be broken down into three phases: where phase 1 is the diffusion of water molecules into the polymer system until full saturation ( $C_s$ ), phase 2 is the initial stages of degradation, and phase 3 is when polymer hydrolysis proceeds far enough along so that small molecule byproducts are able to dissolve into the aqueous media. Molecular weight during hydrolysis can be described by:

$$N(t) = \frac{1}{1 - e^{-k_2 C_s t}}$$

where  $N(t)$  is polymer molecular weight,  $k_2$  is a second order rate constant and  $C_s$  is the solubility of water in the polymer. This equation does not take into account hydrolysis occurring in phase 1 as it is difficult to calculate. Therefore, the rate of hydrolysis during phase 1 is assumed to be 0 until some time  $t_i$ , which is the effective induction time of bulk erosion at which the polymer becomes saturated. We can then incorporate  $t_i$  to get:

$$N(t) = \frac{1}{1 - e^{-k_2 C_s (t - t_i)}}$$

which can be rewritten as:

$$\ln\left(1 - \frac{1}{N(t)}\right) = -k_2 C_s * (t - t_i)$$

Thus, we can utilize molecular weight data to calculate the hydrolysis rate constant. In the early stages of hydrolysis,  $N(t)$  is much greater than 1. The equation now becomes:

$$\frac{1}{N(t)} = k_2 C_s * (t - t_i)$$

We can now plot the reciprocal molecular weight as a function of degradation time to achieve a linear function where the slope is  $k_2 C_s$  and an x-intercept of  $t_i$ . The trends in hydrolytic degradation for polymers **11** – **14** were fitted to these equations and are shown in **Figure 5.6** and the values obtained summarized in **Table 5.1**. Interestingly, we found that polymers **11** and **12** exhibited relatively faster hydrolytic rates of degradation ( $k_2 C_s$ ) than their respective counterparts in polymers **13** and **14**. By combining these findings

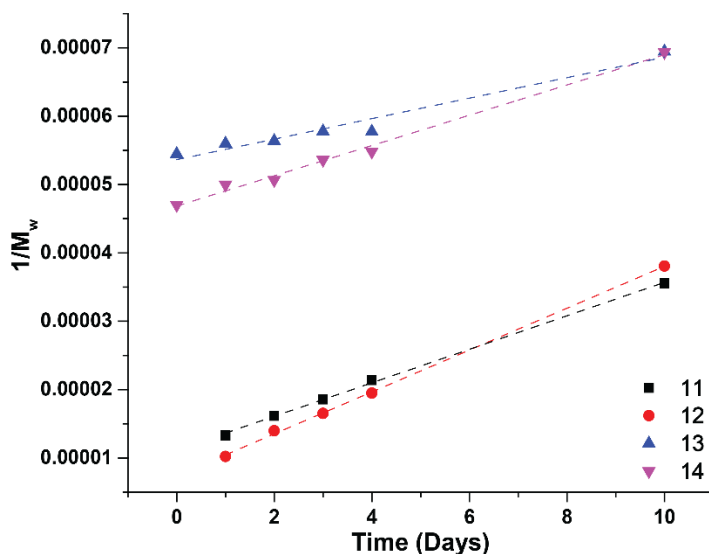


Figure 5.6 Molecular weight data of polymers **11** – **14** fitted to the model proposed by Lyu et al.<sup>140</sup>

Table 5.1 Summary of model degradation kinetics determined using Mw data from polymers **11** – **14** fitted to the model developed by Lyu et al.<sup>140</sup>

Polymer	Model Kinetics $k_2 C_s$ (s <sup>-1</sup> )	$t_i$	R <sup>2</sup>
<b>11</b>	1.70*10 <sup>-9</sup>	-4.5	.9989
<b>12</b>	2.13*10 <sup>-9</sup>	-2.4	.9997
<b>13</b>	1.04*10 <sup>-9</sup>	-36.0	.9598
<b>14</b>	1.54*10 <sup>-9</sup>	-21.2	.9928

with the initial contact angle analysis studies, we were able to determine that the degree of hydrophilic character exhibited by these polymers does not necessarily play as crucial a role in the relative rates of hydrolytic degradation as initially expected. Nevertheless, these findings further support the notion that a crucial determining factor in the relative rates of hydrolytic degradation of these polymer systems is the relative hydrolytic stability of the ketal moiety employed along the polymer backbone. While these findings suggest that the relative rates of hydrolytic degradation are not as dependent of the hydrophilic/hydrophobic character as initially expected, we could not simply disregard these polymer characteristics as negligible in the overall behavior of these systems when subjected to aqueous degradation protocols. Upon further investigation, we found that these inherent polymer characteristics do in fact play a role in the length of time it takes for the aqueous media to diffuse into and fully saturate the polymer system (phase 1), with 1) polymers **13** and **14** exhibiting shorter  $t_i$  times than polymers **11** and **12** and 2) polymers formed using monomer **3** exhibiting shorter  $t_i$  times than with monomer **5**. While the values of  $t_i$  are negative, which is seemingly impossible, these values give qualitative significance to the respective polymer hydrophobic/hydrophilic characteristics and Mw as they pertain to the material behaviour when subjected to aqueous degradation environments.

#### **5.4 Material Properties of Poly(thioether ketal) Thermoplastics**

In general, materials formed by thiol-ene photopolymerization exhibit relatively low mechanical and thermomechanical properties (i.e.  $T_g$  well below room temperature).<sup>141</sup> **Table 5.2** shows a summary of the material properties of all polymers, with the DSC thermograms shown in **Figure C.30 – Figure C.32**. Polymers **9 – 14** all

Table 5.2 Summary of molecular weights, contact angle, and thermal properties of polymers **9** – **14**.

Polymer	Properties		D	Xn	Contact Angle <sup>b</sup>	T <sub>g</sub> (°C)
	M <sub>n</sub> <sup>a</sup> (kDa)	M <sub>w</sub> <sup>a</sup> (kDa)				
<b>9</b>	8.7	19.6	2.25	16.58	92.8°	-12.3
<b>10</b>	10.2	23.4	2.29	16.68	72.9°	10.4
<b>11</b>	16.4	79.3	4.84	33.87	84.9°	-39.9
<b>12</b>	17.7	104.9	5.93	33.52	110.8°	-36.5
<b>13</b>	12.7	27.5	2.17	5.01	48.4°	-61.9
<b>14</b>	13.8	31.6	2.29	5.25	50.1°	-62.5

<sup>a</sup>Initial molecular weights before degradation. <sup>b</sup>Initial water droplet contact angle before submersion in aqueous media.

exhibited  $T_g$  values below room temperature. We found that dithiol monomer selection played a key role in dictating  $T_g$  values, where polymers **9** and **10** exhibited the highest intermediate  $T_g$ , while **13** and **14** gave the lowest values. The reason for these low  $T_g$  values due to the free hydroxyls promoting hydrogen bonding. Polymers **11** and **12** exhibited an values is commonly explained by the inherent flexibility of the thioether linkage along the polymer backbone.<sup>141</sup> We found that polymers **9**, **10**, **11**, and **12** exhibited good film forming properties for our intended degradation procedure, but lacked the mechanical integrity needed to form workable free standing films. Therefore, we determined that they would be best suited for applications such as pressure sensitive adhesives. Since polymers **13** and **14** have PPO segments in the polymer backbone, these systems seem to adopt many of the materials properties commonly associated with PPO – i.e. viscous liquids at room temperature with low  $T_g$ . Developing linear thiol-ene materials with robust thermal and mechanical properties while maintaining hydrolytic degradability remains a challenge, but steps are being taken to improve their inherent thermal and mechanical properties.

## 5.5 Concluding Remarks

In this work, we developed a library of novel poly(thioether ketal) thermoplastics from previously synthesized monomers **3** and **5** and commercially available dithiols *via* radical mediated thiol-ene photopolymerizations. The resulting materials exhibited properties typical of thiol-ene materials – i.e. low mechanical properties and low  $T_g$ . We found that these properties were dependent on dithiol monomer selection. The diketone monomer structure was found to play a key role in influencing the relative rates of hydrolytic degradation for each polymer system. In all cases, polymers formed using monomer **5** exhibited faster rates of hydrolysis than those formed with **3** due to the ability of the ketal moiety to transition from  $sp^2$  to  $sp^3$  more easily. Relating relative rates of hydrolysis based on dithiol monomer selection was found to be difficult due to differing characterization methods and inconsistent  $X_n$  values. Using a set of fundamental equations, we were able to determine the relative rates of hydrolysis ( $k_2C_s$ ) of polymers **11** – **14**, where we found that the predominating factor affecting hydrolysis rate was the relative stability of the ketal moiety employed along the polymer backbone. Furthermore, we found that hydrophobic/hydrophilic character of these polymer systems, as a result of dithiol and bisalkene diketal monomer selection, affected the time it required for the aqueous degradation media to saturate the system ( $t_i$ ). The work herein should provide a framework for facile synthesis of poly(thioether ketals) *via* thiol-ene photopolymerization to produce materials with fast rates of hydrolytic degradation.

## CHAPTER VI Conclusions and Future Work

Thiol-X “click chemistry” has proven to be exceptionally useful in materials science due to it being high yielding, highly efficient, and proceeding without the formation of byproducts. While many types of thiol-X reactions have been identified as “click chemistries”, the work herein sought to utilize radical-mediated thiol-ene photoreactions and base-catalyzed thiol-isocyanate reactions to develop next generation materials exhibiting environmental relevance through reprocessability or hydrolytic degradability. Ultimately, this dissertation focused on utilizing these two chemistries to develop a rapid and efficient route to covalent adaptable networks, as well as a route to hydrolytically labile thermoplastics.

In Chapter III of this dissertation, a “one-pot two-step” approach was developed to achieve ternary thiol-ene/thiourethane CANs through the utilization of both the base-catalyzed thiol-isocyanate reaction and the radical-mediated thiol-ene photoreaction utilizing only commercially sourced materials. The networks produced exhibited excellent reprocessability. Furthermore, it was determined that the virgin material properties of these materials and their material property retention were ultimately dictated by the diisocyanate monomer selection. Networks formed using IPDI and H<sub>12</sub>MDI exhibited dissociative dynamic behavior, imparted by the steric strain on the secondary thiourethane moiety, that was detectable through VTIR analysis. This behavior caused decrease in crosslink density throughout reprocessing, ultimately leading to decreased material property retention.

In Chapter IV of this dissertation, the dynamic exchange equilibria of the ternary thiol-ene/thiourethane was investigated through systematic changes in thiol content of

CAN system formed using HDI as the diisocyanate monomer. As was previously established by Wen and coworkers<sup>72</sup>, the thiourethane moiety exhibits both the associative and dissociative dynamic exchange pathways synergistically when DBN is employed as the exchange catalyst. Through network stress relaxation analysis and small molecule VTIR studies, it was determined that the dynamic equilibria could be shifted to favor the associative or dissociative behavior through altering the free thiol content within the system. Interestingly, networks formed with thiol deficiency exhibited a deviation from Arrhenius behavior to VFT behavior due to increased thiourethane dissociation within the network. The mechanical and thermomechanical properties, as well as the level of property retention throughout reprocessing, were also found to be affected by altering the thiol content present within the networks. Ultimately, networks formed with a thiol deficiency exhibited increased thermal and mechanical properties, however coming at the expense of property retention throughout reprocessing relative to the virgin property.

In Chapter V of this dissertation, radical-mediated thiol-ene photopolymerizations were utilized to develop a series of poly(thioether ketal) thermoplastics. Expanding on work previously described by Alameda et al.<sup>25</sup>, two different bis-alkene diketal monomers were polymerized with a series of commercially available dithiols to produce a library of hydrolytically labile poly(thioether ketals). The structure of the ketal moiety was found to greatly affect the hydrolytic stability of the polymer systems – with polymers formed with the single cyclohexyl derivative being more stable under acidic conditions than that of the dicyclohexyl. This was determined to be due to the ease of transition of the ketal moiety from  $sp^2$  to  $sp^3$ . Additionally, we found that changes in the

hydrophobic/hydrophilic character of the polymer systems was affected by both dithiol and bis-alkene diketal monomer selection. Ultimately, these changes in hydrophobicity/hydrophilicity were found to affect the rate in which each system would become saturated with the degradation media.

Each of these chapters highlight the usefulness of thiol-X “click” chemistries and act as a platform from which further research can be conducted. In particular, the “one-pot two-step” approach described herein offers a route to CANs from all commercially available starting materials. While this simplifies our approach, it does limit the building blocks able to be utilized in altering network architecture. Therefore, the monomer library should be expanded upon through synthetic means. We suggest that a good starting point would be to synthesize a monomer compatible with this system that contains a tethered DBN unit. This will alleviate the need of the addition of external DBN exchange catalyst. Nevertheless, we expect that the work presented herein to serve as a springboard by which further research can be launched.

APPENDIX A - Supplemental Information to Chapter III

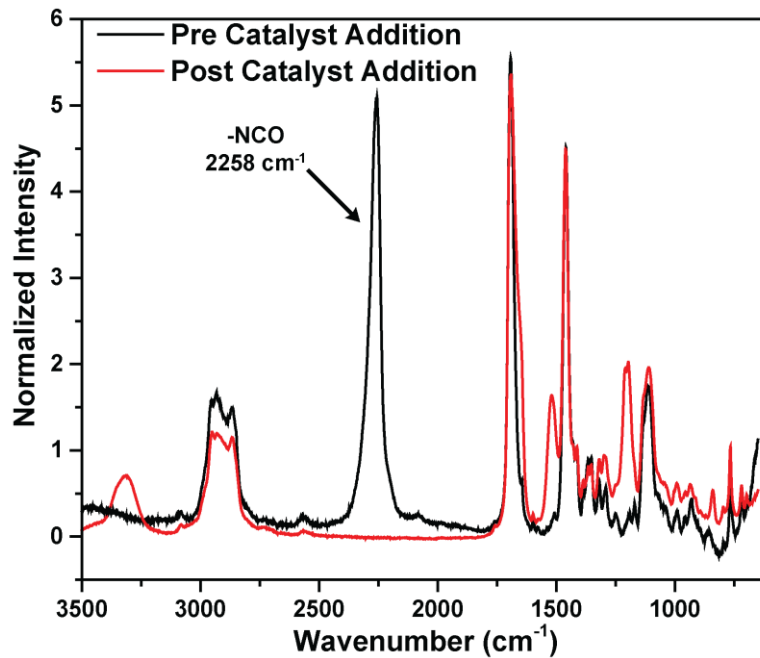


Figure A.1 FTIR analysis of *F2* resin before and after the addition of DBN catalyst.

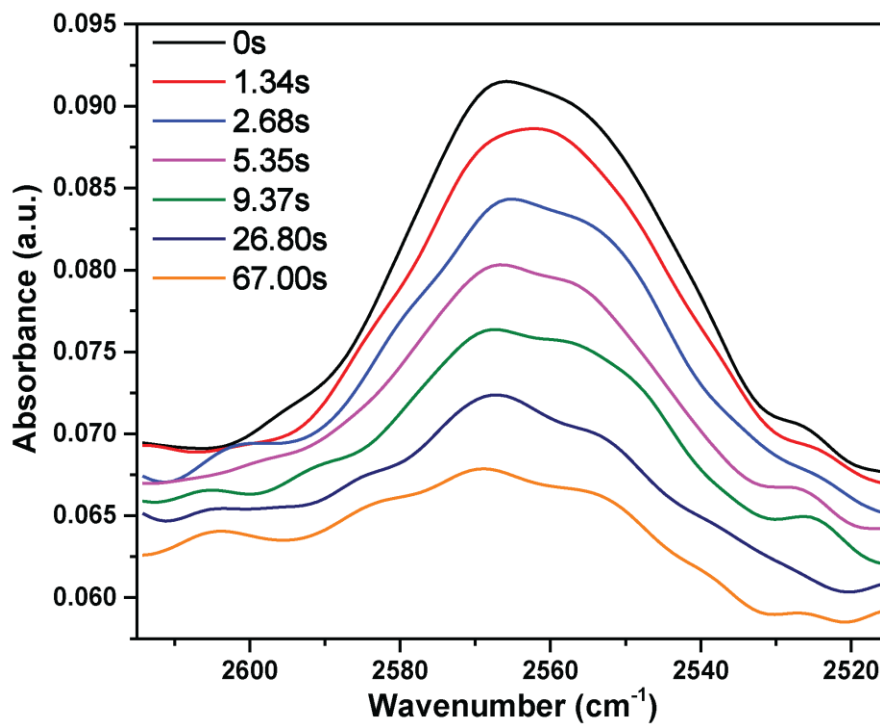


Figure A.2 Reduction in the characteristic thiol peak of *F2* resin due to UV exposure.

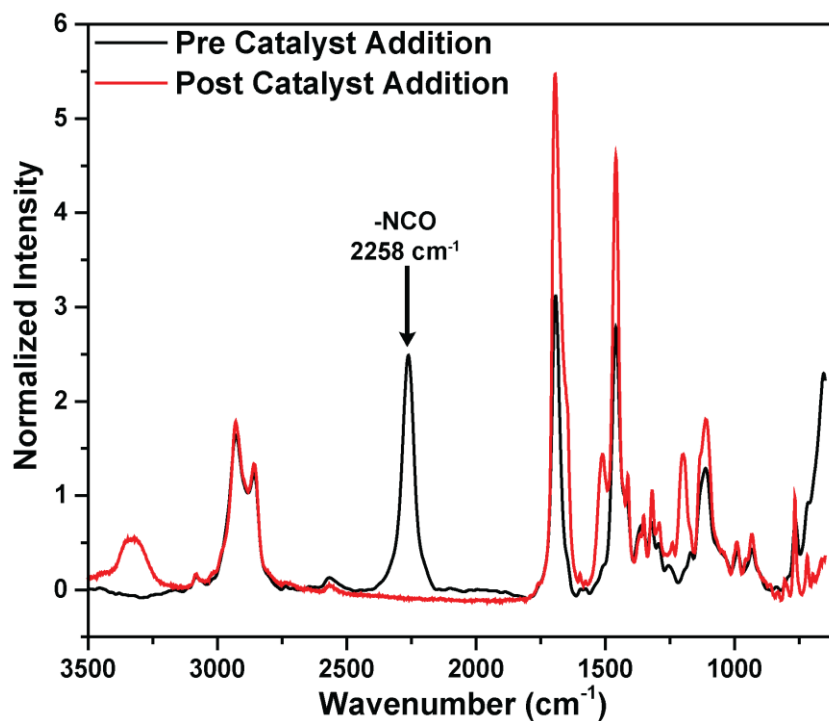


Figure A.3 FTIR analysis of *F3* resin before and after the addition of DBN catalyst.

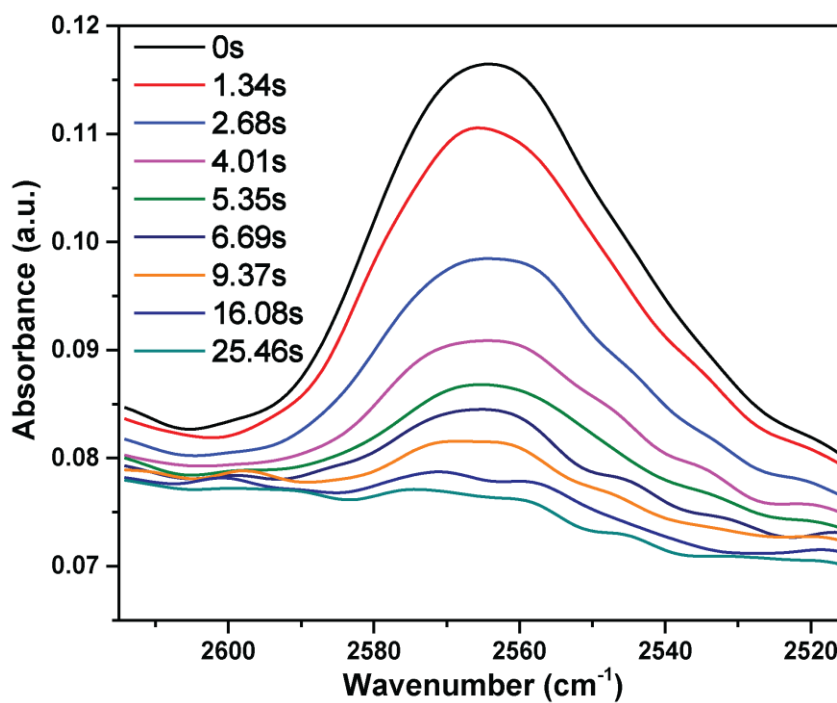


Figure A.4 Reduction in the characteristic thiol peak of *F3* resin due to UV exposure.

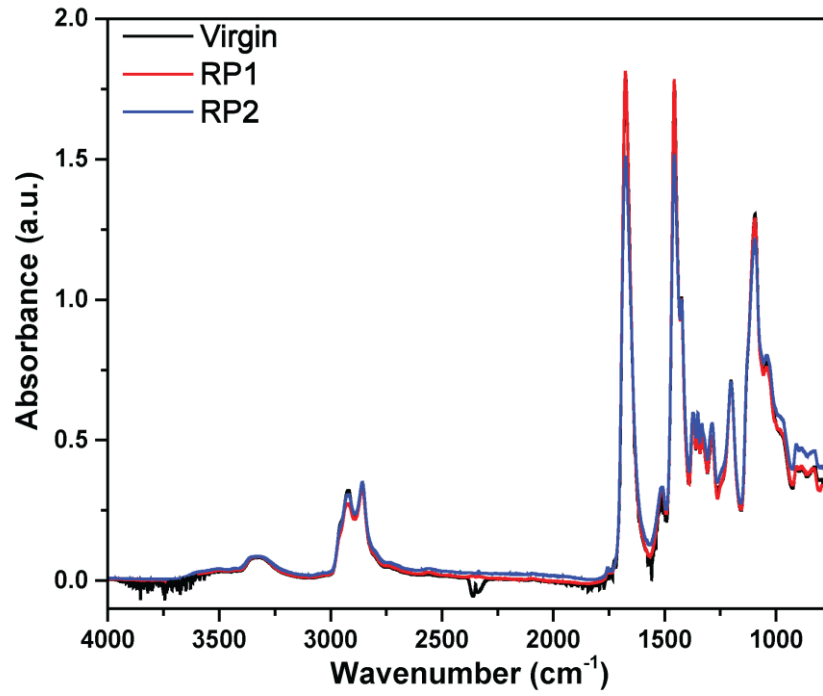


Figure A.5 ATR spectra of **F1** throughout reprocessing.

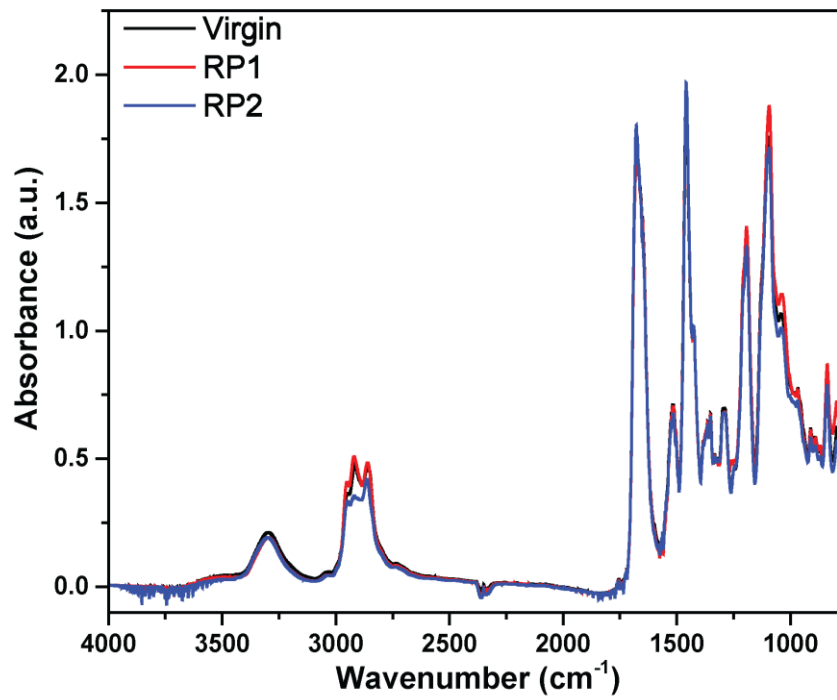


Figure A.6 ATR spectra of **F2** throughout reprocessing.

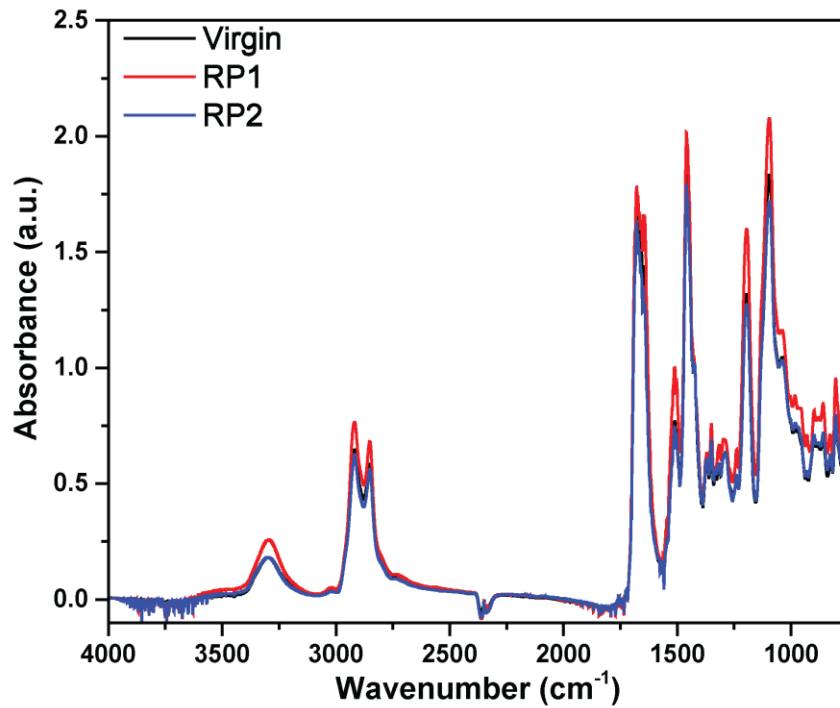


Figure A.7 ATR spectra of **F3** throughout reprocessing.

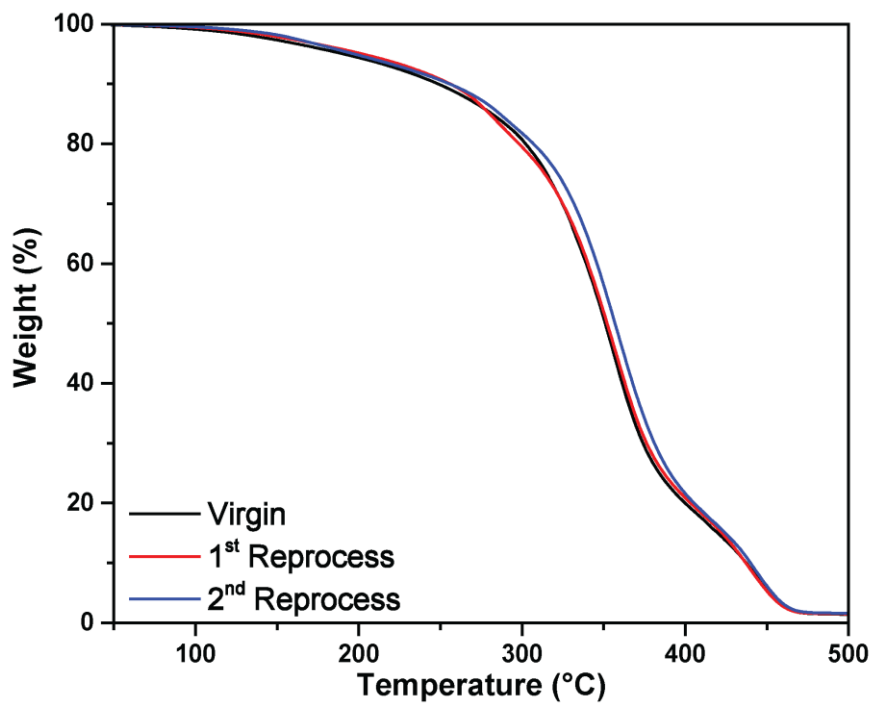


Figure A.8 TGA thermogram of **F1** throughout reprocessing.

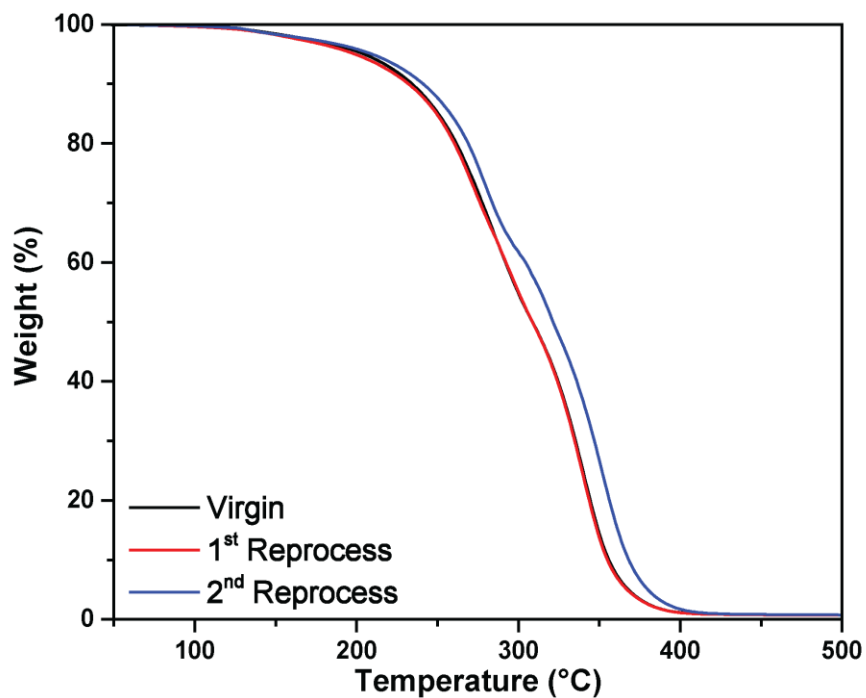


Figure A.9 TGA thermogram of F2 throughout reprocessing.

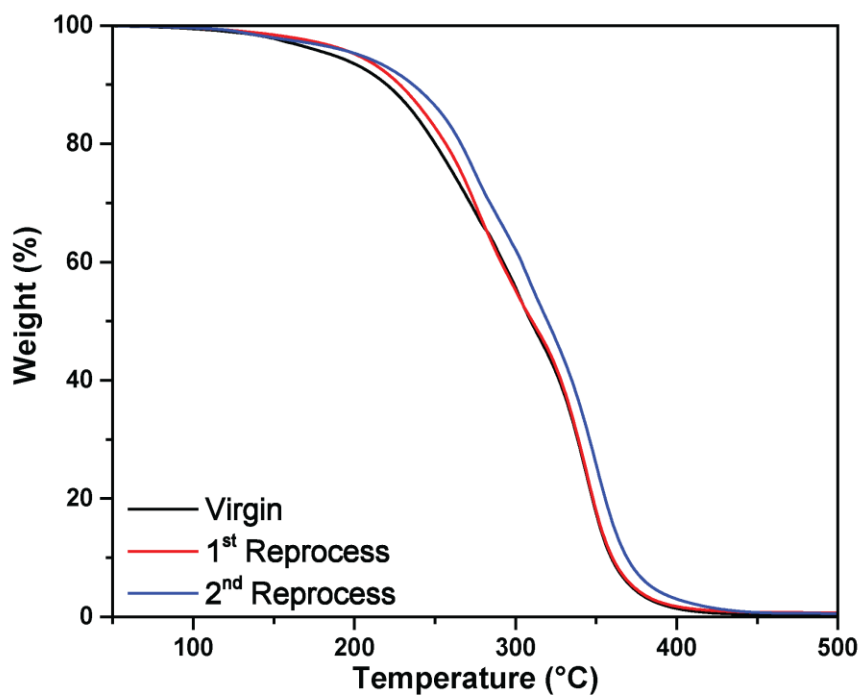


Figure A.10 TGA thermogram of F3 throughout reprocessing.

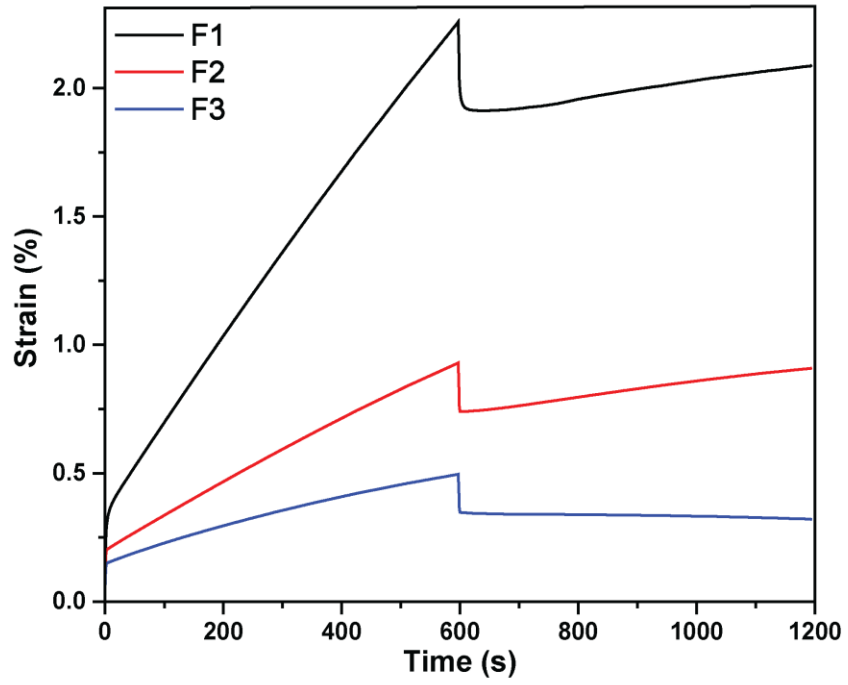


Figure A.11 *Creep/recovery results for F1 – F3.*

APPENDIX B – Supplemental Information to Chapter IV

Table B.1 Summary of  $\tau^*$  values of the excess thiol systems.

Temperature (°C)	F1 $\tau^*$ (s)	+5% $\tau^*$ (s)	+10% $\tau^*$ (s)
80	159.67	65.75	43.82
90	74.33	33.74	30.44
100	46.08	19.62	19.91
110	26.16	11.89	13.68
120	20.50	7.48	8.07

Table B.2 Summary of  $\tau^*$  values of the deficient thiol systems.

Temperature (°C)	-5% $\tau^*$ (s)	-10% $\tau^*$ (s)
70	253.69	1499.76
80	93.55	263.73
90	51.32	179.04
100	27.36	39.80
110	16.26	29.70
120	12.25	15.92
130	9.24	11.20

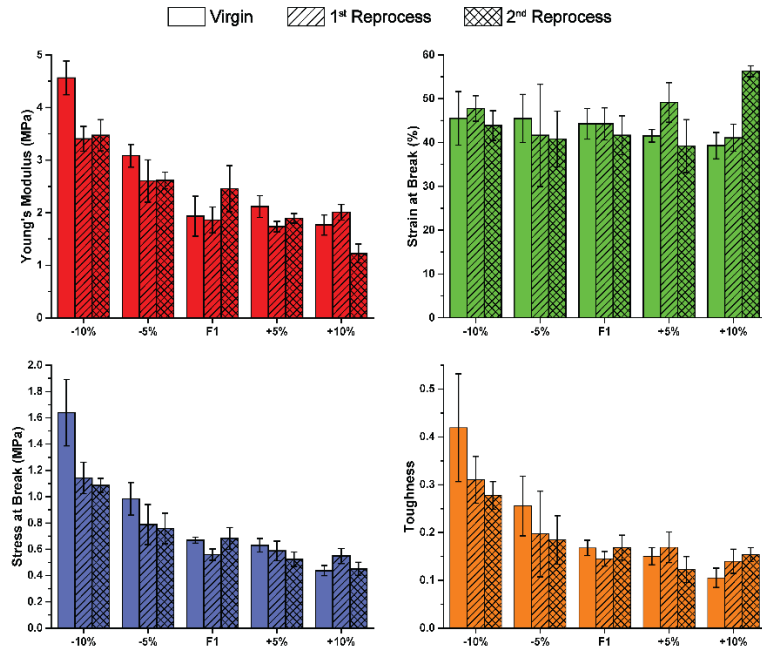


Figure B.1 Bar graphs of key physical properties throughout reprocessing for each of the altered thiol systems.

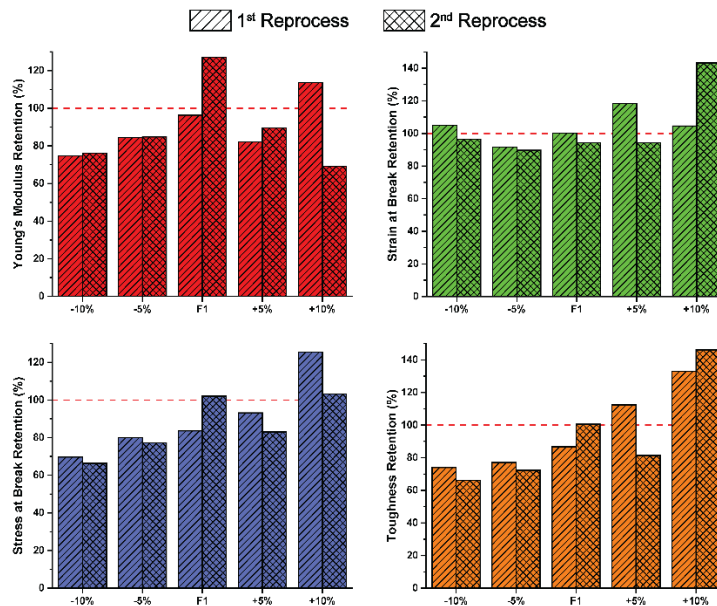


Figure B.2 Bar graphs of key physical property retention throughout reprocessing for each of the altered thiol systems.

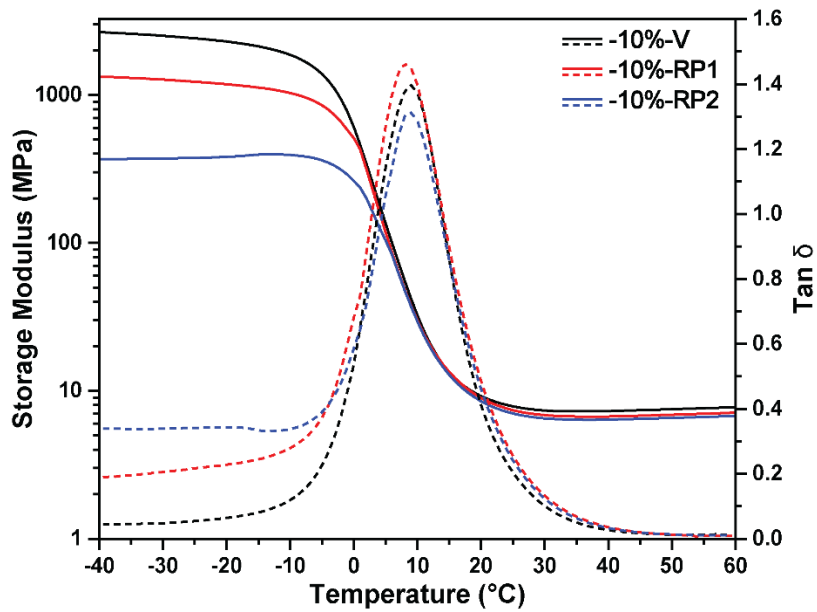


Figure B.3 DMA of the -10% thiol system throughout reprocessing.

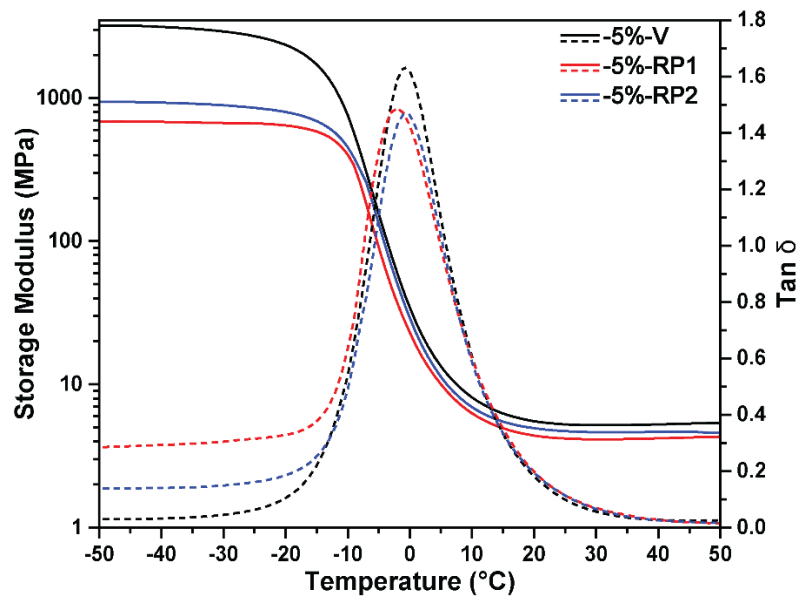


Figure B.4 DMA of the -5% thiol system throughout reprocessing.

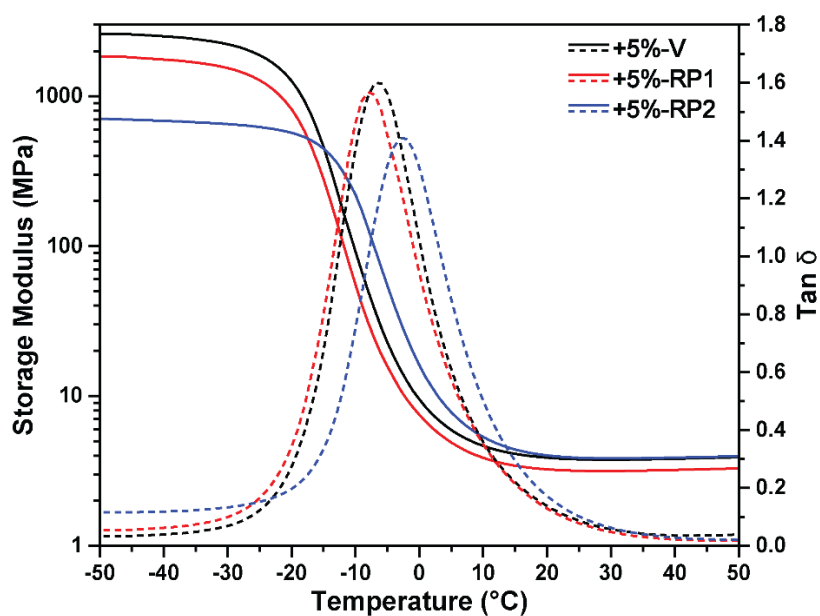
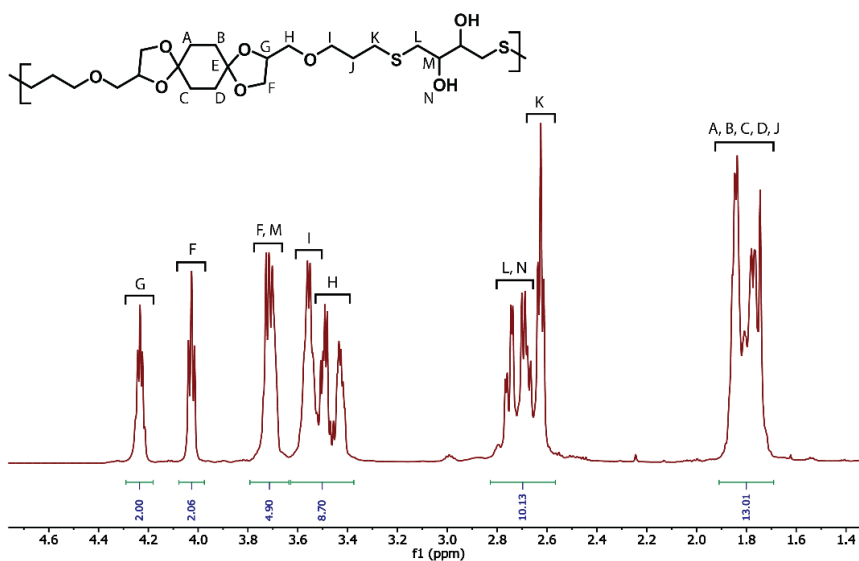


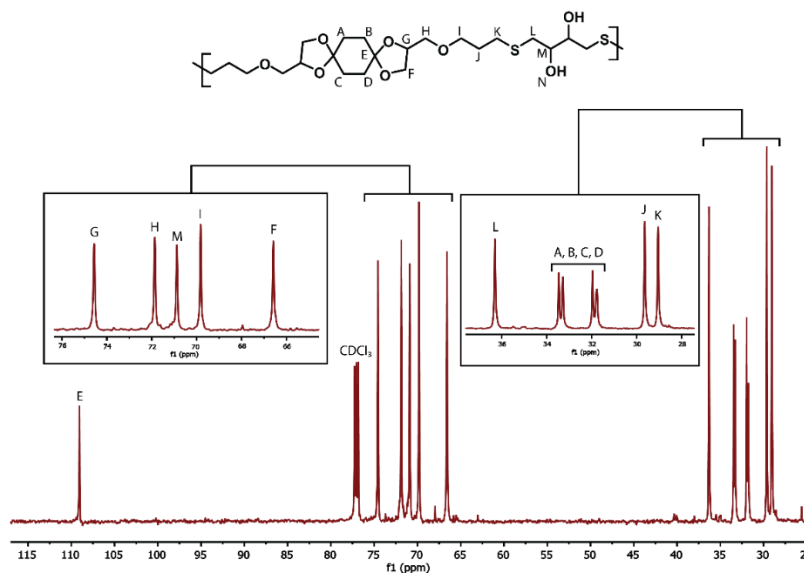
Figure B.5 DMA of the +5% thiol system throughout reprocessing.

APPENDIX C Supplemental Information to Chapter V



$^1\text{H}$  NMR (600 MHz, Chloroform- $d$ )  $\delta$  4.24 (p,  $J$  = 5.58 Hz, 2H), 4.01 (dd,  $J$  = 8.4, 6.4 Hz, 2H), 3.74 – 3.65 (m, 4H), 3.58 – 3.49 (m, 4H), 3.44 (ddd,  $J$  = 37.9, 10.1, 5.1 Hz, 4H), 2.76 – 2.63 (m, 6H), 2.61 (td,  $J$  = 7.2, 1.7 Hz, 4H), 1.87 – 1.69 (m, 12H).

Figure C.1  $^1\text{H}$ -NMR Spectrum of Polymer **9**.



$^{13}\text{C}$  NMR (151 MHz, Chloroform- $d$ )  $\delta$  109.05 (C), 74.58 (CH), 74.55 (CH), 71.88 (CH<sub>2</sub>), 71.85 (CH<sub>2</sub>), 70.88 (CH), 69.82 (CH<sub>2</sub>), 66.59 (CH<sub>2</sub>), 66.57 (CH<sub>2</sub>), 36.30 (CH<sub>2</sub>), 33.46 (CH<sub>2</sub>), 33.30 (CH<sub>2</sub>), 33.27 (CH<sub>2</sub>), 31.96 (CH<sub>2</sub>), 31.96 (CH<sub>2</sub>), 31.80 (CH<sub>2</sub>), 31.76 (CH<sub>2</sub>), 29.64 (CH<sub>2</sub>), 29.05 (CH<sub>2</sub>), 29.03 (CH<sub>2</sub>).

Figure C.2  $^{13}\text{C}$ -NMR Spectrum of Polymer **9**.

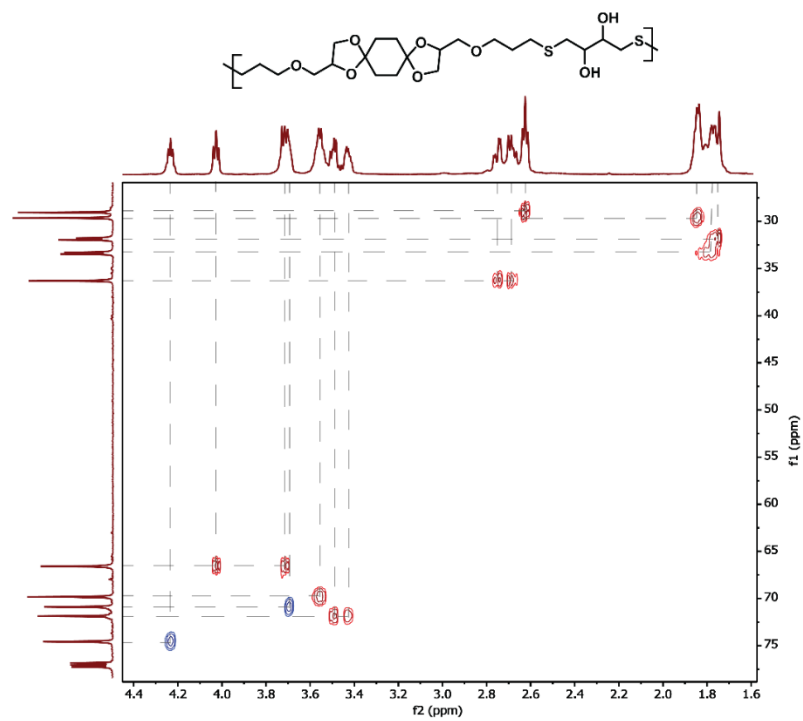


Figure C.3  $^1\text{H}$ - $^{13}\text{C}$  HSQC Spectrum of Polymer **9**.

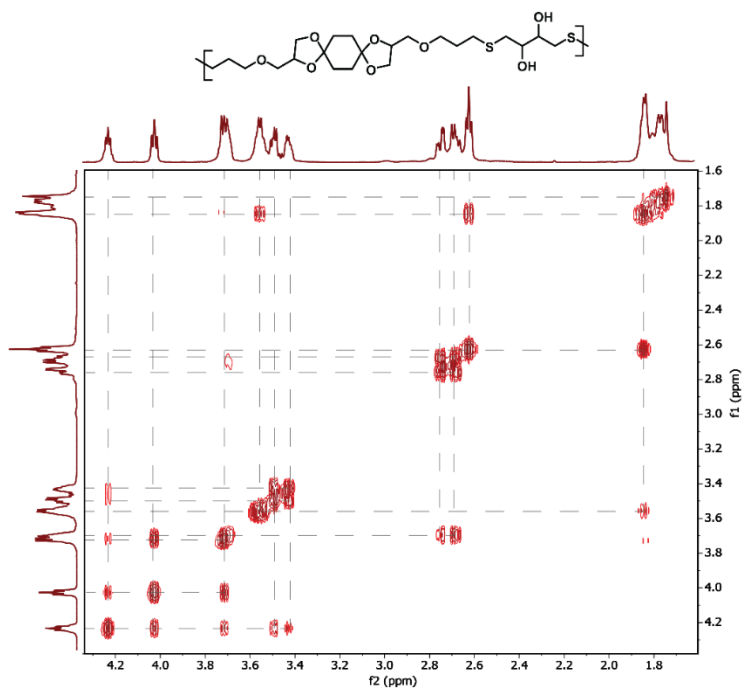
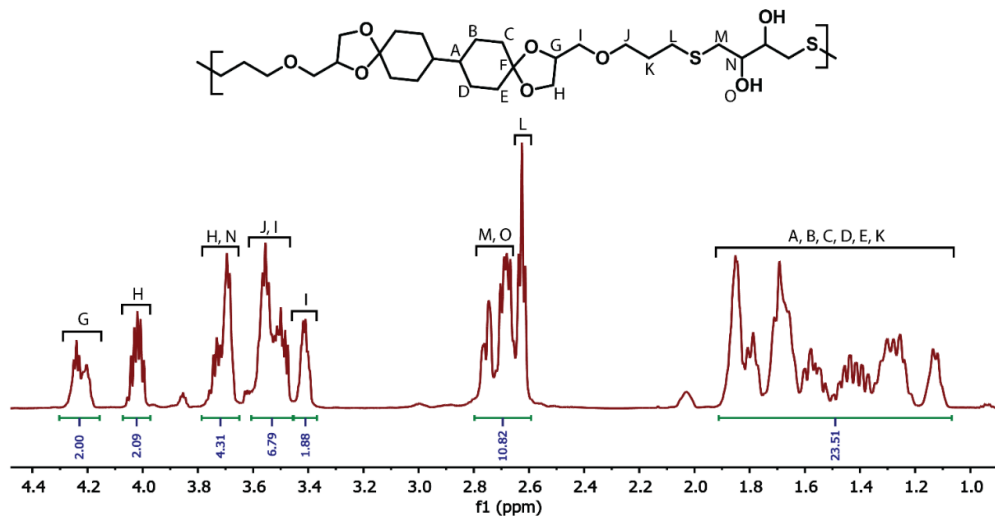
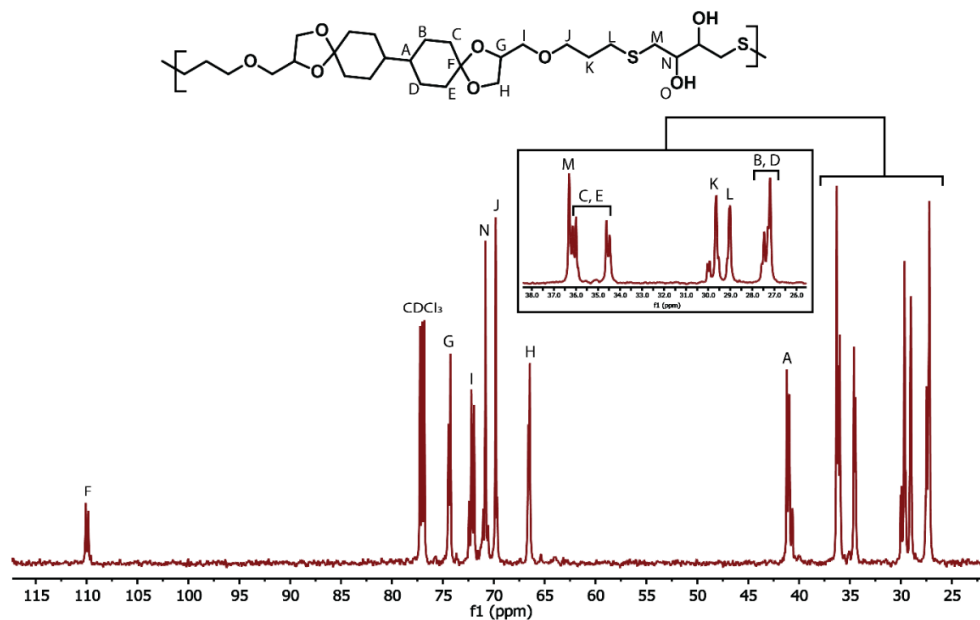


Figure C.4 COSY Spectrum of Polymer **9**.



$^1\text{H-NMR}$  (600 MHz, Chloroform- $d$ )  $\delta$  4.22 – 4.12 (m, 2H), 4.01 – 3.93 (m, 2H), 3.71 – 3.61 (m, 4H), 3.54 – 3.41 (m, 6H), 3.39 – 3.32, 2H), 2.73 – 2.59 (m, 6H), 2.57 (t,  $J = 7.2$  Hz, 4H), 1.80 (qt,  $J = 6.5, 2.6$  Hz, 4H), 1.74 (dt,  $J = 9.6, 3.1$  Hz, 2H), 1.68 – 1.56 (m, 6H), 1.56 – 1.46 (m, 2H), 1.45 – 1.14 (m, 6H), 1.13 – 0.99 (m, 2H).

Figure C.5  $^1\text{H-NMR}$  Spectrum of Polymer 10.



$^{13}\text{C-NMR}$  (151 MHz, Chloroform- $d$ )  $\delta$  110.07 (C), 109.83 (C), 74.44 (CH), 74.25 (CH), 72.42 (CH $_2$ ), 72.18 (CH $_2$ ), 71.93 (CH $_2$ ), 70.81 (CH), 69.81 (CH $_2$ ), 66.59 (CH $_2$ ), 66.47 (CH $_2$ ), 41.20 (CH), 41.04 (CH), 40.96 (CH), 36.31 (CH $_2$ ), 36.14 (CH $_2$ ), 35.99 (CH $_2$ ), 34.62 (CH $_2$ ), 34.47 (CH $_2$ ), 29.67 (CH $_2$ ), 29.64 (CH $_2$ ), 29.52 (CH $_2$ ), 29.14 (CH $_2$ ), 29.05 (CH $_2$ ), 29.00 (CH $_2$ ), 27.47 (CH $_2$ ), 27.29 (CH $_2$ ), 27.19 (CH $_2$ ).

Figure C.6  $^{13}\text{C-NMR}$  Spectrum of Polymer 10.

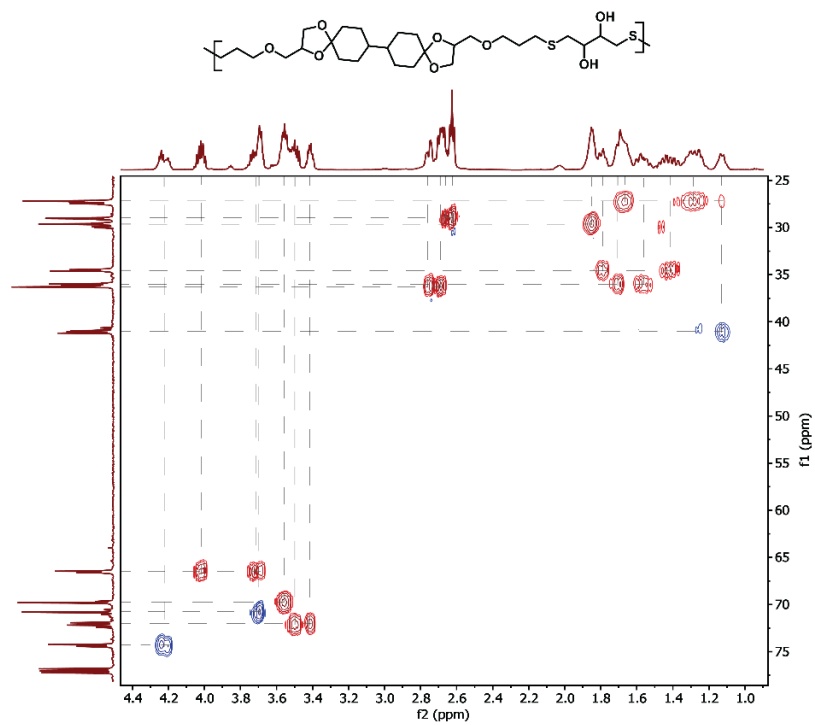


Figure C.7  $^1\text{H}$ - $^{13}\text{C}$  HSQC Spectrum of Polymer 10.

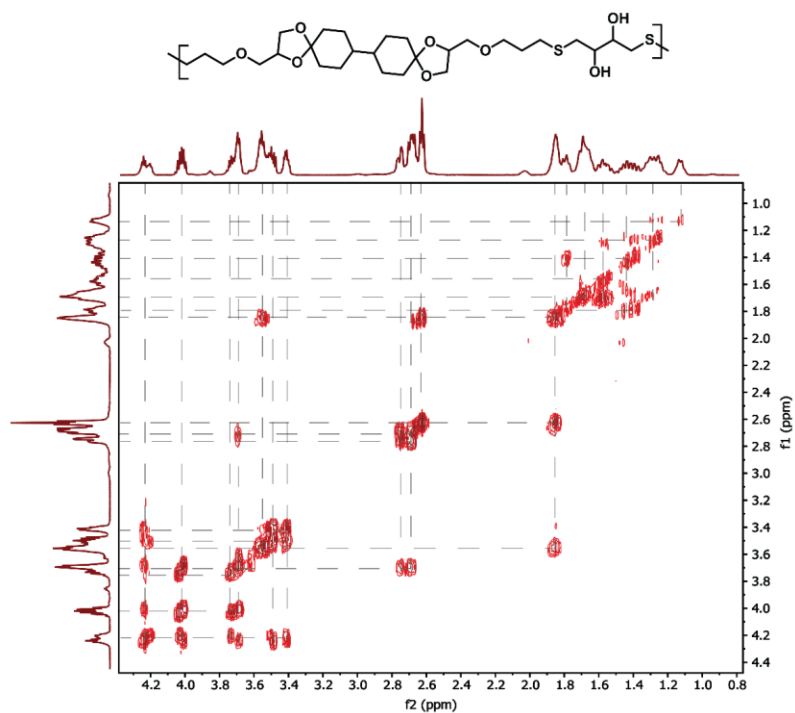
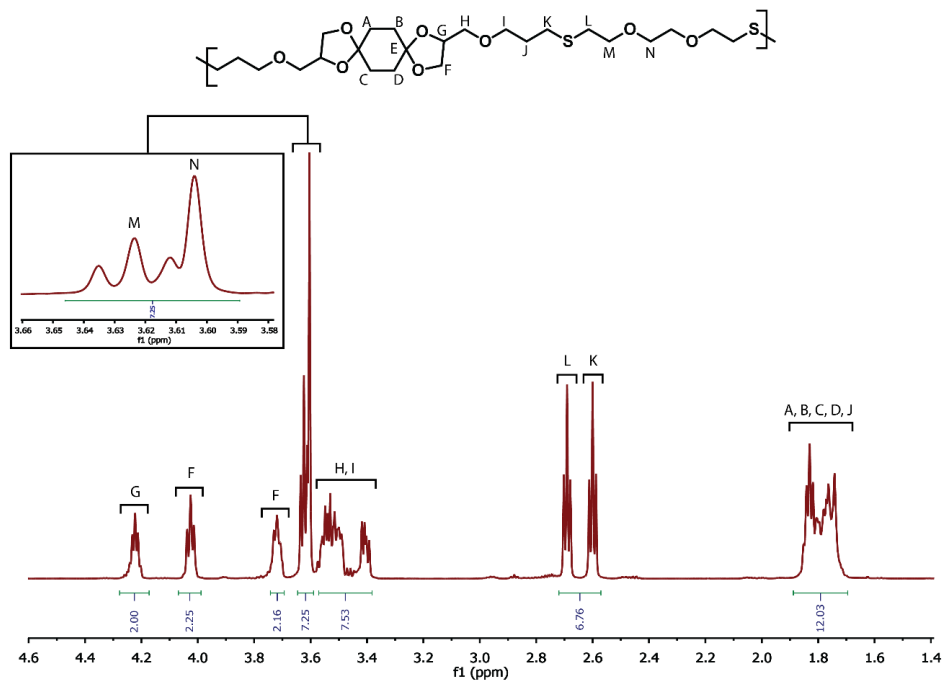
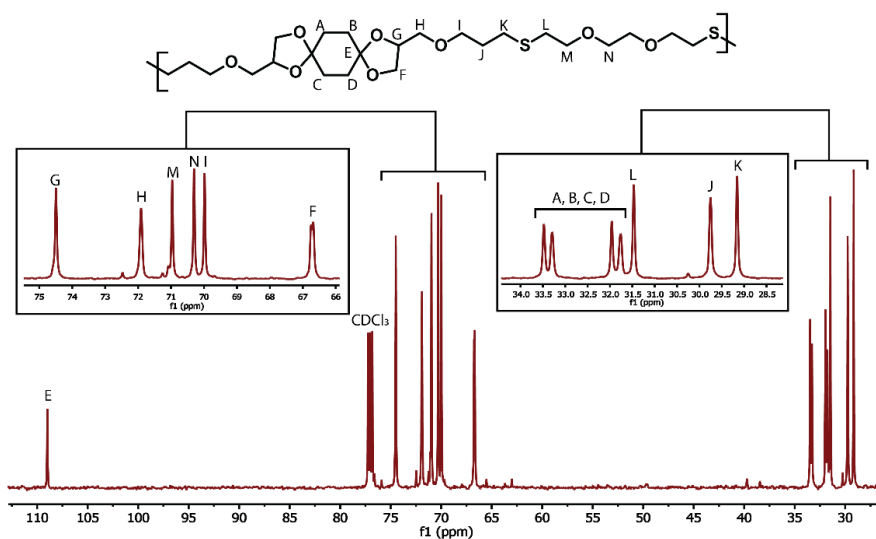


Figure C.8 COSY Spectrum of Polymer 10.



$^1\text{H}$  NMR (600 MHz, Chloroform- $d$ )  $\delta$  4.22 (td,  $J$  = 5.8, 1.7 Hz, 2H), 4.03 (ddd,  $J$  = 8.3, 6.3, 2.0 Hz, 2H), 3.74 – 3.69 (m, 2H), 3.62 (td, 7.1, 0.9 Hz, 4H), 3.60 (s, 4H), 3.58 – 3.38 (m, 8H), 2.69 (td,  $J$  = 7.0, 1.0 Hz, 4H), 2.60 (t,  $J$  = 7.2 Hz, 4H), 1.88 – 1.69 (m, 12H).

Figure C.9  $^1\text{H}$ -NMR Spectrum of Polymer **11**.



$^{13}\text{C}$  NMR (151 MHz, Chloroform- $d$ )  $\delta$  109.00 (C), 108.97 (C), 74.50 (CH), 71.95 (CH $_2$ ), 71.91 (CH $_2$ ), 71.88 (CH $_2$ ), 70.96 (CH $_2$ ), 70.30 (CH $_2$ ), 69.98 (CH $_2$ ), 66.77 (CH $_2$ ), 66.74 (CH $_2$ ), 66.70 (CH $_2$ ), 66.67 (CH $_2$ ), 33.47 (CH $_2$ ), 33.31 (CH $_2$ ), 33.28 (CH $_2$ ), 31.96 (CH $_2$ ), 31.78 (CH $_2$ ), 31.75 (CH $_2$ ), 31.47 (CH $_2$ ), 29.77 (CH $_2$ ), 29.74 (CH $_2$ ), 29.16 (CH $_2$ ).

Figure C.10  $^{13}\text{C}$ -NMR Spectrum of Polymer **11**.

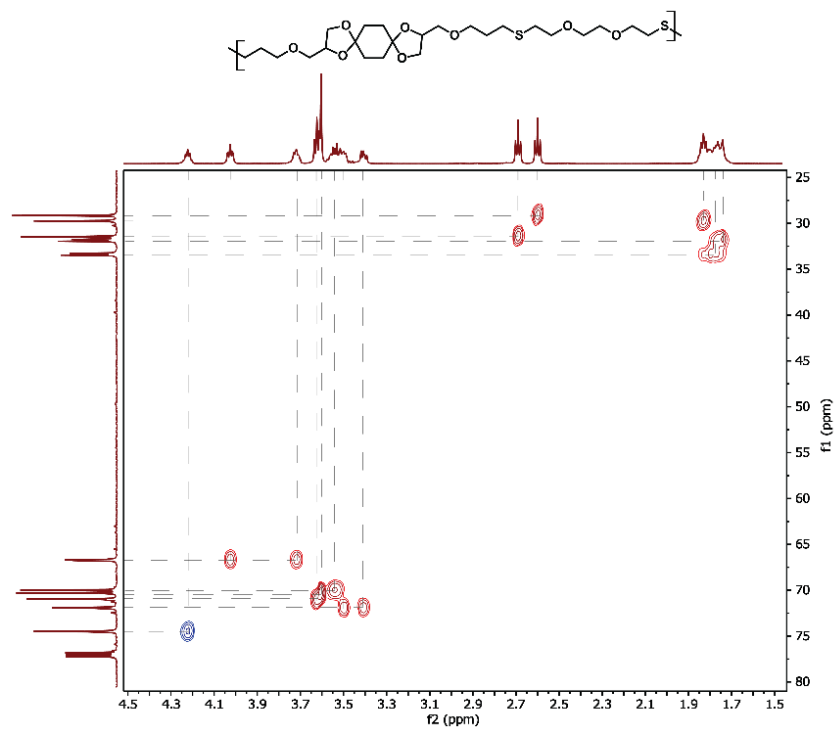


Figure C.11  $^1\text{H}$ - $^{13}\text{C}$  HSQC Spectrum of Polymer 11.

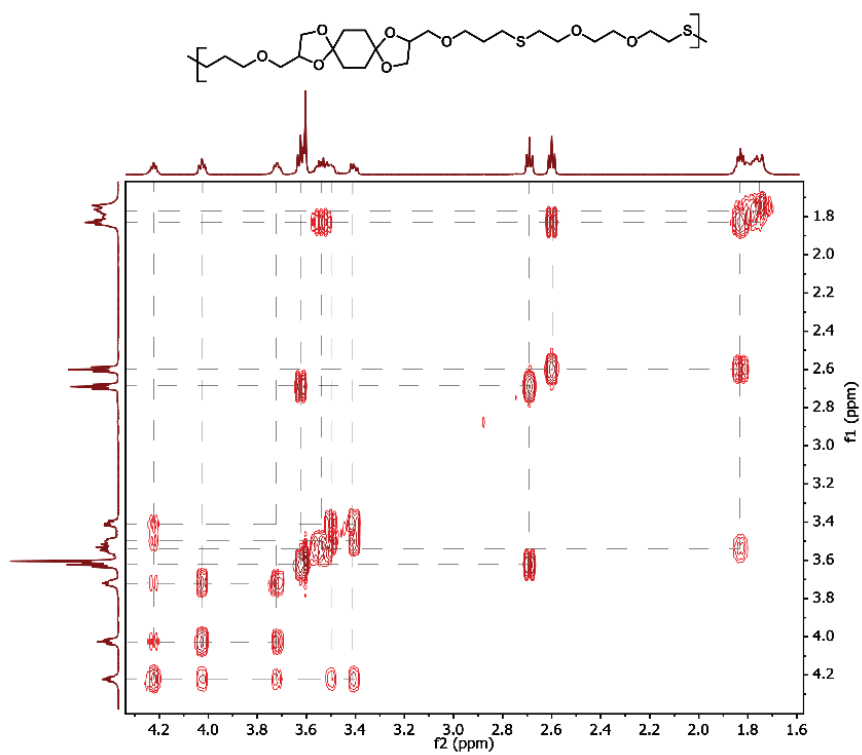
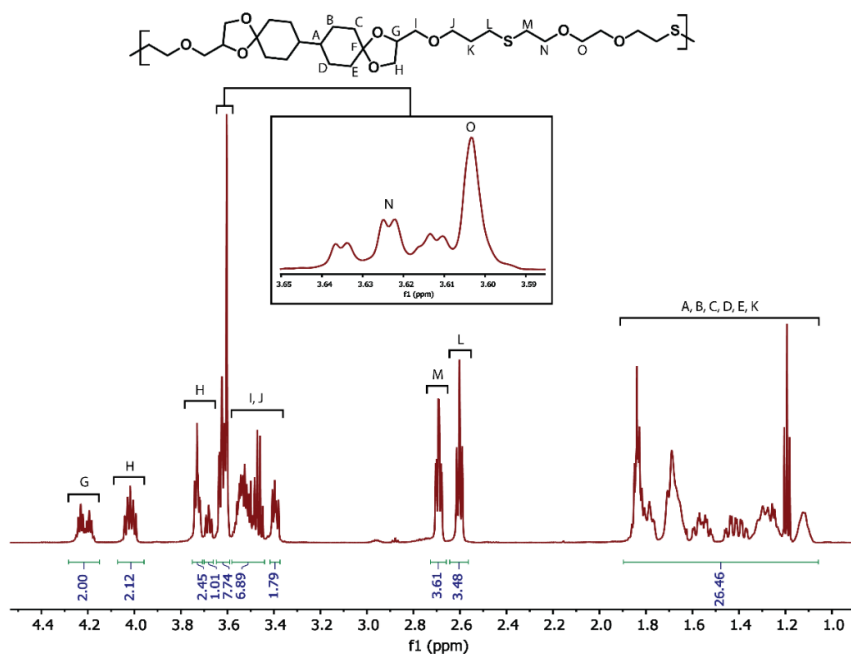
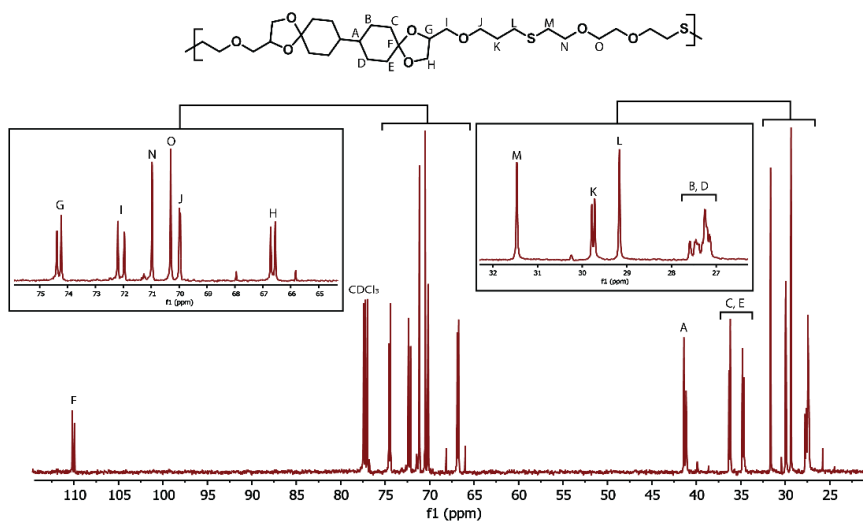


Figure C.12 COSY Spectrum of Polymer 11.



$^1\text{H}$  NMR (600 MHz, Chloroform- $d$ )  $\delta$  4.26 – 4.17 (m, 2H), 4.05 – 3.99 (m, 2H), 3.73 (td,  $J$  = 7.1, 2.0 Hz, 2H), 3.68 (ddd,  $J$  = 8.1, 6.2, 1.4 Hz, 1H), 3.62 (td,  $J$  = 7.1, 2.0 Hz, 4H), 3.60 (s, 4H), 3.58 – 3.44 (m, 6H), 3.39 (dd,  $J$  = 9.9, 5.9 Hz, 2H), 2.69 (td, 7.0, 2.4 Hz, 4H), 2.60 (t,  $J$  = 7.2 Hz, 4H), 1.87 – 1.75 (m, 6H), 1.73 – 1.61 (m, 6H), 1.61 – 1.50 (m, 2H), 1.41 (dtd,  $J$  = 26.3, 13.1, 3.9 Hz, 2H), 1.34 – 1.22 (m, 4H), 1.19 (t,  $J$  = 7.0 Hz, 2H), 1.17 – 1.08 (m, 2H).

Figure C.13  $^1\text{H}$ -NMR Spectrum of Polymer 12.



$^{13}\text{C}$  NMR (151 MHz, Chloroform- $d$ )  $\delta$  110.00 (C), 109.77 (C), 74.38 (CH), 74.23 (CH), 72.20 ( $\text{CH}_2$ ), 71.96 ( $\text{CH}_2$ ), 70.97 ( $\text{CH}_2$ ), 70.30 ( $\text{CH}_2$ ), 69.99 ( $\text{CH}_2$ ), 69.96 ( $\text{CH}_2$ ), 66.72 ( $\text{CH}_2$ ), 66.56 ( $\text{CH}_2$ ), 41.22 (CH), 40.94 (CH), 40.93 (CH), 36.13 ( $\text{CH}_2$ ), 36.00 ( $\text{CH}_2$ ), 34.62

(CH<sub>2</sub>), 34.48 (CH<sub>2</sub>), 31.47 (CH<sub>2</sub>), 29.79 (CH<sub>2</sub>), 29.72 (CH<sub>2</sub>), 29.17 (CH<sub>2</sub>), 27.58 (CH<sub>2</sub>), 28.48 (CH<sub>2</sub>), 27.45 (CH<sub>2</sub>), 27.45 (CH<sub>2</sub>), 27.39 (CH<sub>2</sub>), 27.24 (CH<sub>2</sub>), 27.20 (CH<sub>2</sub>), 27.16 (CH<sub>2</sub>).

Figure C.14 <sup>13</sup>C-NMR Spectrum of Polymer 12.

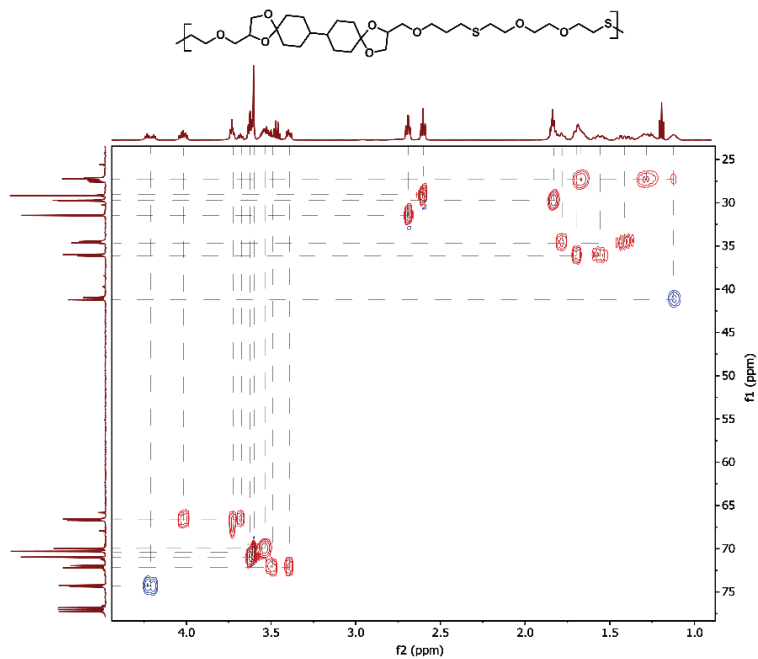


Figure C.15 <sup>1</sup>H-<sup>13</sup>C HSQC Spectrum of Polymer 12.

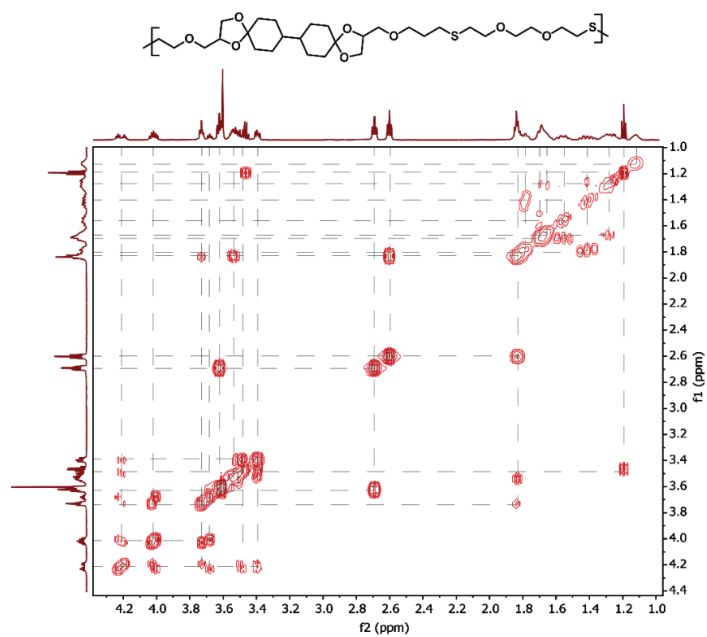
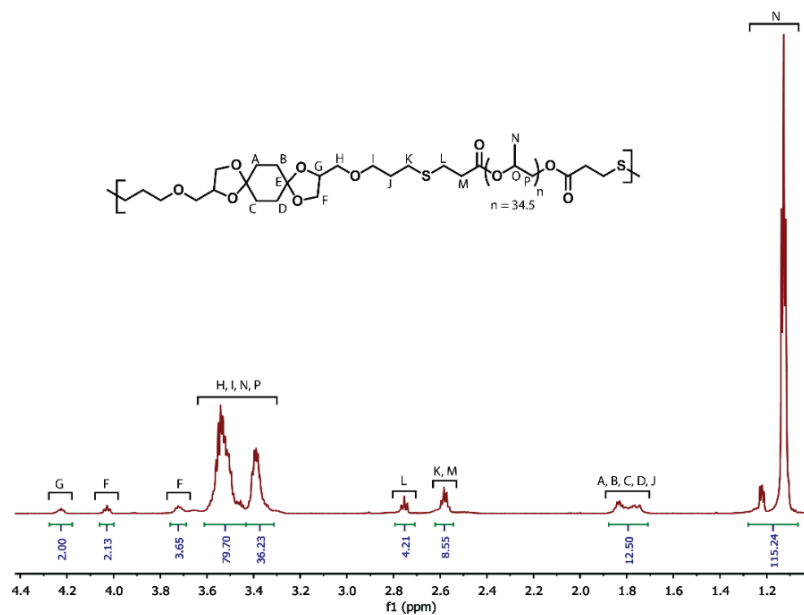
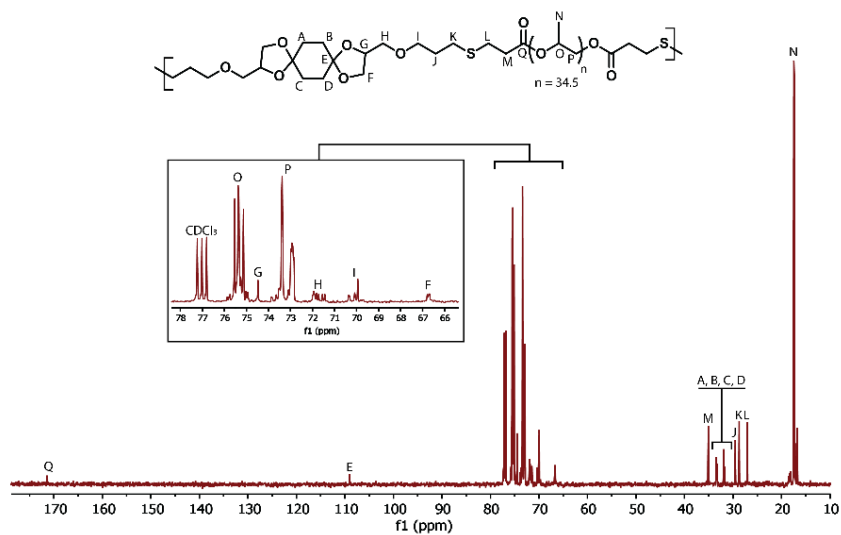


Figure C.16 COSY Spectrum of Polymer 12.



$^1\text{H}$  NMR (600 MHz, Chloroform-d)  $\delta$  4.23 (pt,  $J = 6.0, 2.5$  Hz, 2H), 4.03 (ddd,  $J = 8.3, 6.2, 2.0$  Hz, 2H), 3.75 – 3.69 (m, 2H), 3.61 – 3.44 (m, 78H), 3.38 (qd,  $J = 9.6, 8.2, 3.4$  Hz, 35H), 2.75 (t,  $J = 7.5$  Hz, 4H), 2.58 (td,  $J = 9.5, 8.3, 5.7$  Hz, 8H), 1.87 – 1.72 (m, 12H), 1.22 (dd,  $J = 6.5, 4.3$  Hz, 8H), 1.13 (t,  $J = 5.6, 106\text{H}$ ).

Figure C.17  $^1\text{H}$ -NMR Spectrum of Polymer 13.



$^{13}\text{C}$  NMR (151 MHz, Chloroform-d)  $\delta$  171.40 (C), 108.97 (C), 75.53 (CH), 75.45 (CH), 75.38 (CH), 75.34 (CH), 75.14 (CH), 74.47 (CH), 73.37 (CH<sub>2</sub>), 72.99 (CH<sub>2</sub>), 72.93 (CH<sub>2</sub>), 72.89 (CH<sub>2</sub>), 72.85 (CH<sub>2</sub>), 71.94 (CH<sub>2</sub>), 71.82 (CH<sub>2</sub>), 71.44 (CH<sub>2</sub>), 70.09 (CH<sub>2</sub>), 69.94 (CH<sub>2</sub>), 66.76 (CH<sub>2</sub>), 66.76 (CH<sub>2</sub>), 35.09 (CH<sub>2</sub>), 33.47 (CH<sub>2</sub>), 33.28 (CH<sub>2</sub>), 31.94 (CH<sub>2</sub>), 31.77 (CH<sub>2</sub>), 39.54 (CH<sub>2</sub>), 28.73 (CH<sub>2</sub>), 27.04 (CH<sub>2</sub>), 17.46 (CH<sub>3</sub>), 17.34 (CH<sub>3</sub>).

Figure C.18  $^{13}\text{C}$ -NMR Spectrum of Polymer 13.

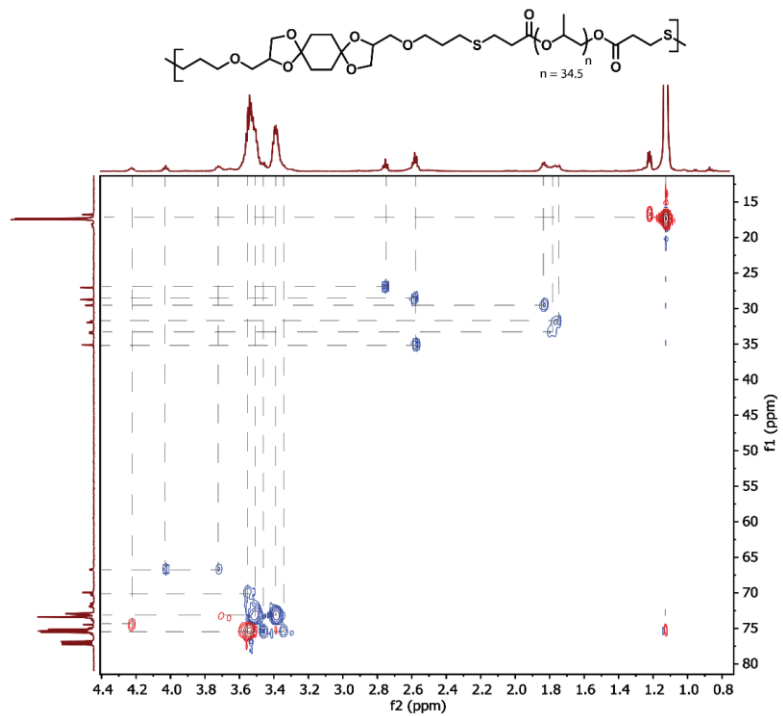


Figure C.19  $^1\text{H}$ - $^{13}\text{C}$  HSQC Spectrum of Polymer 13.

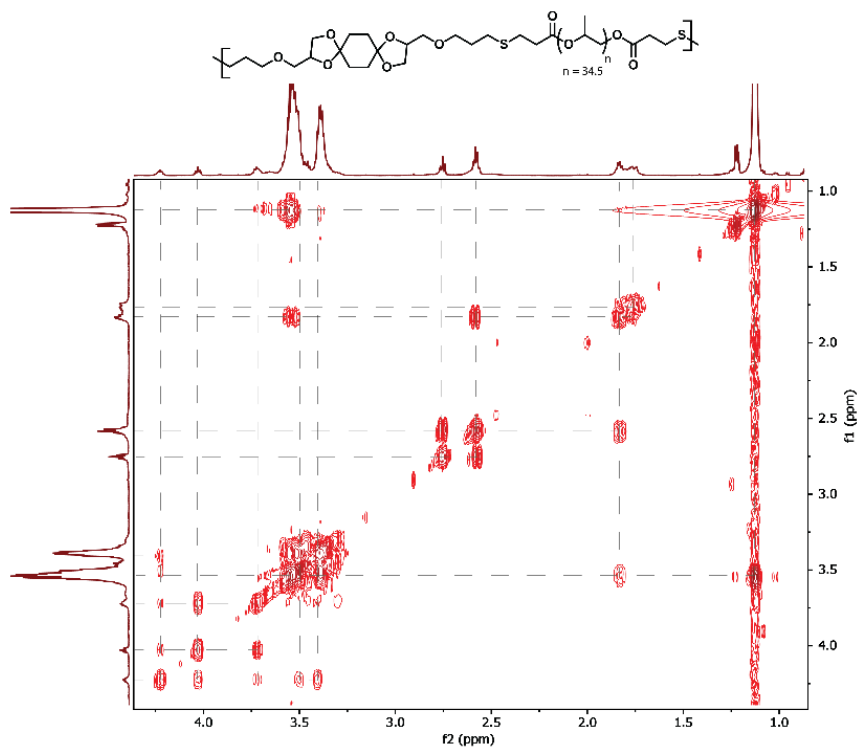
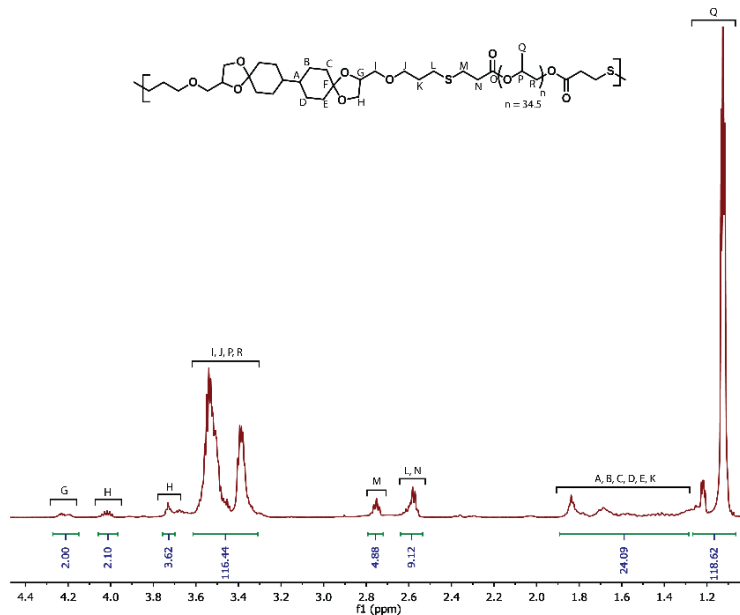
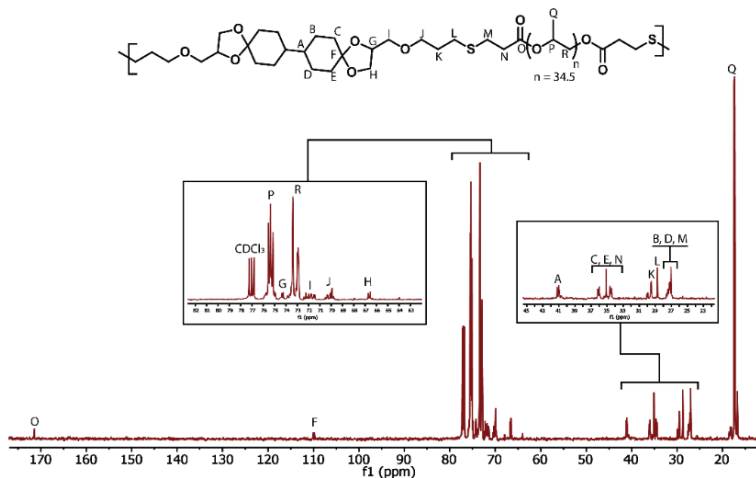


Figure C.20 COSY Spectrum of Polymer 13.



$^1\text{H}$  NMR (600 MHz, Chloroform- $d$ )  $\delta$  4.27 – 4.16 (m, 2H), 4.02 (dt,  $J$  = 14.4, 7.2 Hz, 2H), 3.75 – 3.63 (m, 4H), 3.60 – 3.44 (m, 78H), 3.38 (dq,  $J$  = 14.5, 9.5, 7.6 Hz, 35H), 2.76 (qd,  $J$  = 8.6, 7.4, 2.3 Hz, 4H), 2.58 (dq,  $J$  = 9.2, 7.1 Hz, 9H), 1.89 – 1.75 (m, 6H), 1.75 – 1.62 (m, 6H), 1.62 – 1.51 (m, 2H), 1.51 – 1.31 (m, 4H), 1.35 – 1.24 (m, 4H), 1.22 (dd,  $J$  = 3.5, 4.3 Hz, 8H), 1.12 (t,  $J$  = 5.6 Hz, 106H).

Figure C.21  $^1\text{H}$ -NMR Spectrum of Polymer **14**.



$^{13}\text{C}$  NMR (151 MHz, Chloroform- $d$ )  $\delta$  171.41 (C), 110.01 (C), 109.77 (C), 75.53 (CH), 75.38 (CH), 75.34 (CH), 75.13 (CH), 74.36 (CH), 74.21 (CH), 73.40 (CH<sub>2</sub>), 73.37 (CH<sub>2</sub>), 72.98 (CH<sub>2</sub>), 72.93 (CH<sub>2</sub>), 72.89 (CH<sub>2</sub>), 72.84 (CH<sub>2</sub>), 72.22 (CH<sub>2</sub>), 71.98 (CH<sub>2</sub>), 71.81 (CH<sub>2</sub>), 71.71 (CH<sub>2</sub>), 71.55 (CH<sub>2</sub>), 70.35 (CH<sub>2</sub>), 70.08 (CH<sub>2</sub>), 69.95 (CH<sub>2</sub>), 69.92 (CH<sub>2</sub>), 69.79 (CH<sub>2</sub>), 66.73 (CH<sub>2</sub>), 66.55 (CH<sub>2</sub>), 41.22 (CH), 40.95 (CH), 36.15 (CH<sub>2</sub>), 35.99 (CH<sub>2</sub>), 35.09 (CH<sub>2</sub>), 34.63 (CH<sub>2</sub>), 34.46 (CH<sub>2</sub>), 29.57 (CH<sub>2</sub>), 29.50 (CH<sub>2</sub>), 28.73 (CH<sub>2</sub>), 27.45 (CH<sub>2</sub>), 27.19 (CH<sub>2</sub>), 27.03 (CH<sub>2</sub>), 18.22 (CH<sub>3</sub>), 17.46 (CH<sub>3</sub>), 17.34 (CH<sub>3</sub>), 16.75 (CH<sub>3</sub>).

Figure C.22  $^{13}\text{C}$ -NMR Spectrum of Polymer **14**.

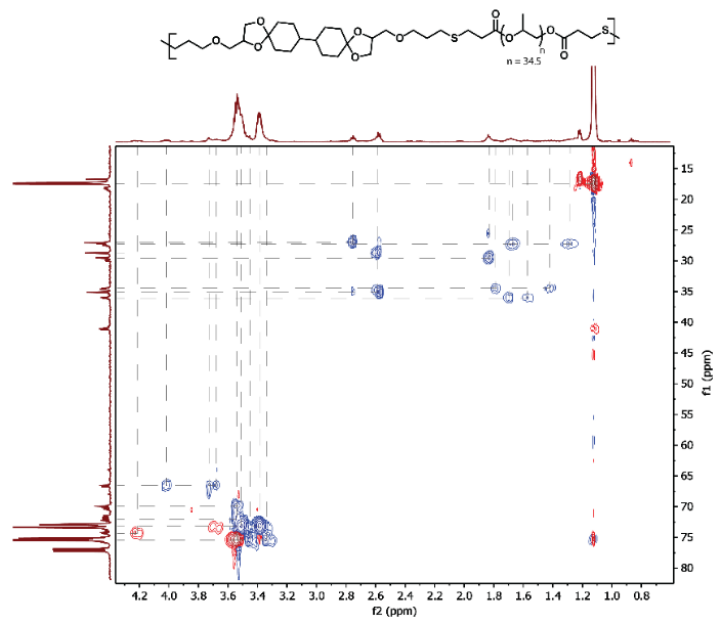


Figure C.23  $^1\text{H}$ - $^{13}\text{C}$  HSQC Spectrum of Polymer 14.

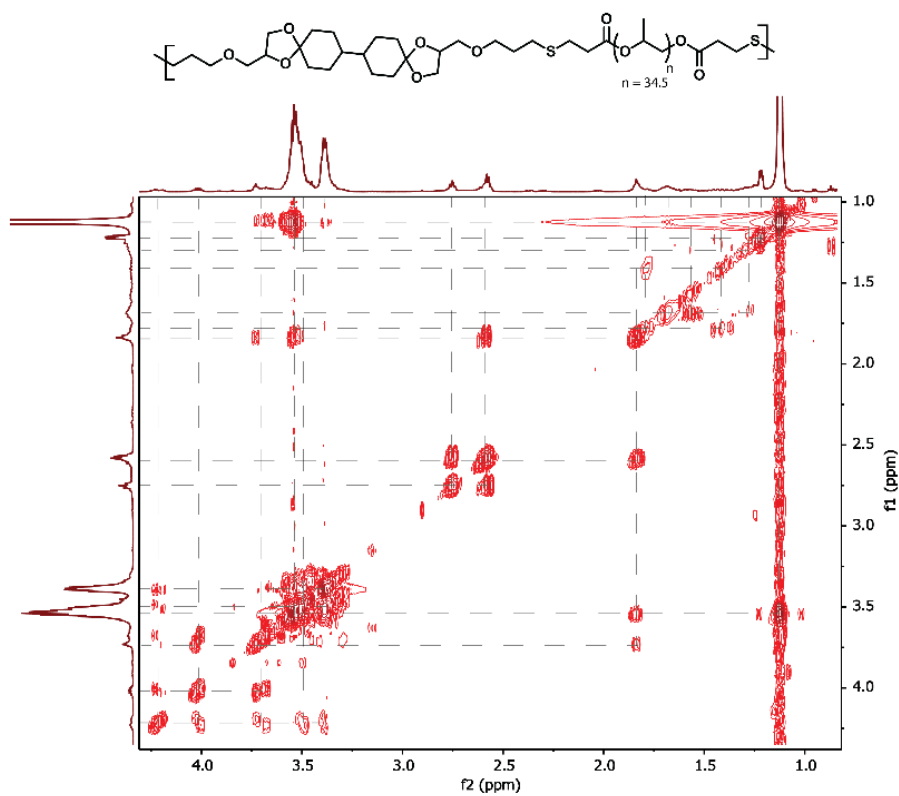


Figure C.24 COSY Spectrum of Polymer 14.

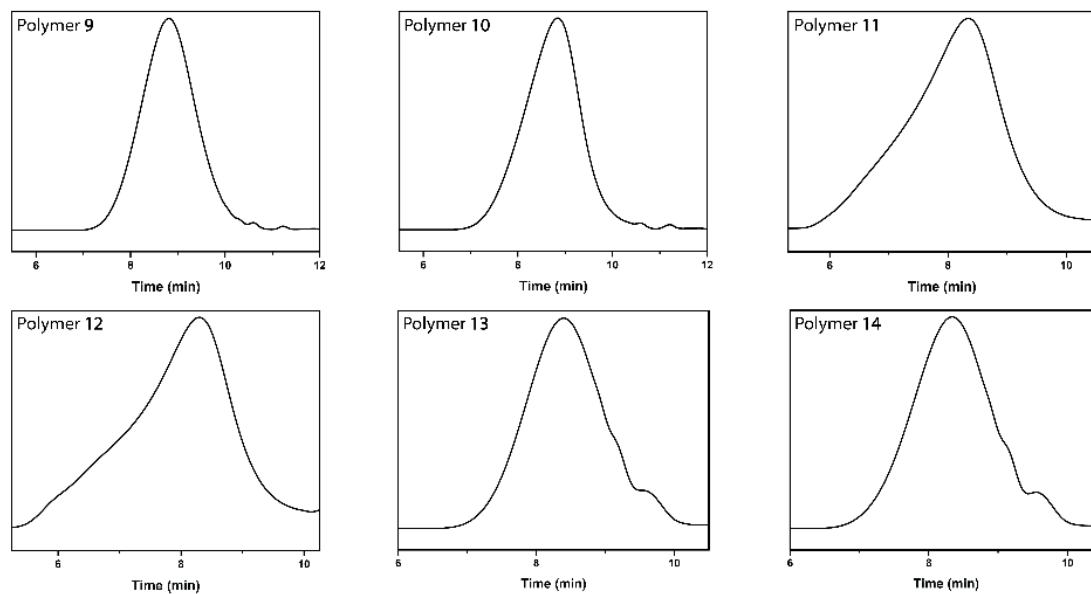


Figure C.25 Initial SEC chromatograms of polymers 9-14.

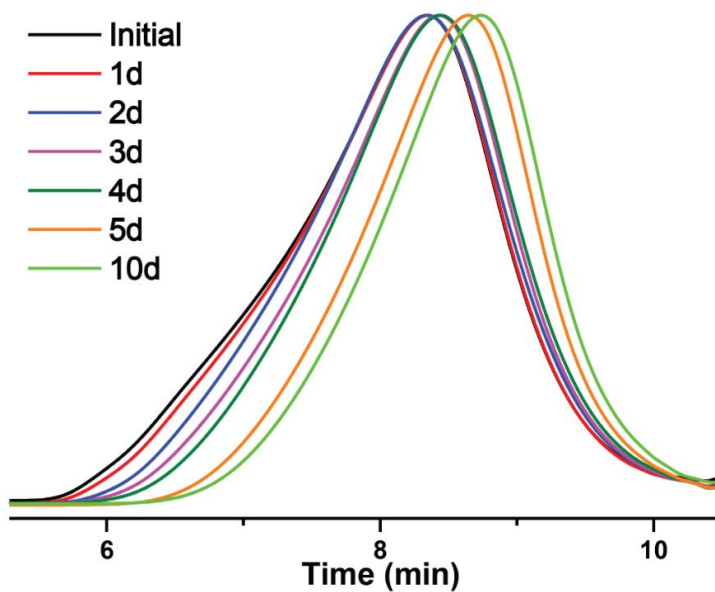


Figure C.26 SEC Chromatograms of Polymer 11 Throughout Degradation Under Acidic Conditions

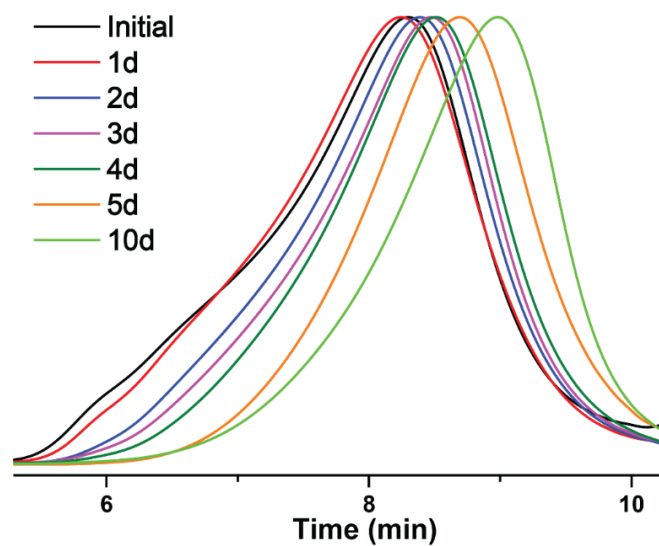


Figure C.27 SEC Chromatograms of Polymer 12 Throughout Degradation Under Acidic Conditions

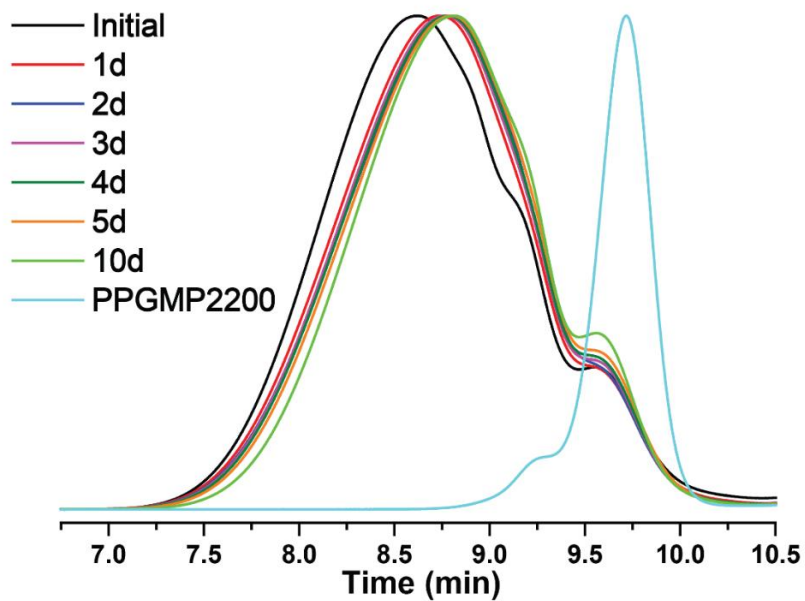


Figure C.28 SEC Chromatograms of Polymer 13 Throughout Degradation Under Acidic Conditions

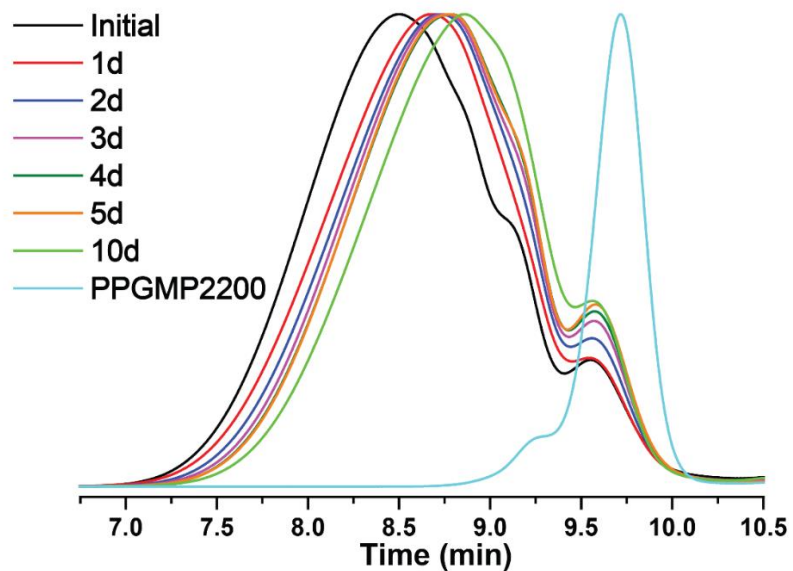


Figure C.29 SEC Chromatograms of Polymer 14 Throughout Degradation Under Acidic Conditions

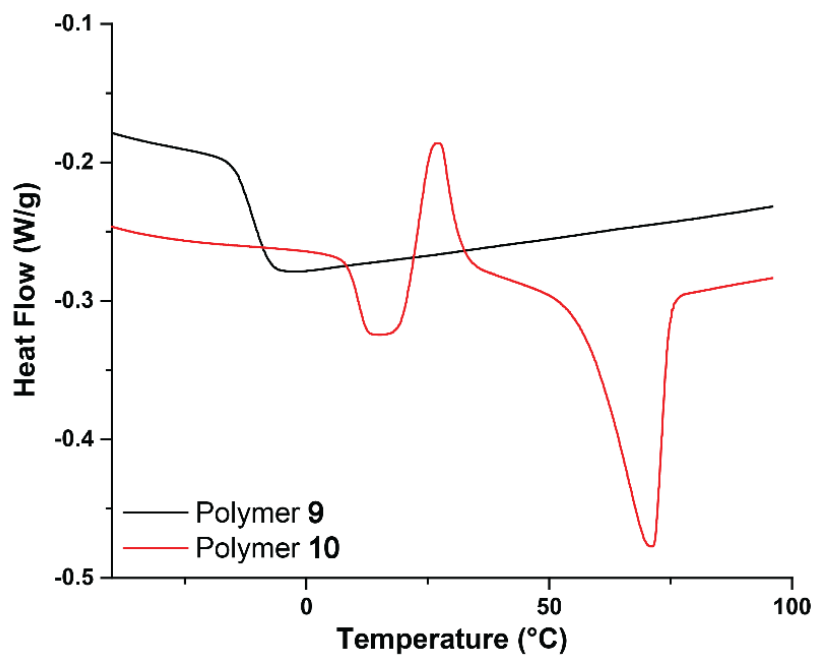


Figure C.30 DSC Thermograms of Polymers 9 and 10.

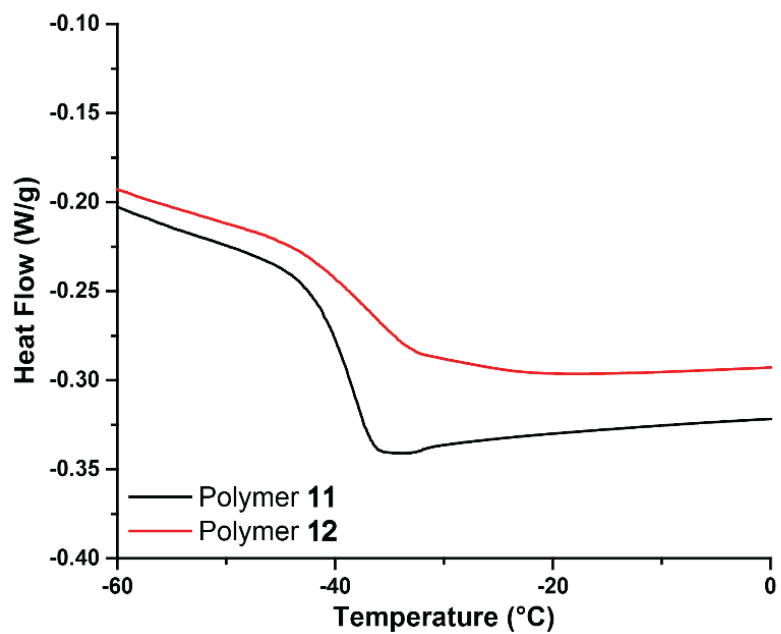


Figure C.31 DSC Thermograms of Polymers 11 and 12.

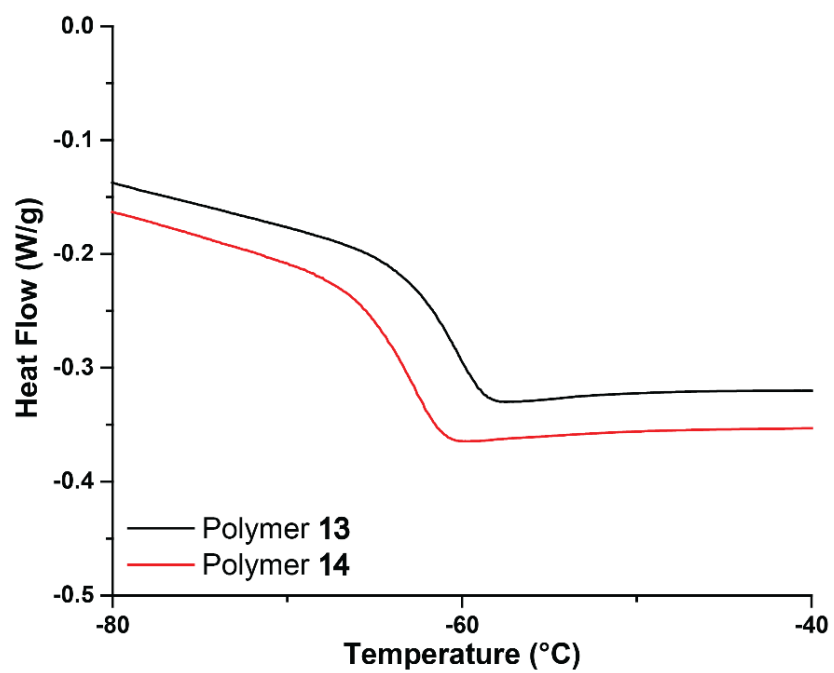


Figure C.32 DSC Thermograms of Polymers 13 and 14

## REFERENCES

1. Geyer, R.; Jambeck, J. R.; Law, K. L., Production, use, and fate of all plastics ever made. *Sci. Adv.* **2017**.
2. Garcia, J. M.; Robertson, M. L., The future of plastics recycling. *Science* **2017**, 358 (6365), 870-872.
3. Scheutz, G. M.; Lessard, J. J.; Sims, M. B.; Sumerlin, B. S., Adaptable Crosslinks in Polymeric Materials: Resolving the Intersection of Thermoplastics and Thermosets. *J Am Chem Soc* **2019**, 141 (41), 16181-16196.
4. Kolb, H. C.; Finn, M. G.; Sharpless, K. B., Click Chemistry: Diverse Chemical Function from a Few Good Reactions. *Angew. Chem. Int. Ed.* **2001**, 40, 2004-2021.
5. Hoyle, C. E.; Lowe, A. B.; Bowman, C. N., Thiol-click chemistry: a multifaceted toolbox for small molecule and polymer synthesis. *Chem Soc Rev* **2010**, 39 (4), 1355-87.
6. Xi, W.; Scott, T. F.; Kloxin, C. J.; Bowman, C. N., Click Chemistry in Materials Science. *Advanced Functional Materials* **2014**, 24 (18), 2572-2590.
7. Scanlan, E. M.; Corce, V.; Malone, A., Synthetic applications of intramolecular thiol-ene "click" reactions. *Molecules* **2014**, 19 (11), 19137-51.
8. Lowe, A. B., Thiol-ene "click" reactions and recent applications in polymer and materials synthesis: a first update. *Polym. Chem.* **2014**, 5 (17), 4820-4870.
9. Lowe, A. B., Thiol-ene "click" reactions and recent applications in polymer and materials synthesis. *Polym. Chem.* **2010**, 1 (1), 17-36.
10. Hoyle, C. E.; Bowman, C. N., Thiol-Ene Click Chemistry. *Angew. Chem. Int. Ed.* **2010**, 49, 1540-1573.
11. Carioscia, J. A.; Stansbury, J. W.; Bowman, C. N., Evaluation and Control of Thiol-ene/Thiol-epoxy Hybrid Networks. *Polymer (Guildf)* **2007**, 48 (6), 1526-1532.
12. Nair, D. P.; Podgórski, M.; Chatani, S.; Gong, T.; Xi, W.; Fenoli, C. R.; Bowman, C. N., The Thiol-Michael Addition Click Reaction: A Powerful and Widely Used Tool in Materials Chemistry. *Chemistry of Materials* **2013**, 26 (1), 724-744.
13. Dyer, E.; Glenn, J. F.; Lendrat, E. G., The Kinetics of the Reactions of Phenyl Isocyanate with Thiols. *J. Org. Chem.* **1960**, 26, 2919-2925.
14. Droger, N.; Primel, O.; Halary, J. L., Characterization of the viscoelastic and mechanical properties of tightly cross-linked polythiourethane networks. *Journal of Applied Polymer Science* **2008**, 107 (1), 455-462.
15. Li, Q.; Zhou, H.; Wicks, D. A.; Hoyle, C. E.; Magers, D. H.; McAlexander, H. R., Comparison of Small Molecule and Polymeric Urethanes, Thiourethanes, and Dithiourethanes: Hydrogen Bonding and Thermal, Physical, and Mechanical Properties. *Macromolecules* **2009**, 42, 1824-1833.
16. Shin, J.; Lee, J.; Jeong, H. M., Properties of polythiourethanes prepared by thiol-isocyanate click reaction. *Journal of Applied Polymer Science* **2018**, 135 (14).
17. Durmaz, H.; Sanyal, A.; Hizal, G.; Tunca, U., Double click reaction strategies for polymer conjugation and post-functionalization of polymers. *Polym. Chem.* **2012**, 3 (4), 825-835.
18. Alim, M. D.; Childress, K. K.; Baugh, N. J.; Martinez, A. M.; Davenport, A.; Fairbanks, B. D.; McBride, M. K.; Worrell, B. T.; Stansbury, J. W.; McLeod, R. R.;

- Bowman, C. N., A photopolymerizable thermoplastic with tunable mechanical performance. *Materials Horizons* **2020**, 7 (3), 835-842.
19. Hensarling, R. M.; Rahane, S. B.; LeBlanc, A. P.; Sparks, B. J.; White, E. M.; Locklin, J.; Patton, D. L., Thiol–isocyanate “click” reactions: rapid development of functional polymeric surfaces. *Polym. Chem.* **2011**, 2 (1), 88-90.
20. Harant, A. W.; Khire, V. S.; Thibidaux, M. S.; Bowman, C. N., Thiol–Ene Photopolymer Grafts on Functionalized Glass and Silicon Surfaces. *Macromolecules* **2006**, 39 (4), 1461-1466.
21. Herwig, G.; Dove, A. P., Synthesis of Rapidly Surface Eroding Polyorthoesters and Polyacetals Using Thiol–ene Click Chemistry. *ACS Macro Letters* **2019**, 8 (10), 1268-1274.
22. Lyon, G. B.; Cox, L. M.; Goodrich, J. T.; Baranek, A. D.; Ding, Y.; Bowman, C. N., Remoldable Thiol–Ene Vitrimers for Photopatterning and Nanoimprint Lithography. *Macromolecules* **2016**, 49 (23), 8905-8913.
23. Cramer, N. B.; Davies, T.; O’Brian, K. A.; Bowman, C. N., Mechanism and Modeling of a Thiol-Ene Photopolymerization. *Macromolecules* **2003**, 36 (12), 4631-4636.
24. Reddy, S. K.; Cramer, N. B.; Bowman, C. N., Thiol-Vinyl Mechanisms. 1. Termination and Propagation Kinetics in Thiol-Ene Photopolymerizations. *Macromolecules* **2006**, 39, 3673-3680.
25. Alameda, B. M.; Palmer, T. C.; Sisemore, J. D.; Pierini, N. G.; Patton, D. L., Hydrolytically degradable poly( $\beta$ -thioether ester ketal) thermosets via radical-mediated thiol–ene photopolymerization. *Polymer Chemistry* **2019**, 10 (41), 5635-5644.
26. Amato, D. N.; Amato, D. V.; Mavrodi, O. V.; Martin, W. B.; Swilley, S. N.; Parsons, K. H.; Mavrodi, D. V.; Patton, D. L., Pro-Antimicrobial Networks via Degradable Acetals (PANDAs) Using Thiol–Ene Photopolymerization. *ACS Macro Letters* **2017**, 6 (2), 171-175.
27. Khire, V. S.; Lee, T. Y.; Bowman, C. N., Synthesis, Characterization and Cleavage of Surface-Bound Linear Polymers Formed Using Thiol-Ene Photopolymerizations. *Macromolecules* **2008**, 41, 7440-7447.
28. Movassagh, B.; Soleiman-Beigi, M., Synthesis of Thiocarbamates from Thiols and Isocyanates Under Catalyst- and Solvent-Free Conditions. *Monatshefte für Chemie - Chemical Monthly* **2008**, 139 (2), 137-140.
29. Cui, C.; Chen, X.; Ma, L.; Zhong, Q.; Li, Z.; Mariappan, A.; Zhang, Q.; Cheng, Y.; He, G.; Chen, X.; Dong, Z.; An, L.; Zhang, Y., Polythiourethane Covalent Adaptable Networks for Strong and Reworkable Adhesives and Fully Recyclable Carbon Fiber-Reinforced Composites. *ACS Appl Mater Interfaces* **2020**, 12 (42), 47975-47983.
30. Gamardella, F.; Serra, A.; Ramis, X.; De la Flor, S., Actuator Behaviour of Tailored Poly(thiourethane) Shape Memory Thermosets. *Polymers (Basel)* **2021**, 13 (10).
31. Jia, Y.; Shi, B.; Jin, J.; Li, J., High refractive index polythiourethane networks with high mechanical property via thiol-isocyanate click reaction. *Polymer* **2019**, 180.
32. Kloxin, C. J.; Scott, T. F.; Adzima, B. J.; Bowman, C. N., Covalent Adaptable Networks (CANs): A Unique Paradigm in Crosslinked Polymers. *Macromolecules* **2010**, 43 (6), 2643-2653.

33. Denissen, W.; Winne, J. M.; Du Prez, F. E., Vitrimers: permanent organic networks with glass-like fluidity. *Chem Sci* **2016**, *7* (1), 30-38.
34. Van Zee, N. J.; Nicolaÿ, R., Vitrimers: Permanently crosslinked polymers with dynamic network topology. *Progress in Polymer Science* **2020**, *104*.
35. Seiffert, S.; Sprakel, J., Physical chemistry of supramolecular polymer networks. *Chem Soc Rev* **2012**, *41* (2), 909-30.
36. Cordier, P.; Tournilhac, F.; Soulie-Ziakovic, C.; Leibler, L., Self-healing and thermoreversible rubber from supramolecular assembly. *Nature* **2008**, *451* (7181), 977-80.
37. Fox, J. D.; Rowan, S. J., Supramolecular Polymerizations and Main-Chain Supramolecular Polymers. *Macromolecules* **2009**, *42* (18), 6823-6835.
38. Burattini, S.; Greenland, B. W.; Merino, D. H.; Weng, W.; Seppala, J.; Colquhoun, H. M.; Hayes, W.; Mackay, M. E.; Hamley, I. W.; Rowan, S. J., A Healable Supramolecular Polymer Blend Based on Aromatic  $\pi$ - $\pi$  Stacking and Hydrogen-Bonding Interactions. *J Am Chem Soc* **2010**, *132*, 12051-12058.
39. Burnworth, M.; Tang, L.; Kumpfer, J. R.; Duncan, A. J.; Beyer, F. L.; Fiore, G. L.; Rowan, S. J.; Weder, C., Optically healable supramolecular polymers. *Nature* **2011**, *472* (7343), 334-7.
40. Bowman, C. N.; Kloxin, C. J., Covalent adaptable networks: reversible bond structures incorporated in polymer networks. *Angew Chem Int Ed Engl* **2012**, *51* (18), 4272-4.
41. Zheng, J.; Png, Z. M.; Ng, S. H.; Tham, G. X.; Ye, E.; Goh, S. S.; Loh, X. J.; Li, Z., Vitrimers: Current research trends and their emerging applications. *Materials Today* **2021**.
42. Zheng, N.; Xu, Y.; Zhao, Q.; Xie, T., Dynamic Covalent Polymer Networks: A Molecular Platform for Designing Functions beyond Chemical Recycling and Self-Healing. *Chem Rev* **2021**, *121* (3), 1716-1745.
43. Chen, X.; Dam, M. A.; Ono, K.; Mal, A.; Shen, H.; Nutt, S. R.; Sheran, K.; Wudl, F., A Thermally Re-mendable Cross-Linked Polymeric Material. *Science* **2002**, *295*, 1698-1702.
44. Reutenauer, P.; Buhler, E.; Boul, P. J.; Candau, S. J.; Lehn, J. M., Room temperature dynamic polymers based on Diels-Alder chemistry. *Chemistry* **2009**, *15* (8), 1893-900.
45. Willocq, B.; Khelifa, F.; Brancart, J.; Van Assche, G.; Dubois, P.; Raquez, J. M., One-component Diels-Alder based polyurethanes: a unique way to self-heal. *RSC Adv.* **2017**, *7* (76), 48047-48053.
46. Li, L.; Qin, X.; Mei, H.; Liu, L.; Zheng, S., Reprocessed and shape memory networks involving poly(hydroxyl ether ester) and polydimethylsiloxane through Diels-Alder reaction. *European Polymer Journal* **2021**, *160*.
47. Zhang, B.; Digby, Z. A.; Flum, J. A.; Chakma, P.; Saul, J. M.; Sparks, J. L.; Konkolewicz, D., Dynamic Thiol-Michael Chemistry for Thermoresponsive Rehealable and Malleable Networks. *Macromolecules* **2016**, *49* (18), 6871-6878.
48. Higaki, Y.; Otsuka, H.; Takahara, A., A Thermodynamic Polymer Cross-Linking System Based on Radically Exchangeable Covalent Bonds. *Macromolecules* **2006**, *39*, 2121-2125.

49. Deng, G.; Li, F.; Yu, H.; Liu, F.; Liu, C.; Sun, W.; Jiang, H.; Chen, Y., Dynamic Hydrogels with an Environmental Adaptive Self-Healing Ability and Dual Responsive Sol–Gel Transitions. *ACS Macro Letters* **2012**, *1* (2), 275-279.
50. Deng, G.; Tang, C.; Li, F.; Jiang, H.; Chen, Y., Covalent Cross-Linked Polymer Gels with Reversible Sol–Gel Transition and Self-Healing Properties. *Macromolecules* **2010**, *43* (3), 1191-1194.
51. Ying, H.; Zhang, Y.; Cheng, J., Dynamic urea bond for the design of reversible and self-healing polymers. *Nat Commun* **2014**, *5*, 3218.
52. Zhang, Y.; Ying, H.; Hart, K. R.; Wu, Y.; Hsu, A. J.; Coppola, A. M.; Kim, T. A.; Yang, K.; Sottos, N. R.; White, S. R.; Cheng, J., Malleable and Recyclable Poly(urea-urethane) Thermosets bearing Hindered Urea Bonds. *Adv Mater* **2016**, *28* (35), 7646-51.
53. Zheng, N.; Fang, Z.; Zou, W.; Zhao, Q.; Xie, T., Thermoset Shape-Memory Polyurethane with Intrinsic Plasticity Enabled by Transcarbamoylation. *Angew Chem Int Ed Engl* **2016**, *55* (38), 11421-5.
54. Denissen, W.; Droesbeke, M.; Nicolay, R.; Leibler, L.; Winne, J. M.; Du Prez, F. E., Chemical control of the viscoelastic properties of vinylogous urethane vitrimers. *Nat Commun* **2017**, *8*, 14857.
55. Montarnal, D.; Capelot, M.; Tournilhac, F.; Leibler, L., Silica-Like Malleable Materials from Permanent Organic Networks. *Science* **2011**, *334*, 965-968.
56. Capelot, M.; Montarnal, D.; Tournilhac, F.; Leibler, L., Metal-catalyzed transesterification for healing and assembling of thermosets. *J Am Chem Soc* **2012**, *134* (18), 7664-7.
57. Altuna, F. I.; Pettarin, V.; Williams, R. J. J., Self-healable polymer networks based on the cross-linking of epoxidised soybean oil by an aqueous citric acid solution. *Green Chemistry* **2013**, *15* (12).
58. Brutman, J. P.; Delgado, P. A.; Hillmyer, M. A., Polylactide Vitrimers. *ACS Macro Letters* **2014**, *3* (7), 607-610.
59. Debnath, S.; Kaushal, S.; Ojha, U., Catalyst-Free Partially Bio-Based Polyester Vitrimers. *ACS Applied Polymer Materials* **2020**, *2* (2), 1006-1013.
60. Liu, T.; Zhao, B.; Zhang, J., Recent development of repairable, malleable and recyclable thermosetting polymers through dynamic transesterification. *Polymer* **2020**, *194*.
61. Salaeh, S.; Das, A.; Wießner, S.; Stapor, M., Vitrimer-like material based on a biorenewable elastomer crosslinked with a dimeric fatty acid. *European Polymer Journal* **2021**, *151*.
62. Van Lijsebetten, F.; Spiesschaert, Y.; Winne, J. M.; Du Prez, F. E., Reprocessing of Covalent Adaptable Polyamide Networks through Internal Catalysis and Ring-Size Effects. *J Am Chem Soc* **2021**, *143* (38), 15834-15844.
63. Scott, T. F.; Schneider, A. D.; Cook, W. D.; Bowman, C. N., Photoinduced Plasticity in Cross-Linked Polymers. *Science* **2005**, *308*, 1615-1617.
64. Nicolaÿ, R.; Kamada, J.; Van Wassen, A.; Matyjaszewski, K., Responsive Gels Based on a Dynamic Covalent Trithiocarbonate Cross-Linker. *Macromolecules* **2010**, *43* (9), 4355-4361.

65. Amamoto, Y.; Kamada, J.; Otsuka, H.; Takahara, A.; Matyjaszewski, K., Repeatable photoinduced self-healing of covalently cross-linked polymers through reshuffling of trithiocarbonate units. *Angew Chem Int Ed Engl* **2011**, *50* (7), 1660-3.
66. Denissen, W.; Rivero, G.; Nicolaj, R.; Leibler, L.; Winne, J. M.; Du Prez, F. E., Vinylogous Urethane Vitrimers. *Advanced Functional Materials* **2015**, *25* (16), 2451-2457.
67. Canadell, J.; Goossens, H.; Klumperman, B., Self-Healing Materials Based on Disulfide Links. *Macromolecules* **2011**, *44* (8), 2536-2541.
68. Michal, B. T.; Jaye, C. A.; Spencer, E. J.; Rowan, S. J., Inherently Photohealable and Thermal Shape-Memory Polydisulfide Networks. *ACS Macro Letters* **2013**, *2* (8), 694-699.
69. Pepels, M.; Filot, I.; Klumperman, B.; Goossens, H., Self-healing systems based on disulfide–thiol exchange reactions. *Polymer Chemistry* **2013**, *4* (18).
70. Imbernon, L.; Oikonomou, E. K.; Norvez, S.; Leibler, L., Chemically crosslinked yet reprocessable epoxidized natural rubber via thermo-activated disulfide rearrangements. *Polymer Chemistry* **2015**, *6* (23), 4271-4278.
71. Ji, F.; Liu, X.; Sheng, D.; Yang, Y., Epoxy-vitrimer composites based on exchangeable aromatic disulfide bonds: Reprocessibility, adhesive, multi-shape memory effect. *Polymer* **2020**, *197*.
72. Wen, Z.; Han, X.; Fairbanks, B. D.; Yang, K.; Bowman, C. N., Development of thiourethanes as robust, reprocessable networks. *Polymer* **2020**, *202*.
73. Li, L.; Chen, X.; Torkelson, J. M., Reprocessable Polymer Networks via Thiourethane Dynamic Chemistry: Recovery of Cross-link Density after Recycling and Proof-of-Principle Solvolysis Leading to Monomer Recovery. *Macromolecules* **2019**, *52* (21), 8207-8216.
74. Huang, S.; Podgórski, M.; Han, X.; Bowman, C. N., Chemical recycling of poly(thiourethane) thermosets enabled by dynamic thiourethane bonds. *Polymer Chemistry* **2020**, *11* (43), 6879-6883.
75. Gamardella, F.; Munoz, S.; De la Flor, S.; Ramis, X.; Serra, A., Recyclable Organocatalyzed Poly(Thiourethane) Covalent Adaptable Networks. *Polymers (Basel)* **2020**, *12* (12).
76. Gamardella, F.; Guerrero, F.; De la Flor, S.; Ramis, X.; Serra, A., A new class of vitrimers based on aliphatic poly(thiourethane) networks with shape memory and permanent shape reconfiguration. *European Polymer Journal* **2020**, *122*.
77. Gamardella, F.; De la Flor, S.; Ramis, X.; Serra, A., Recyclable poly(thiourethane) vitrimers with high Tg. Influence of the isocyanate structure. *Reactive and Functional Polymers* **2020**, *151*.
78. Fan, C.-J.; Wen, Z.-B.; Xu, Z.-Y.; Xiao, Y.; Wu, D.; Yang, K.-K.; Wang, Y.-Z., Adaptable Strategy to Fabricate Self-Healable and Reprocessable Poly(thiourethane-urethane) Elastomers via Reversible Thiol–Isocyanate Click Chemistry. *Macromolecules* **2020**, *53* (11), 4284-4293.
79. Erice, A.; Ruiz de Luzuriaga, A.; Azcune, I.; Fernandez, M.; Calafel, I.; Grande, H. J.; Rekondo, A., New injectable and self-healable thermoset polythiourethane based on S-aromatic thiourethane dissociative exchange mechanism. *Polymer* **2020**, *196*.

80. Meng, F.; Saed, M. O.; Terentjev, E. M., Elasticity and Relaxation in Full and Partial Vitrimer Networks. *Macromolecules* **2019**, *52* (19), 7423-7429.
81. Chakma, P.; Konkolewicz, D., Dynamic Covalent Bonds in Polymeric Materials. *Angew Chem Int Ed Engl* **2019**, *58* (29), 9682-9695.
82. Chakma, P.; Rodrigues Possarle, L. H.; Digby, Z. A.; Zhang, B.; Sparks, J. L.; Konkolewicz, D., Dual stimuli responsive self-healing and malleable materials based on dynamic thiol-Michael chemistry. *Polymer Chemistry* **2017**, *8* (42), 6534-6543.
83. Wang, C.; Mavila, S.; Worrell, B. T.; Xi, W.; Goldman, T. M.; Bowman, C. N., Productive Exchange of Thiols and Thioesters to Form Dynamic Polythioester-Based Polymers. *ACS Macro Letters* **2018**, *7* (11), 1312-1316.
84. Albertsson, A. C. K., S, Degradable polymers for the future. *Acta Polymerica* **1995**, *46* (2), 114-123.
85. Schneiderman, D. K.; Hillmyer, M. A., 50th Anniversary Perspective: There Is a Great Future in Sustainable Polymers. *Macromolecules* **2017**, *50* (10), 3733-3749.
86. Hou, S.; Hoyle, D. M.; Blackwell, C. J.; Haernvall, K.; Perz, V.; Guebitz, G. M.; Khosravi, E., Hydrolytic degradation of ROMP thermosetting materials catalysed by bio-derived acids and enzymes: from networks to linear materials. *Green Chemistry* **2016**, *18* (19), 5190-5199.
87. Rehmann, M. S.; Garibian, A. C.; Kloxin, A. M., Hydrolytically degradable thiol-ene hydrogels for protein release. *Macromol Symp* **2013**, *329* (1), 58-65.
88. Inkinen, S.; Hakkarainen, M.; Albertsson, A. C.; Sodergard, A., From lactic acid to poly(lactic acid) (PLA): characterization and analysis of PLA and its precursors. *Biomacromolecules* **2011**, *12* (3), 523-32.
89. Poetz, K. L. D., Olivia Z.; Shipp, Devon A., Polyanhydride Nanoparticles by 'Click' Thiol-Ene Polymerization. *Polym. Chem.* **2015**, *6*, 5464-5469.
90. Rutherglen, B. G.; McBath, R. A.; Huang, Y. L.; Shipp, D. A., Polyanhydride Networks from Thiol-Ene Polymerizations. *Macromolecules* **2010**, *43* (24), 10297-10303.
91. Gopferich, A. T., J., Polyanhydride degradation and erosion. *Advanced Drug Delivery Reviews* **2002**, *54* (7), 911-931.
92. Amato, D. V.; Amato, D. N.; Blancett, L. T.; Mavrodi, O. V.; Martin, W. B.; Swilley, S. N.; Sandoz, M. J.; Shearer, G.; Mavrodi, D. V.; Patton, D. L., A bio-based pro-antimicrobial polymer network via degradable acetal linkages. *Acta Biomater* **2018**, *67*, 196-205.
93. Paramonov, S. E. B., Eric M.; Beaudette, Tristan T.; Standley, Stephany M.; Lee, Cameron C.; Dashe, Jesse; and Frechet, Jean M. J., Fully Acid Degradable Biocompatible Polyacetal Microparticles for Drug Delivery. *Bioconjugate Chemistry* **2008**, *19* (4), 911-919.
94. Wang, Y.; Morinaga, H.; Sudo, A.; Endo, T., Synthesis of amphiphilic polyacetal by polycondensation of aldehyde and polyethylene glycol as an acid-labile polymer for controlled release of aldehyde. *Journal of Polymer Science Part A: Polymer Chemistry* **2011**, *49* (3), 596-602.
95. Heffernan, M. J. M., Niren, Polyketal Nanoparticles: A New pH-Sensitive Biodegradable Drug Delivery Vehicle. *Bioconjugate Chemistry* **2005**, *16* (6), 1340-1342.

96. Shenoi, R. A.; Narayanannair, J. K.; Hamilton, J. L.; Lai, B. F.; Horte, S.; Kainthan, R. K.; Varghese, J. P.; Rajeev, K. G.; Manoharan, M.; Kizhakkedathu, J. N., Branched multifunctional polyether polyketals: variation of ketal group structure enables unprecedented control over polymer degradation in solution and within cells. *J Am Chem Soc* **2012**, *134* (36), 14945-57.
97. Whiting, B. T.; Coates, G. W., Synthesis and polymerization of bicyclic ketals: a practical route to high-molecular weight polyketals. *J Am Chem Soc* **2013**, *135* (30), 10974-7.
98. Lee, S. Y., Stephen C.; Heffernan, Michael J.; Taylor, W. Robert; Murthy, Niren, Polyketal Microparticles: A New Delivery Vehicle for Superoxide Dismutase. *Bioconjugate Chemistry* **2007**, *18* (1), 4-7.
99. Fiore, V. F. L., Megan C.; Roser-Page, Susanne; Yang, Stephen C.; Roman, Jesse; Murthy, Niren; Barker, Thomas H., Polyketal microparticles for therapeutic delivery to the lung. *Biomaterials* **2010**, *31* (5), 810-817.
100. Liu, B.; Thayumanavan, S., Substituent Effects on the pH Sensitivity of Acetals and Ketals and Their Correlation with Encapsulation Stability in Polymeric Nanogels. *J Am Chem Soc* **2017**, *139* (6), 2306-2317.
101. Brogan, J. B.; Richard, J. E.; Zercher, C. K., Preparation of Diallyl Ketals. *Synthetic Communications* **1995**, *25* (4), 587-593.
102. Cordes, E. H. B., H. G., Mechanism and catalysis for hydrolysis of acetals, ketals, and ortho esters. *Chemical Reviews* **1974**, *74* (5), 581-603.
103. Marvel, C. S. C., R. R., Polyalkylene Sulfides from Diolefins and Dimercaptans. *J Am Chem Soc* **1948**, *70* (3), 993-998.
104. Jasinski, F.; Rannée, A.; Schweitzer, J.; Fischer, D.; Lobry, E.; Croutxé-Barghorn, C.; Schmutz, M.; Le Nouen, D.; Criqui, A.; Chemtob, A., Thiol–Ene Linear Step-Growth Photopolymerization in Miniemulsion: Fast Rates, Redox-Responsive Particles, and Semicrystalline Films. *Macromolecules* **2016**, *49* (4), 1143-1153.
105. Jin, K.; Leitsch, E. K.; Chen, X.; Heath, W. H.; Torkelson, J. M., Segmented Thermoplastic Polymers Synthesized by Thiol–Ene Click Chemistry: Examples of Thiol–Norbornene and Thiol–Maleimide Click Reactions. *Macromolecules* **2018**, *51* (10), 3620-3631.
106. Lluch, C. R., Joan C.; Galia, Marina; Lligadas, Gerard; Cadiz, Virginia, Rapid Approach to Biobased Telechelics through Two One-Pot Thiol–Ene Click Reactions. *Biomacromolecules* **2010**, *11* (6), 1646-1653.
107. Sarapas, J. M.; Tew, G. N., Poly(ether–thioethers) by Thiol–Ene Click and Their Oxidized Analogues as Lithium Polymer Electrolytes. *Macromolecules* **2016**, *49* (4), 1154-1162.
108. van den Berg, O.; Dispinar, T.; Hommez, B.; Du Prez, F. E., Renewable sulfur-containing thermoplastics via AB-type thiol-ene polyaddition. *European Polymer Journal* **2013**, *49* (4), 804-812.
109. Türünç, O.; Meier, M. A. R., The thiol-ene (click) reaction for the synthesis of plant oil derived polymers. *European Journal of Lipid Science and Technology* **2013**, *115* (1), 41-54.

110. Lillie, L. M.; Tolman, W. B.; Reineke, T. M., Degradable and renewably-sourced poly(ester-thioethers) by photo-initiated thiol–ene polymerization. *Polymer Chemistry* **2018**, *9* (23), 3272-3278.
111. Zheng, N.; Fang, G.; Cao, Z.; Zhao, Q.; Xie, T., High strain epoxy shape memory polymer. *Polymer Chemistry* **2015**, *6* (16), 3046-3053.
112. Ding, Z.; Yuan, L.; Liang, G.; Gu, A., Thermally resistant thermadapt shape memory crosslinked polymers based on silyl ether dynamic covalent linkages for self-folding and self-deployable smart 3D structures. *Journal of Materials Chemistry A* **2019**, *7* (16), 9736-9747.
113. Krishnakumar, B.; Sanka, R. V. S. P.; Binder, W. H.; Parthasarthy, V.; Rana, S.; Karak, N., Vitrimers: Associative dynamic covalent adaptive networks in thermoset polymers. *Chemical Engineering Journal* **2020**, 385.
114. Elling, B. R.; Dichtel, W. R., Reprocessable Cross-Linked Polymer Networks: Are Associative Exchange Mechanisms Desirable? *ACS Cent Sci* **2020**, *6* (9), 1488-1496.
115. Hubbard, A. M.; Ren, Y.; Konkolewicz, D.; Sarvestani, A.; Picu, C. R.; Kedziora, G. S.; Roy, A.; Varshney, V.; Nepal, D., Vitrimer Transition Temperature Identification: Coupling Various Thermomechanical Methodologies. *ACS Applied Polymer Materials* **2021**, *3* (4), 1756-1766.
116. Wen, Z.; McBride, M. K.; Zhang, X.; Han, X.; Martinez, A. M.; Shao, R.; Zhu, C.; Visvanathan, R.; Clark, N. A.; Wang, Y.; Yang, K.; Bowman, C. N., Reconfigurable LC Elastomers: Using a Thermally Programmable Monodomain To Access Two-Way Free-Standing Multiple Shape Memory Polymers. *Macromolecules* **2018**, *51* (15), 5812-5819.
117. Ying, H.; Cheng, J., Hydrolyzable Polyureas Bearing Hindered Urea Bonds. *Journal of the American Chemical Society* **2014**, *136* (49), 16974-16977.
118. Stowell, J. C.; Padegimas, S. J., Urea dissociation. Measure of steric hindrance in secondary amines. *The Journal of Organic Chemistry* **1974**, *39* (16), 2448-2449.
119. Zhang, L.; Rowan, S. J., Effect of Sterics and Degree of Cross-Linking on the Mechanical Properties of Dynamic Poly(alkylurea–urethane) Networks. *Macromolecules* **2017**, *50* (13), 5051-5060.
120. Yun, S. M.; Lee, H. M.; Ahmed, S.; Kim, G. Y.; Kim, J. C.; Cheong, I. W., Effect of diisocyanate structure on steric restructuring of hindered urea bonds for self-healable coating. *Progress in Organic Coatings* **2022**, *165*, 106730.
121. Nishimura, Y.; Chung, J.; Muradyan, H.; Guan, Z., Silyl Ether as a Robust and Thermally Stable Dynamic Covalent Motif for Malleable Polymer Design. *Journal of the American Chemical Society* **2017**, *139* (42), 14881-14884.
122. Guerre, M.; Taplan, C.; Winne, J. M.; Prez, F. E. D., Vitrimers: directing chemical reactivity to control material properties. *Chem. Sci.* **2020**, *11*, 4855-4870.
123. McNair, O. D.; Brent, D. P.; Sparks, B. J.; Patton, D. L.; Savin, D. A., Sequential thiol click reactions: formation of ternary thiourethane/thiol-ene networks with enhanced thermal and mechanical properties. *ACS Appl Mater Interfaces* **2014**, *6* (9), 6088-97.
124. Jing, B. B.; Evans, C. M., Catalyst-Free Dynamic Networks for Recyclable, Self-Healing Solid Polymer Electrolytes. *J Am Chem Soc* **2019**, *141* (48), 18932-18937.

125. Samanta, S.; Kim, S.; Saito, T.; Sokolov, A. P., Polymers with Dynamic Bonds: Adaptive Functional Materials for a Sustainable Future. *J Phys Chem B* **2021**, *125* (33), 9389-9401.
126. Wu, J. B.; Li, S. J.; Liu, H.; Qian, H. J.; Lu, Z. Y., Dynamics and reaction kinetics of coarse-grained bulk vitrimers: a molecular dynamics study. *Phys Chem Chem Phys* **2019**, *21* (24), 13258-13267.
127. Beaupre, D. M.; Weiss, R. G., Thiol- and Disulfide-Based Stimulus-Responsive Soft Materials and Self-Assembling Systems. *Molecules* **2021**, *26* (11).
128. Lillie, L. M.; Tolman, W. B.; Reineke, T. M., Degradable and renewably-sourced poly(ester-thioethers) by photo-initiated thiol-ene polymerization. *Polym Chem* **2018**, *9*, 3272-3278.
129. Poetz, K. L.; Durham, O. Z.; Shipp, D. A., Polyanhydride Nanoparticles by 'Click' Thiol-Ene Polymerization. *Polym. Chem.* **2015**, *6*, 5464-5469.
130. Cramer, N. B. D., Tanner; O'Brian, K. Allison; Bowman, Christopher N., Mechanism and Modeling of a Thiol-Ene Photopolymerization. *Macromolecules* **2003**, *36* (12), 4631-4636.
131. von Burkersroda, F. S., Luise; Gopferich, Achim, Why degradable polymers undergo surface erosion or bulk erosion. *Biomaterials* **2002**, *23* (21), 4221-4231.
132. Gopferich, A., Mechanisms of polymer degradation and erosion. *Biomaterials* **1996**, *17* (2), 103-114.
133. Tzafriri, A. R., Mathematical modeling of diffusion-mediated release from bulk degrading matrices. *Journal of Controlled Release* **2000**, *63* (1), 69-79.
134. Shah, S. S. K., M. G.; Mashelkar, R. A., Release kinetics of pendant substituted bioactive molecules from swellable hydrogels: role of chemical reaction and diffusive transport. *Journal of Membrane Science* **1990**, *51* (1), 83-104.
135. Sevim, K.; Pan, J., A model for hydrolytic degradation and erosion of biodegradable polymers. *Acta Biomater* **2018**, *66*, 192-199.
136. Sackett, C. K.; Narasimhan, B., Mathematical modeling of polymer erosion: consequences for drug delivery. *Int J Pharm* **2011**, *418* (1), 104-14.
137. Laycock, B.; Nikolić, M.; Colwell, J. M.; Gauthier, E.; Halley, P.; Bottle, S.; George, G., Lifetime prediction of biodegradable polymers. *Progress in Polymer Science* **2017**, *71*, 144-189.
138. Bat, E. Z., Zheng; Feijen, Jan; Grijpma, Dirk W.; Poot, Andre, A., Biodegradable elastomers for biomedical applications and regenerative medicine. *Regenerative Medicine* **2014**, *9* (3), 385-398.
139. Kenley, R. A. O. L., Maryann; Mahoney, Randolph; Sanders, Lynda M., Poly(lactide-co-glycolide) decomposition kinetics in vivo and in vitro. *Macromolecules* **1987**, *20* (10), 2398-2403.
140. Lyu, S.; Sparer, R.; Untereker, D., Analytical solutions to mathematical models of the surface and bulk erosion of solid polymers. *Journal of Polymer Science Part B: Polymer Physics* **2005**, *43* (4), 383-397.
141. Li, Q.; Zhou, H.; Wicks, D. A.; Hoyle, C. E., Thiourethane-based thiol-ene highT<sub>g</sub> networks: Preparation, thermal, mechanical, and physical properties. *Journal of Polymer Science Part A: Polymer Chemistry* **2007**, *45* (22), 5103-5111.